



DOCTORAL THESIS

3rd Cycle Doctoral (D-LMD)

Presented by

Khadra HAOUARI

With a view to obtaining the doctoral diploma in 3rd Cycle Doctoral (D-LMD)

Branch: Mechanic

Specialty: Energetic

Topic

Numerical study of heat and mass transfer in venturi

Supported, on 19/05 /2022, before the jury composed of:

Last and first name	Grade	Institution of affiliation	Designation
Mr Brahim Khalil HACHI	Professor	University of Djelfa	President
Mr Kouider RAHMANI	Professor	University of Djelfa	Supervisor
Mr Abdelhalim BENTEBBICHE	Professor	University of Bab Ezzouar-Alger	Examiner
Mr Sahraoui KHERRIS	Professor	University of Tissemsilt	Examiner
Mr Lakhdar AIDAOUI	Professor	University of Djelfa	Examiner
Mr Amar KOUADRI	MCA	University of Djelfa	Examiner



Dedicate to

My parents

My sisters and my brothers

My friends

Acknowledgements

First of all, I thank Allah who aided me to complete my thesis

*I'm very grateful to my supervisor, **Pr. Kouider RAHMANI**. Thankful for his advice, guidance, and support throughout this work. Also thank **Dr. Toufik Tayeb NAAS** for his assistance during the achievement of this work.*

*I express my deep gratitude to **Mr. Brahim Khalil HACHI** chairing the jury.*

*I would also like to thank **Mr. Abdelhalim BENTEBBICHE**, Professor at the University of Bab Ezzouar in Algiers, **Mr. Sahraoui KHERRIS**, Professor at the University Center of Tissemsilt, **Mr. Lakhdar AIDAOU**I, professor at the University of Djelfa, and **Mr. Amar KOUADRI**, lecturer professor at the University of Djelfa.*

I extend my sincere thanks to my professors at the Department of Mechanical Engineering, Faculty of Science and Technology, University of Djelfa.

*I would also like to thank **Miss. Djemaa BALAKHAL** and **Miss. Zohour ALLAM** from the Department of Physics, Faculty of mathematic and informatics, University of Djelfa.*

ملخص


يعتبر جهاز تنقية الغاز الفنتوري من أهم الأجهزة التي تنظف الغازات المستخدمة في العديد من التطبيقات الصناعية. في هذا العمل ، قمنا بفحص كفاءة جهاز تنقية الغاز في تنظيف الغازات الناتجة عن الكتلة الحيوية ودرسنا ظاهرة انتقال الحرارة والكتلة في هذا الجهاز. تستخدم هذه الدراسة كود CFD التجاري (ANSYS FLUENT) للتحقيق في المحاكاة الرقمية ثنائية الأبعاد لتدفقات غاز الكتلة الحيوية والمياه في جهاز فنتوري مع ظروف حدية ممثلة بسرعات مدخل غاز تبلغ 15 و 20 و 25 و 30 م / ث و تدفق كتلة مدخل الماء 0.02 و 0.04 و 0.06 كجم / ثانية. تم استخدام نموذج $k - \epsilon$ و نموذج النقل الجماعي لمعالجة التدفق المضطرب ونقل الكتلة. تم عرض تطور السرعة والضغط وعدد نسلت ، وكذلك نتائج دالة كثافة الاحتمال (PDF) لانتقال الكتلة والحرارة. أوضحت النتائج أن كفاءة جهاز تنقية الغاز الفنتوري في تنظيف الغاز الناتج عن تغويز الكتلة الحيوية تصل إلى 98٪ بسرعة غاز 30 م / ث مع أدنى معدل تدفق سائل وأن ظاهرتي الانتقال الحراري والكتلي لهما تأثير ضئيل على أداء فنتوري.

الكلمات الرئيسية: جهاز تنقية الغاز الفنتوري ، نقل الكتلة ، نقل الحرارة ، دالة الكثافة الاحتمالية ، كفاءة الإزالة .

Abstract :

The venturi Scrubber is one of the most important gas cleaner devices used in many industrial applications. In this work, we examined the efficiency of the venturi scrubber in cleaning gases from biomass and studied the phenomenon of heat and mass transfer in this device. In this study, a commercial CFD code (ANSYS FLUENT) was used as a 2D numerical simulation support for the calculations of the biomass gas and water flows in the venturi device with boundary conditions represented by the inlet gas velocities of 15, 20, 25 and 30 m/s and inlet water mass flow rates of: 0.02, 0.04 and 0.06 kg/s. The $k - \varepsilon$ model and the transport species model are used to treat the turbulent flow and the mass transfer. The evolutions of velocity, pressure, and Nusselt number are presented, as well as the results of the probability density function (PDF) for mass and heat transfer. The results showed that the efficiency of the venturi scrubber in cleaning the gas resulting from the gasification of biomass reaches 98% at a gas velocity of 30 m/s with the lowest liquid flow rate and that the transfer phenomena of heat and mass have a little effect on the venturi scrubber performance.

KEYWORDS: Venturi scrubber, Mass transfer, Heat transfer, Probability density function, Removal efficiency.



Résumé:

Le venturi Laveur est l'un des dispositifs le plus important nettoyeur des gaz utilisés dans de nombreuses applications industrielles. Dans ce travail, nous avons examiné l'efficacité du venturi laveur dans le nettoyage des gaz issus de biomasse, et étudié le phénomène de transfert de chaleur et de masse dans ce dispositif. Dans cette étude, on a utilisé un code commercial CFD (ANSYS FLUENT) comme support de simulation numérique en 2D pour les calculs des flux de gaz de biomasse et d'eau dans le dispositif venturi avec des conditions aux limites représentées par les vitesses d'entrée de gaz de 15, 20, 25 et 30 m/s et les débits massiques de l'eau d'entrée de : 0,02, 0,04 et 0,06 kg/s. Le modèle $k - \varepsilon$ et le modèle des espèces de transport sont utilisés pour traiter l'écoulement turbulent et le transfert de masse. Les évolutions de la vitesse, de la pression et du nombre de Nusselt sont présentée, ainsi que les résultats de la fonction de densité de probabilité (PDF) pour le transfert de masse et de chaleur. Les résultats ont montré que l'efficacité du venturi laveur dans le nettoyage du gaz issu de la gazéification de la biomasse atteint 98% à une vitesse de gaz de 30 m/s avec le plus faible débit de liquide et que les phénomènes de transfert de chaleur et de masse ont peu d'effet sur le performance de laveur venturi.

MOTS CLÉS : Laveur venturi, Transfert de masse, Transfert de chaleur, Fonction de densité de probabilité, Efficacité d'élimination

TABLE OF CONTENTS

NOMENCLATURE.....	I
LIST OF FIGURES	III
LIST OF TABLES	VII

CHAPTER I: General introduction

I.1 Venturi scrubber.....	1
I.2 Types of venturi scrubber	2
I.3 Advantages and disadvantages of venturi scrubber.....	4
I.4 Objectives of the Research.....	5
I.5 Thesis plan.....	5

CHAPTER II: Literature review

II.1 Introduction.....	7
II.2 Experimental studies	7
II.3 Theoretical studies.....	12
II.4 Numerical simulation using CFD.....	17
II.5 Conclusion.....	25

CHAPTER III: Computational models and methods

III.1 Introduction	27
III.2 Computational models	27
III.2.1 Physical model.....	27
III.2.2 Governing equations.....	28
III.2.3 The $k - \varepsilon$ Model.....	29
III.2.3.1 Turbulent kinetic energy equation k	29
III.2.3.2 Equation of the dissipation rate ε of turbulent kinetic energy.....	29

III.2.4 Species transport model expression	30
III.2.5 Reynolds number expression	31
III.2.6 Nusselt number expression	31
III.2.7 Probability density function PDF	31
III.2.8 The removal efficiency	32
III.2.9 The removal energy cost	32
III.2.10 Fluid properties	32
III.2.11 The boundary conditions	34
III.3 Numerical methodology	34
III.3.1 Solution methodology	34
III.3.2 Grid independency tests	35
III.4 Conclusion	36

CHAPTER IV: Flows behavior in the venturi scrubber

IV.1 Introduction	38
IV.2 Validation	38
IV.3 The velocity evolution.....	39
IV.4 The evolution of pressure.....	44
IV.5 Pressure drops assessment.....	51
IV.6 The evolution of turbulent kinetic energy	52
IV.7 The evolution of turbulent dissipation rate.....	54
IV.8 Turbulent viscosity	56
IV.9 Conclusion	59

CHAPTER V: Heat and mass transfer in the venturi scrubber

V.1 Introduction	61
V.2 Evolution of temperature	61

V.3 The local Nusselt number evolutions	65
V.4 Mass fraction variations	68
V.4.1 Mass fraction of gas.....	68
V.4.2 Mass fraction of water.....	72
V.5 The probability density function (PDF)	77
V.6 Removal efficiency and the removal energy cost	79
V.7 Conclusion.....	80
General Conclusion.....	82
References	85

NOMENCLATURE

Letter

$(A/F)_{\text{stoic}}$	Stoichiometric air-PG ratio	kg air/kg PG
c	Specific heat capacity	j/kg.k
c_i	Mass fraction	-
C_{in}	Mass fraction at inlet water	-
C_o	Mass fraction at outlet	-
\bar{C}_{Pm}	Molar specific heat capacity at constant pressure at NTP	kJ/(kmol.K)
\bar{C}_{Pv}	Molar specific heat capacity at constant volume at NTP	kJ/(kmol.K)
d	Diameter	m
D_h	Hydraulic diameter	m
$D_{\text{air-mixt}}$	Diffusion coefficient	m^2/s
$D_{i,m}$	Mass diffusion coefficient	m^2/s
$D_{T,i}$	Thermal diffusion coefficient	$\text{m}^2/\text{s.K}$
D_t	Turbulent diffusivity	m^2/s
E_R	Collection efficiency	-
F_α	Function of a scalar field	
g	Gravitational acceleration	m/s^2
h	Convection coefficient	$\text{W}/\text{m}^2.\text{K}$
J_i	Diffusion flux	$\text{Kg}/\text{m}^2.\text{s}$
k	Turbulent kinetic energy	m^2/s^2
K_m	Thermal conductivity	$\text{W}/(\text{m.K})$
l	Unit tensor	-
L	Length	m
LHV_m	Lower Heating Value	kJ/m^3
M_m	Molar mass	kg/kmol
\dot{m}	Mass flow rate	Kg/s
Nu	Nusselt number	-
P	Pressure	Pa
Q	Flow rate	m^3/s

Re	Reynolds number	-
REC	Removal Energy Cost	W
SG	Specific gravity at NTP	-
S_L	Laminar burning velocity	m/s
\bar{s}_m°	Absolute entropy of PG	kJ/(kmol.K)
(A/F)stoic	Stoichiometric air-PG ratio	kg air/kg PG
T	Temperature	K
T_{adfl}	Adiabatic Flame Temperature	K
u	Velocity	m/s
V_{gth}	Throat gas velocity	m/s
WI	Wobbe Index	kJ/m ³
W_{rev}	Reversible Work	kJ/kmol
x_i	Coordinate along the X axis	m
x_j	Coordinate along the Y axis	m

Greek symbols

ρ	Density	Kg/m ³
Δp	Pressure drop	Pa
μ	Dynamic viscosity	Kg/m.s
μ_m	Absolute viscosity	Kg/(m.s)
μ_t	Turbulent viscosity	Kg/m.s
ε	Turbulent dissipation rate	m ² /s ³
λ	Thermal conductivity	W/m.k
α	Scalar field	

Abbreviations

CFD	Computational Fluid Dynamics
NTP	Normal Temperature of 298 K and Pressure of 1 atm
PG	Producer gas
PDF	Probability density function
VOF	Volume of Fluid

LIST OF FIGURES

Figure I.1: Venturi scrubber description	2
Figure I.2: Operating modes of venturi scrubbers	3
Figure I. 3: Geometry of ejector-venturi	4
Figure II.1: Effect of liquid-to-gas flow rate on the overall pressure drop.....	16
Figure II.2: Effect of the liquid flow rate on the pressure drop: $V_g = 64$ [m/s]	17
Figure II.3: Pressure drop for different static pressures given at water inlet.....	18
Figure II.4: Pressure at throat for different gas mass flow rates.....	18
Figure II.5: Comparison of experimental and simulation results of dust removal efficiency	19
Figure II.6: Numerical pressure drop results for water mass flow rate of 0.013 kg/s	20
Figure II.7: Pressure drop results for water mass flow rate of 0.038 kg/s	20
Figure II.8: Centerline pressure for different cases	21
Figure II.9: The velocity contours of square tube and circular tube.....	22
Figure II.10: The effect of throat gas velocity on the pressure drop	23
Figure II.11: Particulate collection efficiency at specific gas and liquid mass flow rates.....	23
Figure II.12: Structure of self-priming venturi scrubber	24
Figure II.13: Comparison of simulation and experimental removal efficiency of iodine	25
Figure III.1: Geometry description of venturi scrubber	27
Figure III 2: Grid sensitivity study	35
Figure III 3: Mesh study for: (a) Single phase(gas) , (b) Two phases(gas-water).....	36
Figure IV.1: Validation using CFD code	38
Figure IV.2: Evolution of velocity in venturi scrubber with mass flow rate equals 0.06 kg/s and different gas velocities.....	39
Figure IV.3: Velocity profiles for different mass flow rate at the middle of the venturi with gas velocity of 15 (m/s).....	40
Figure IV.4: Velocity profiles for different mass flow rate at the middle of the venturi with gas velocity of 20 (m/s).....	40

Figure IV.5: Velocity profiles for different mass flow rate at the middle of the venturi with gas velocity of 25 (m/s).....	41
Figure IV.6: Velocity profiles for different mass flow rate at the middle of the venturi with gas velocity of 30 (m/s).....	41
Figure IV.7: Contours of velocity magnitude	43
Figure IV.8: Contours of static pressure.	46
Figure IV. 9: The comparison of static pressure values for different gas velocities	47
Figure IV.10: The comparison of dynamic pressure values for different gas velocities.	48
Figure IV.11: Contours of dynamic pressure	50
Figure IV.12: Effect of inlet gas velocity on pressure drop.....	51
Figure IV.13: Effect of inlet water mass flow rate on pressure drop.....	51
Figure IV.14: Contours of turbulent kinetic energy in the throat near the wall	52
Figure IV. 15: The evolution of turbulent kinetic energy in the axial position	53
Figure IV.16: Contours of turbulent dissipation rate in the throat near the wall	54
Figure IV.17: The evolution of turbulent dissipation rate in the axial position.....	55
Figure IV.18: Evolution of turbulent viscosity in different sections of the venturi with gas velocity of 15 m / s for different water mass flow rates.....	56
Figure IV.19: Evolution of turbulent viscosity in different sections of the venturi with gas velocity of 20 m / s for different water mass flow rates.....	57
Figure IV.20: Evolution of turbulent viscosity in different sections of the venturi with gas velocity of 25 m / s for different water mass flow rates.....	58
Figure IV.21: Evolution of turbulent viscosity in different sections of the venturi with gas velocity of 30 m / s for different water mass flow rates.....	59
Figure V.1: Contours of temperature	63
Figure V.2: Temperature profiles in the axial position with different gas velocities for different water mass flow rates.	64
Figure V.3: The evolution of the local Nusselt number on the length of venturi with gas velocity of 15 m/s.....	65
Figure V.4: The evolution of the local Nusselt number on the length of venturi with gas velocity of 20 m/s.....	66

Figure V.5: The evolution of the local Nusselt number on the length of venturi with gas velocity of 25 m/s.....	67
Figure V.6: The evolution of the local Nusselt number on the length of venturi with gas velocity of 30 m/s.....	68
Figure V.7: Contours of the gas mass faction	70
Figure V.8: Mass fraction evolution of gas at along the venturi scrubber axis.	71
Figure V.9: Mass fraction of gas at X-position in the venturi throat	72
Figure V.10: Contours of water mass faction	74
Figure V.11: Mass fraction evolution of water at along the venturi scrubber axis.	75
Figure V.12: Mass fraction of water at X-position in venturi throat	76
Figure V.13: The probability density functions of water mass fraction... ..	77
Figure V.14: The probability density function of temperature... ..	78
Figure V.15: Removal Efficiency of venturi system at different fluid flow rates.	79
Figure V.16: Effect the temperature on the Removal Efficiency.....	80
Figure V.17: Removal Efficiency of venturi system at different fluid flow rates.	80

LIST OF TABLES

Table III. 1: Physical characteristics of the venturi scrubber	28
Table III. 2: Properties of gas generated from biomass.....	33
Table III. 3: Properties of water liquid	34

Chapter I:

General Introduction

Gas cleaning is an important process in many industrial applications. Due to the role, it plays in protecting the environment from fine particles and toxic gases as well as for protecting equipment that operates by industrial gases. One of the most important devices used in gas cleaning is the venturi scrubber. It is a simple design and easy to maintain a device that relies on atomizing the liquid into droplets in the throat due to the high velocity of the gas. These drops work to encapsulate the particles and thus clean the gases.

The venturi scrubber is used in a Vented Filter Containment System in a nuclear power plant to remove gaseous pollutants in the event of a serious accident [1]. Venturi scrubber is also used in the cleaning of exhaust gases resulting from the combustion of fuels such as fuel oil, natural gas, biofuels, and coal in factories and engines from chemical pollutants SO_x , NO_x , and particulate matter[2]. Venturi scrubber can also be used in the cleaning of gases resulting from the gasification of biomass. The gas produced from this process contains hydrogen, carbon monoxide, a large amount of methane, carbon dioxide, steam, and nitrogen, as well as some pollutants such as tar and unwanted particles[3] that cause damage to the equipment that is powered by the gas gasification.

I.1 Venturi scrubber

Venturi scrubbers are highly efficient in removing particulates, tars, metallic fumes, and acidic gas from gases stream. They are simple devices consisting of three main sections, the convergence section, the throat section, and the diffuser section. It also contains orifices for the liquid introduction, as shown in Figure I.1.

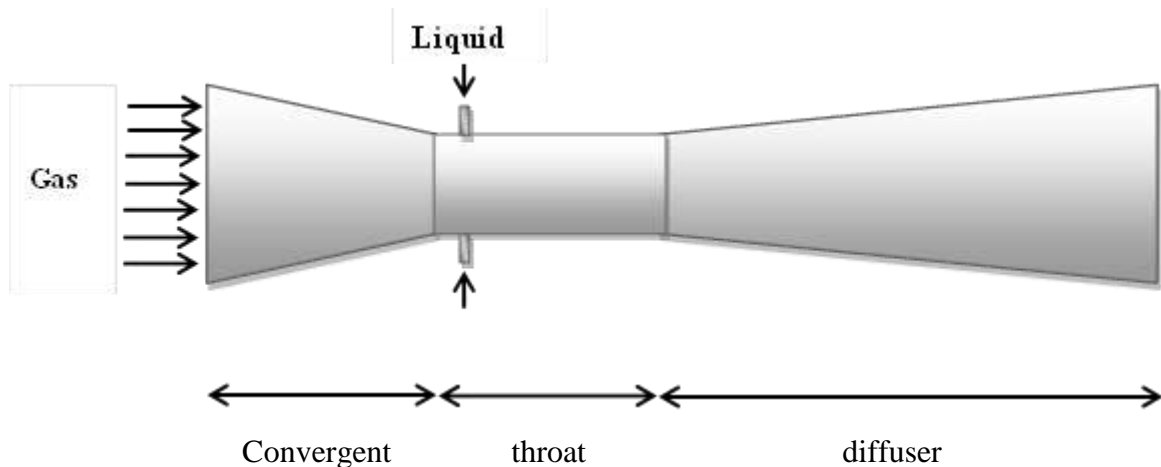


Figure I.1: Venturi scrubber description.

Venturi uses the high energy produced by accelerating the gas in the convergence section to break up the liquid into droplets in the throat. These droplets are responsible for cleaning the gas as they encapsulate and trap the particles.

I.2 Types of venturi scrubber

Venturi devices divide into several types according to the place of the liquid is entered, operating modes and pressure loss across the unit:

- According to the place of the liquid is entered, the venturi scrubber divides into two types[4]:
 - **Pease-Anthony:** In a venturi of this type, the liquid is introduced through orifices in the throat.
 - **Wetted approach:** The liquid is introduced as a film on the walls before the convergent. Most of the liquid is atomized at the throat by the shearing action of the gas flow. This type was chosen to be studied in this work.
- According to the operating modes, The venturi scrubber divides into three types as shown in Figure I.2 [5][6]:
 - **Forced feed mode:** A pump introduces liquid into the venturi scrubber, and a regulating valve allows the liquid flow rate to be adjusted independently of the gas flow. This mode was used in this study.

- **Self-priming mode:** In this mode, the operation is based on the reduced static pressure of the gas flowing into the venturi caused by the acceleration of the gas in the convergent section, the liquid supply through a surrounding water tank.
- **Submerged mode:** in this mode, the operation is based on the scrubbing liquid being passively driven into the throat by the radial pressure difference across the throat orifices.

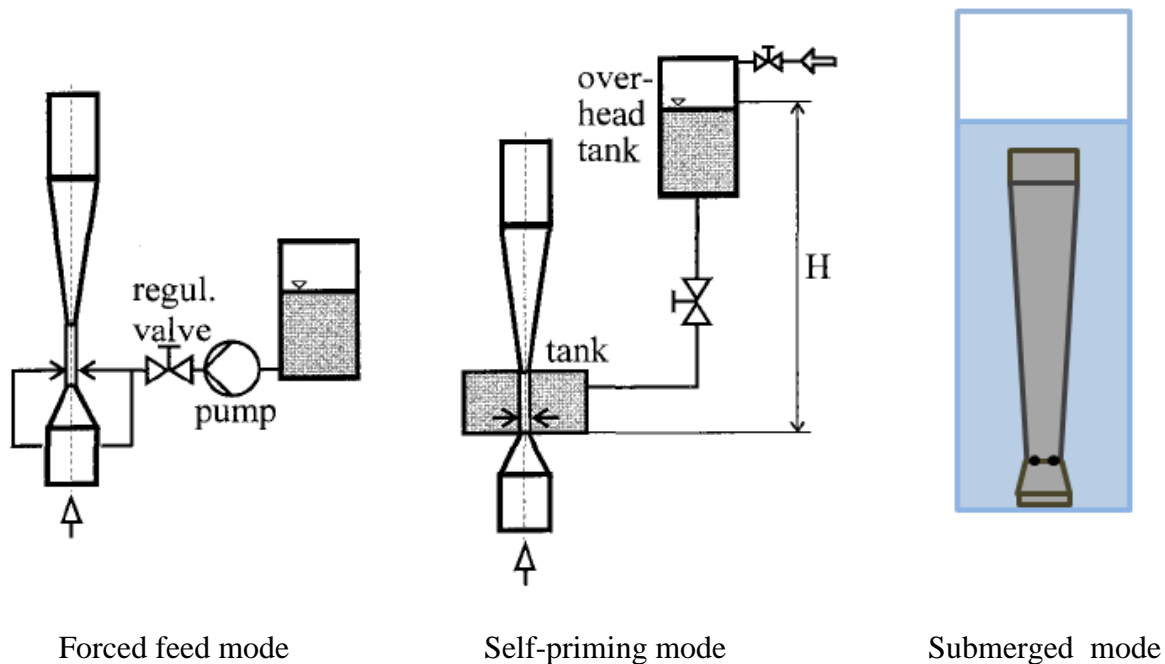


Figure I.2: Operating modes of venturi scrubbers [5][6].

- According pressure loss across the unit, The venturi scrubber divides into three types[7]:
 - **Low-energy venturi scrubbers** (pressure drops up to 2:42 KPa).
 - **Medium-energy venturi scrubbers** (pressure drops from 2.42 to 4:9 KPa).
 - **High -energy venturi scrubbers** (above 4:9 KPa).
- There is another type of venturi called ejector-venturi as shown in Figure I.3. In this type, liquid enter through axial nozzles using mechanical sprays[7].

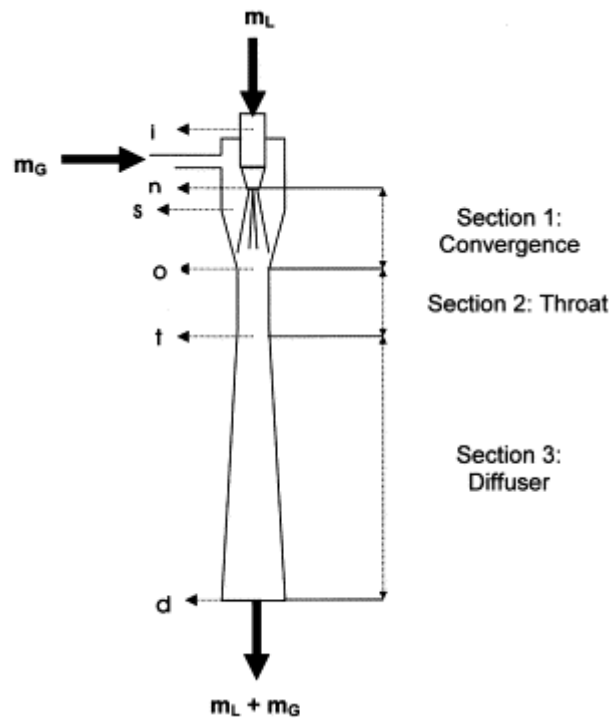


Figure I.3: Geometry of ejector-venturi [8].

I.3 Advantages and disadvantages of venturi scrubber[9-10]

A. Advantages

- ❖ Simple in design and easy to install relatively low maintenance.
- ❖ High collection efficiency.
- ❖ Cleaning with a lower risk of gas laden with flammable and explosive dust.
- ❖ The cleaning of gas laden with fine particles.
- ❖ Cleaning of gaseous pollutants.

B. Disadvantages

- ❖ Environmental pollution.
- ❖ A problem of collecting liquid waste.
- ❖ Corrosion of the dust collector.

I.4 Objectives of the Research

Much research has been done on venturi scrubber, most of which focus on hydrodynamic mechanisms and the effect of geometry on the collection efficiency of venturi. Most of the studies have studied the efficiency of venturi in removing particles and toxic gases from the air and did not give much importance to studying the cleaning of other gases in venturi, as well as to studying the phenomenon of heat and mass transfer in venturi scrubber.

The subject of this thesis is focused on to the study of the cleaning of the gas generated by biomass and the processes of thermal and mass transfer in venturi scrubber, where the conversion of potential energy into kinetic energy while passing through the convergence section atomizing of the liquid into droplets and the formation of a film on the walls of the venturi, which traps the pollutants present in the gas flow. Heat transfer occurs at the walls of the venturi scrubber because they are areas of heat exchange with the surrounding environment.

The main objective of this work is to study the performance of venturi in the cleaning of gases resulting from biomass gasification. And a study of forced convection, mass transfer phenomenon in venturi scrubber also the hydrodynamic mechanisms that occur in venturi.

I.5 Thesis Plan

This thesis has been divided into four chapters:

- The first chapter is a general introduction.
- The second chapter is a bibliographical study of the previous works on venturi scrubbers, they have been distributed into three sections; experimental works, mathematical models, and numerical simulations.
- The third chapter includes the physical model of this study, the properties of the fluids used, the mathematical models, the solution methodology, and sensitivity mesh tests.
- The fourth chapter contains the CFD code validation and the results of the hydrodynamic behavior of the flow within the venturi scrubber.
- The results of heat and mass transfer in venturi were represented in the fifth chapter.
- Finally general conclusion.

Chapter II:

Literature Review

II.1 Introduction

This chapter represented previous work carried out by other authors on venturi scrubbers related to pressure drop, collection efficiency, venturi scrubber dimensions, and operating conditions. We classified previous works into the following topics: experimental studies, theoretical studies, and numerical studies using CFD code.

II.2 Experimental studies

T. J. Overcamp and S. R. Bowen (1983) [11] provided experimental measurements of the total pressure loss and pressure recovery in a diffuser on a laboratory scale a venturi with throat and diffusers variable to study the effect of throat length and diffuser angles on pressure loss. The tests were carried out with different throat lengths between 1 and 53.7 cm and a cross-section of 4 cm × 1.5 cm three diffusers with angles 5, 10, 19 degrees and lengths 48, 24, and 12 cm. With gas velocities soaring at gas velocities 35, 45, 55, and 65 m/s and liquid-to-gas ratios of 0, 0.5, 1, 1.5, and 2 l/m³. The results showed that venturi with a wide diffuser angle gave better pressure recovery.

To study the effects of changing liquid-to-gas ratios and gas velocity on fluid and membrane flow measurements in a venturi scrubber. **S. Vlswanathan and Alex W. Gnyp (1984)** [12] took flow rate measurements at a pilot plant scale venturi scrubber of Pease-Anthony of throat gas velocities are 150, 200, 250 watts and different water mass flow.

S. Vlswanathan and Alex W. Gnyp (1985) [13] validated the annular flow model by taking measurements of pressure gradients, film flow rates, and liquid-to-gas ratios for throat velocities between 45.7 and 76.2 m/s and liquid-to-gas ratios between 4.0×10^{-4} and 1.9×10^{-3} m³ liquid/m³ air. The experiments have used a venturi scrubber of a pilot-plant-scale venturi made of glass sheets. The results were compared with three models to predict pressure drop (Hesketh correlation, modified Calvert model, and Poole model).

To develop data on the performance of venturi with operating conditions on a large scale, **S. N. Rudnlck et al (1986)** [14] measured the particle collection efficiencies of venturi scrubbers with annular diameters of 3.2, 5.4 and 7.6 cm with four kinds of injection of liquid, throat gas velocities between 21 to 160 m/s, and liquid-to-gas ratios volume between 0.00019 to 0.0043. He compared the results with widely used theoretical models.

To examine the effect of venturi geometry and fluid distribution, **H. Haller, E. Muschelknautz, and T. Schultz (1989)** [15] achieved an experimental work using a venturi with a diameter of 70 mm with different fluid loads between 1 and 2 (l/m^3), Where have taken the results of measurements of pressure, fluid distribution, and collection efficiency The results showed that the venturi, which gives a uniform distribution of the liquid through the injection orifices, that the assembly process is along with the first 20 mm downstream from the injection level, and that shortening the venturi throat gives less energy consumption.

B. J. Azzopardi (1992) [16] studied the importance of boundary layer separation in the diffuser through experimental work on three venturi devices. The difference between them is in the diffuser angle only. He concluded that the separation of the boundary layer leads to a loss of pressure recovery as well as the use of a smaller divergence angle leads to a significant decrease in the pressure drop.

R. W. K. Allen and A. Van Santen (1996) [17] carried out experimental work on two venture devices, one with a short throat and the other with a long throat, with a wide range of operating conditions. To investigate the effect of gas flow rate and throat velocity, liquid flow rate and liquid-to-gas ratio, venturi geometry, and axial and radial position along with the venturi on dry and wet pressure. This work concluded that long-throat venturi devices do not offer any advantages in the collection efficiency and operation cost.

S. Viswanathan (1998) [18] carried out experimental work to examine the properties of the liquid film and its effect on the prediction of pressure drop using a venturi device with 9 orifices with diameters of 2.108, 2.565, 3.175, and 3.860 mm and throat gas velocities between 45.7 and 76.2 m/s. Been measured the film flow, thickness film, pressure drop, throat gas velocity, and fluid loading. He found the calculated film velocities increase with increasing throat gas velocity and liquid loading and decrease continuously along the axial direction.

D. Fernandez Alonso et al (1999) [19] realized experimental work on two venturi scrubbers with different throat lengths and throat gas velocities of 53 –73 $m s^{-1}$ and liquid to gas ratios in the range of 0.75 –2 $l m^3$, which measured the film flow rates at the end of the throat and the end of the diffuser. The results show that a significant fraction of the liquid remains as a film.

X. Gamisansa et al (2002) [7] experimentally studied the effect of throat diameter, length, and spray angle on the performance of the venturi scrubbers and investigated the suitability of the available models to predict pressure drop for venturi. It was concluded that the higher pressure drop increases with increasing atomization angle and that the effect of throat length on pressure is small.

To understand the effect of the pressure drop, the liquid-to-gas ratio, and the amount of S_iH_4 gas on Submicron particle removal efficiency. **C. J. Tsai et al (2005)** [20] designed and tested a venturi scrubber system that uses fine-water mist to reduce the temperature of the exhaust gas and allow the particles below micronized growth to micron size. The most significant results they concluded are that the maximum removal efficiency obtained for particles with a diameter of 478 nm is much greater than that of a traditional scrubber. The effect of the liquid-to-gas ratios and amount of S_iH_4 gas on the removal efficiency is not significant. The removal efficiency of a traditional scrubber is less than 30% in this study.

M. A. Martins Costa et al (2005) [21] conducted experimental work to study the efficiency of fine powder collection using a rectangular venturi. This study includes three variables: the velocity of the throat between 58 m/s and 75 m/s, the rate of fluid flow between 280 ml/min and 900 ml/min, and the length of the throat and throat length (63, 90, and 117 mm). The liquid injects through one orifice in the throat. They have used rock minerals dust, insoluble in water, with an average diameter of 5.8 μm and a density of 3030 kg/m^3 . They concluded that collection efficiency increases with an increase in the throat velocity and the increase in the use of the liquid to a certain extent.

To improve the efficiency of the submicron particle control, **C. Huang, C. Tsai, and Y. Wang (2007)** [22] presented an experimental study based on mixing saturated vapor at 100°C with a waste stream natural temperature before a venturi device to increase particle size from Submicron to the micron. The effect of liquid-to-gas ratio and gas flow rate on the efficiency of fine particle control was investigated using a venturi with a 1 cm diameter and 3 cm long throat. The liquid is injected transversely at the entrance to the throat. Flow rates of 200, 250, and 300 l/min were used, liquid-to-gas ratios were 1.5, 2.0, and 2.5 l/m^3 , and gas velocities were from 42.4 to 63.7 m/s at the throat. They have found that the particulate control efficiency of the venturi scrubber used in this work is much greater than traditional venturi scrubbing while the

pressure drop is much lower. The addition of saturated steam is effective in enhancing the efficiency of submicron particle control.

To study the effect of gas velocity and liquid flow rate and the type of liquid injection (film or spray), **A.M. Silva et al (2009)** [23] took measurements of the pressure drop in a venturi device with an inlet diameter of 250 mm, throat diameter of 122.5 mm with gas flow rates from 0.4835 to 0.987 kg/s, and liquid flows from 0.013 to 0.075 kg/s. The results obtained in this work showed that the pressure drop depends on the gas flow rates and liquid flow rates also the type of injection fluid.

I. G. O. S. Wendsida et al (2012) [24] studied the effects of hydrodynamics thermal and mass transfer phenomena on collection efficiency through experimental work on wet approach venturi with different operating conditions. The most prominent results included in this work are that the majority of evaporation of the liquid occurs in the throat. Condensation of film evaporation leads to better collection efficiency. The collection efficiency increases with the increase in the liquid flow rate and the increase in the gas velocity.

V. G. Guerra (2012) [25] has experimentally studied the distribution of fluid in venturi's throat and the effect of the number of fluid injection orifices using optical imaging techniques. Experimental tests were achieved using a venturi made of a rectangular cross-section of 0.040 m x 0.027 m, having orifices in the throat of 0.001 m in diameter with different numbers of orifices from one to three. The operating conditions are throat gas velocities of 59, 64, 69, and 74 m/s and the fluid flow rate from 2×10^{-6} to 3×10^{-5} m³/s. The results showed that the number of orifices affects the fluid distribution and does not affect the pressure drop.

A. Majid et al (2013) [26] focused on the efficiency of collecting dust particles in venturi scrubber devices through experimental work. Titanium dioxide particles were used throat gas velocities between 130 and 200 m/s, and the liquid flow between 0.3 and 1 g/m³. The hydrophobic titanium dioxide (TiO₂) uses as dust particles with a density of 4.23 g/cm³ and an average diameter of 1 with a dust concentration ranging between 0.1 and 1 g/m³. He has concluded that the efficiency increases with increasing throat velocity and fluid flow rate. The maximum dust particle removal efficiency in the venturi is 99.5% with a gas velocity is 200 m/s at the throat.

R. Desai and O. P. Sahu (2014) [27] used a venturi scrubber to reduce air pollution in the pesticide industry. His work has used a gas flow of $15\text{m}^3/\text{s}$ and a temperature of 80°C and was used different cleaning liquids (caustic soda, potash, water, and lime) with a flow of $0.014\text{m}^3/\text{s}$ and a temperature of 30°C . His results showed that the removal efficiency was 99.1%.

Y. Zhou et al (2015) [28] research, the performance of venturi was examined in collecting barium sulfate and titanium dioxide particles with a size of less than 0.5 mm used as aerosols. The results of this work indicated that the effect of velocity increases with a decrease in the injection flow rate. The removal efficiency is excellent with a long-throat venturi or small diffuser angle, the removal efficiency is 99 % at a gas velocity of 200 m/s and an appropriate injection rate. The length of the throat and the smaller angles of the diffuser have little effect on the pressure drop.

To study the effect of a venturi scrubber on improving the efficiency of tar removal from gas produced by biomass gasification, **S. Unyaphan et al (2017)** [29] achieved experimental work using a venturi scrubber and regeneration absorbent. Two liters of canola oil were used in the venturi scrubber as a cleaning fluid for 10 hours. The results showed that: tar removal efficiency was 98% in the first use of oil, and the tar removal efficiency was higher than 90% for the refined oil.

To investigate the efficiency of removing dust particles in venturi gas scrubbers, **S. Ali et al (2020)** [30] conducted experimental work. Alumina particles (Al_2O_3) use treated as aerosols as dust particles with a density of 3950 kg/m^3 and a diameter of 0.4 mm. Gas flow rates were between 3 and $6\text{ m}^3/\text{h}$, flow rates The liquid is between 0.009 and $0.025\text{ m}^3/\text{h}$. The results represent that the efficiency of the removals is affected by the throat velocity and the head liquid head, the efficiency increases with their increase, especially the velocity of the throat, the maximum removal efficiency was 87.5% in the case of an airflow rate of $6\text{ m}^3/\text{h}$ and a fluid head of 3 feet.

II.3 Theoretical studies

In **Calvert's (1970)** [31] model for predicting pressure drop and collection efficiency in venturi devices, it is considering that the velocity gas was constant and that the pressure drop was due to loss of acceleration due to friction with fixed surfaces. And the efficiency is calculated through the inertial correlation of Walton and Woolcock's experimental work.

R. A. Pulley (1970) [4] extended Azoubardi 's model of venturi particle collection to include predictions of particle collection in venturi and to verify their validity compare them with experimental data for pressure drop and feature collection in venturi devices with either a wetted approach or liquid injection at the throat. The results showed that this model gave better predictions than previous models.

R. H. Boll (1973) [32] proposed a mathematical model containing differential equations for momentum change, drop motion, and particle impaction on droplets. This model was applied to all venturi parts to predict particle collection and pressure drop. Boll also focused on the effect of particle size, venturi geometry, and operating conditions.

Based on Boll's model with a difference in the law used to define the drag coefficient for droplets. **K. G. T. Hollands and K. C. Goel (1975)** [33] presented a study that presented general solutions of drop pressure and the dimensionless liquid velocities in the style of graphs and closed-form equations that aid in estimating the pressure drop inside the venturi devices when designed.

Also, based on Boll's model, **K. C. Advance et al (1977)** [34] paper extended Hollands' s study to include general solutions of differential equations for the collection efficiency in venturi devices. This work presented graphs to estimate the total collection efficiency on the basis that the particle collection efficiency is related to pressure loss. The results of the predictions were verified with data from Calvert et al.

Through modification of differential equation to predict the performance of a scrubber for the Claver model, **S. C. Yung (1978) et all** [35] presented a new model for the efficiency of particle collection in venturi devices, assuming that the particles collected in the throat with atomized liquid. This paper also gave the relationship of the maximum length of the throat with the assembly efficiency and pressure drop, as it has shown that the collection efficiency has

increased slightly with the length of the throat, so the length of the throat is not increased except when necessary because this leads to a decrease in pressure.

T. D. Placek and L. K. Peters 's (1982) [36] paper presented a theoretical model to determine the particle collection efficiency of the venturi scrubber. It takes into account the heat and mass transfer. It was concluded that increasing the temperature of the gas leads to an increase in its density and thus to a decrease in the velocity of the gas in the throat, which affects the efficiency of collection. Also, the temperature of the liquid affects the efficiency of the collection as the cold liquid enhances the efficiency of collection due to the condensation process.

To improve venturi's performance, **D. W. Cooper and D. Leith (1984)** [37] studied the effect of used fluid and energy, as well as venturi geometry, through developing a model in which actual values of the drag coefficient and venturi geometry are using. The results of this model show that the geometry of the scrubber affects the efficiency of liquid use and the efficiency of energy use. The operating conditions suitable for obtaining the optimum venturi performance change with the throat velocity, particle diameter and the geometry of the scrubber.

An annular flow pressure drop model was developed by **S. Viswanathan and A. W. Gnyp (1985)** [13] to predict the pressure drop in the venturi scrubbers and flow losses by calculating the effects of friction and acceleration of liquid droplets and films flowing on the walls and recovery in the diffuser. This model takes into account the liquid to gas ratio, throat gas velocity, venturi geometry, and liquid film flow rate.

Through the momentum integration equation, **T. R Azzopardi (1991)** [38] developed a model containing the boundary layer growth in the diffuser of the venturi devices to predict the pressure drop in the diffuser section.

N. V. A. and S. Viswanathan (1998) [39] tested a model bi-dimensional simplified depending on the experimental data for prediction of to predict liquid flux distribution and collection efficiency in a venturi scrubber, the effect of throat gas velocity, liquid to gas ratio, aspect ratio, and nozzle diameter. The results showed that increasing the gas velocity enhances the consistency of the flow distribution and increases the collection efficiencies, the flow distribution becomes non uniform, and the collection efficiency decreases if the ratio of liquid to gas increases or decreases from the optimum value.

J. A. S. Gonçalves et al (2001) [40] evaluated the models available to predict pressure drop in venturi by comparing the mathematical equations for these models with experimental data. He concluded that: These models have to be taken into account the venturi geometry and the fraction of liquid. Empirical correlations are not valid for all operating conditions.

H. Sun and B. J. Azzopardi (2003) [41] extended the boundary layer model in the diffuser section to include a description of the boundary layer in the three venturi sections to predict the pressure loss for cylindrical venturis type Pearce–Anthony at high pressure. This model showed the importance of including the boundary layer phenomenon and its effect on the prediction of pressure drop in venturi devices. Also, it gave good predictions under high-pressure conditions.

S. Viswanathan et al (2005) [42] proposed an improved algorithm based on a prediction of minimum pressure drop prediction to improve venturi performance. It takes into account the design and operating parameters (liquid to gas ratio, throat gas velocity, number of nozzles, nozzle diameter, and throat aspect ratio). This algorithm is applied cylindrical and rectangular venturi devices of the type of Pease-Anthony. The algorithm data were compared with the experimental data for validation. The optimization algorithm provided an efficient and effective method for optimizing scrubbers.

To investigate the effects of heat and mass transfer on venturi and its removal efficiency, **A. Rahimi, M. Taheri, and J. Fathikakajahi (2005)** [43] developed a mathematical model composed of differential equations for energy, momentum, and material exchange in an isothermal venturi. The results indicate that the temperature difference of the liquid and gas affects the collection efficiency.

S. Nasseh et al (2006) [44] relied on the artificial neural networks approach to predict the pressure drop in the venturi. He applied the design of three independent artificial neural networks using three data sets of five different venturi scrubbers each network has three layers and follows the forward propagation back-forward algorithm to train the input data. The input vectors for the first mesh are the gas velocity of the venturi scrubber throat , the ratio of the liquid-to-gas flow rate, and the axial distance of the venturi scrubber the second grid evaluating the input dry pressure drop is the velocity of the gas in the scrubber's throat and the axial distance of the venturi scrubber relative to the third grid the input throat diameter, and the liquid flow rate, throat gas velocity, an axial distance of a venturi scrubber.

The results indicated that a neural network approach is a powerful tool for well-predicting pressure drop in the venturi scrubber.

A. A. Economopoulou and R. M. Harrison (2007) [45] worked on the development of graphical tools to estimate the overall collection efficiency of venturi scrubber devices under the defined operating conditions. To aid environmental engineers in conducting appropriate reports of venturi performance and alternative designs assessments.

Artificial neural networks design was also used by **M. Taheri et al (2007)** [46], based on a genetic algorithm, where he used experimental data to create these artificial neural networks to predict the collection efficiency of venturi scrubber. Three networks were designed to study the efficiency of particle collection in venturi, and one network to study the collection efficiency of CO₂. The inputs to these neural networks are the ratio of the liquid to gas flow rate ratio, pressure drop across the venturi scrubber, gas throat velocity, liquid nozzle diameter, and the angle of the divergent section, the output of these neural networks is the collection efficiency as an output. Comparing the results of the improved genetic algorithm-artificial neural networks with the results of the artificial neural networks shows that the improved neural network is more efficient, as well as determines the effect of the ratio of liquid-to-gas flow rate, throat gas velocity, and particle diameter on the collection efficiency.

A. Kumar et al (2008) [47] have developed a mathematical model to study the drop Reynolds number effect on the collection of small particles less than 3 mm in a venturi scrubber. They concluded that the gas velocity affects the penetration of particles that the effective collection of these particles is at a high throat velocity of up to 80 m/s and above, and that increasing the length of the throat does not significantly affect the efficiency of the collection.

S. Nasseh et al (2008) [48] used the improved neural networks to estimate the collection efficiency and predict the pressure drop in venturi devices. Two neural networks trained first to predict wet pressure drop and the second to predict dry pressure drop based on experimental data from seven different venturi scrubbers. The first network inputs are the gas velocity in the throat, the liquid-to-gas flow rate and the distance along with the venturi scrubber, the hydraulic diameter of the throat, and the length of the throat. The second network inputs are the gas velocity in the throat, the hydraulic diameter of the throat, and the

length of the throat. This work concluded that the use of neural networks gave good and reliable predictions for pressure drop.

A. Rahimi, A. Niksiar, and M. Mobasher (2011) [49] examined the effect of heat and mass transfer on the pressure drop prediction through a descriptive model focusing on mass and energy equations. A correction factor associated with sets of empirical data has also been added to improve predictions in the divergent section. The results showed that the phenomenon of heat and mass transfer reduces the pressure drop (see Figure II.1).

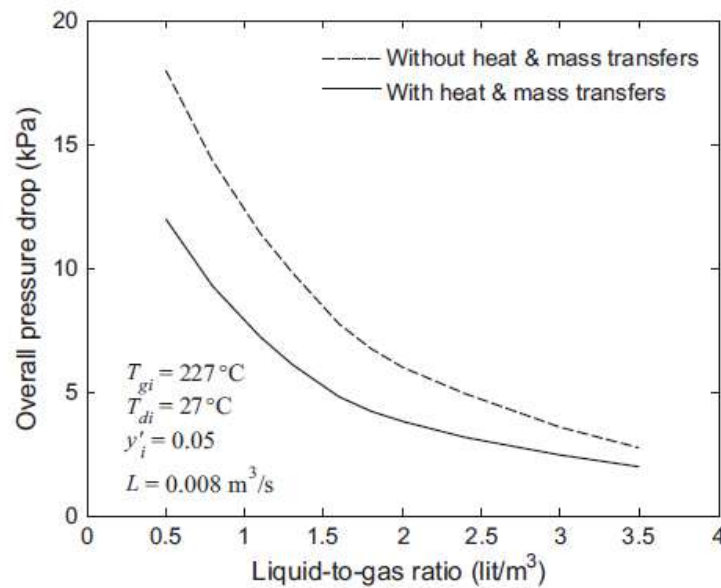


Figure II.1: Effect of liquid-to-gas flow rate on the overall pressure drop [49].

A. A. Shraiber et al (2015) [50] developed a three-phase mathematical model focused on examining the effect of gas flow turbulence on the efficiency of removal of particles and the collision of particles with droplets.

J. Kim, J. W. Park, and S. Korea (2016) [51] conducted a comparative study on three one-dimensional models in terms of collection efficiency in venturi devices. This comparison was using experimental data and 2D model data with main parameters of particle size, gas velocity, and flow rate. The results showed that the Calvert and Yung models gave relatively better results with pilot scale data compared to the Boll model.

II.4 Numerical studies using CFD

V. G. Guerra et al (2012) [25] performed a three-dimensional simulation of rectangular section venturi devices with one, two, or three orifices in the throat using ANSYS Fluent 12. The multi-phase flow was treated using (VOF), the turbulent has treated using the $k-\epsilon$ model. The results showed that the VOF model was able to give pressure profiles and pressure drops in venturi and that the number of orifices affects the fluid distribution but does not big effect the pressure drop as shown in the experimental results (see Figure II.2).

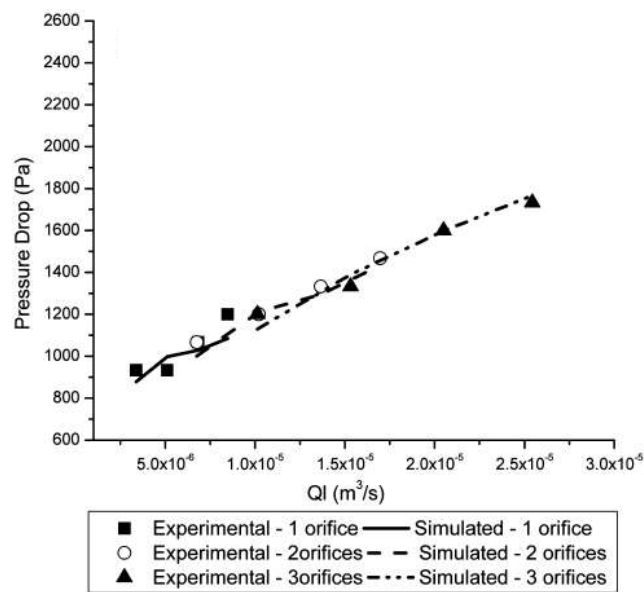


Figure II.2: Effect of the liquid flow rate on the pressure drop: $V_g = 64$ m/s [25].

M. Ali et al (2012) [52- 54] performed a 3D simulation on the venturi scrubber based on Euler's model by CFX and presented their work through three scientific papers. The first paper focused on the prediction of pressure drop in venturi gas scrubbers using ANSYS CFX. In this simulation, Euler-Lagrangian model and the $k-\epsilon$ model have used. The boundary conditions were: the mass flow rate of gas at the inlet, static pressure at the water inlet. The most important results of this paper are that: the pressure drop increases with increasing gas flow rate and static pressure at the water inlet (see Figure II.3).

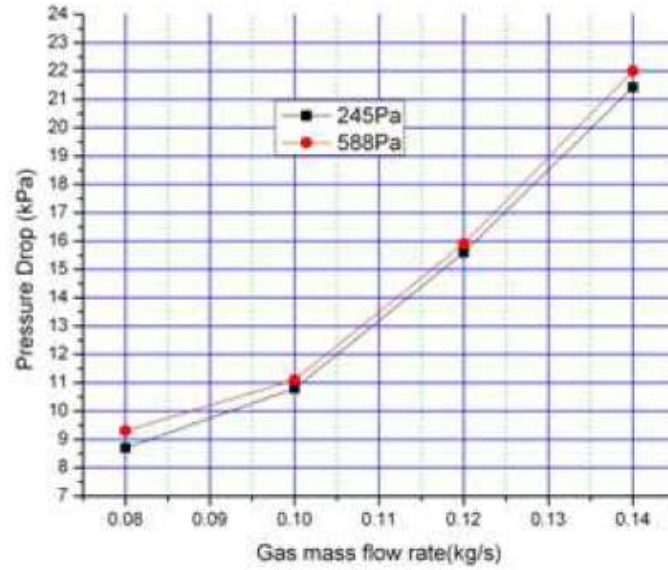


Figure II.3: Pressure drop for different static pressure given at water inlet [52].

The second paper presented the evaluation of pressure in the throat and the study of fluid dynamics in the venturi using the same tool (ANSYS CFX) and the same models used in the previous paper with different conditions at inlet represented by gas mass flows 0.09, 0.12, 0.14 kg/s, and liquid mass flows 0.103, 0.118, 0.131 kg/s. The simulation results gave good agreement with the experimental results of the pressure drop in the venturi's throat (see Figure II.4).

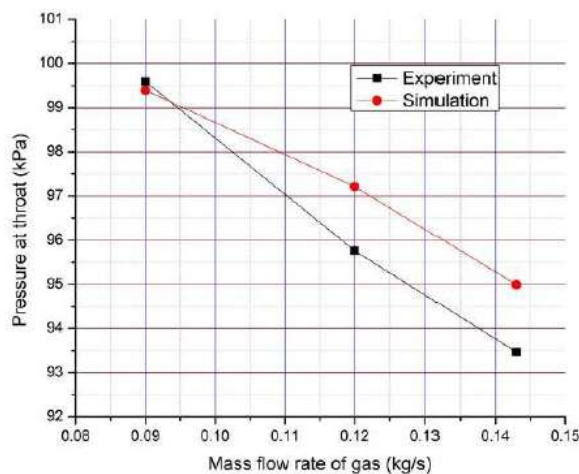


Figure II.4: Pressure at throat for different gas mass flow rate [54].

The third paper includes the examination of dust particles removal efficiency and gas velocity in the throat of the venturi gas scrubber based on ANSYS CFX, the eulerian-Lagrangian method used; the $k-\epsilon$ turbulent flow model, and the cascading dissolution and dissociation model to predict the liquid dissociation in a venturi scrubber, boundary conditions for gas flow rate at 0.09, 0.115, and 0.14 kg/s and liquid flow rate at 0.1 and 0.13 and 0.16 kg/s. The titanium dioxide (TiO_2) is used as dust particles with a diameter of 1 meter, its density of 4.23 g/cm. This paper concluded that: the dust particles removal efficiency increases with the increase in the mass flow rate of gas and the liquid flow rate (see Figure II.5).

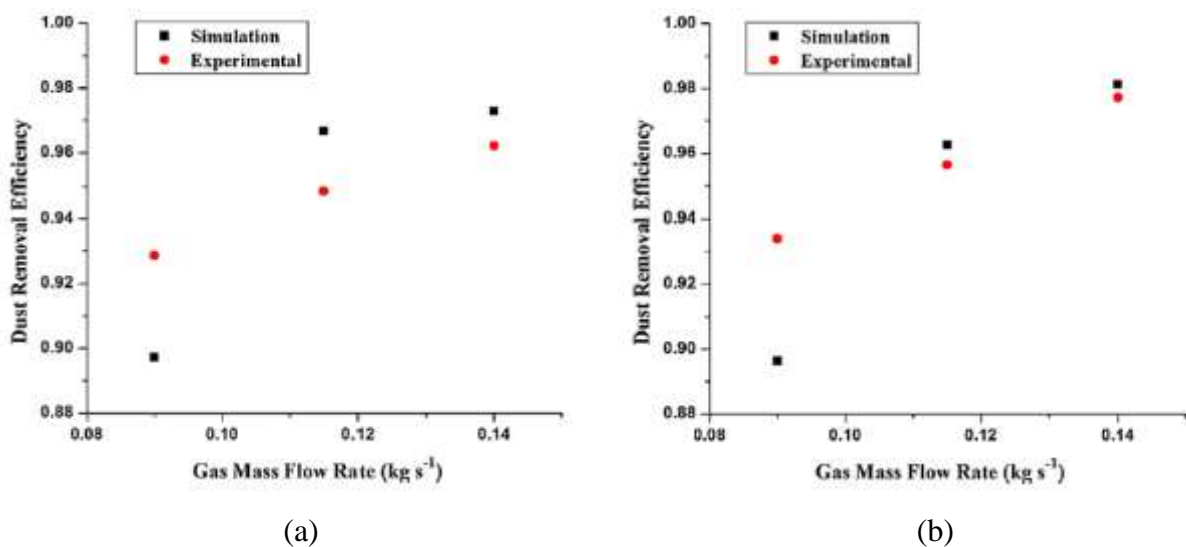


Figure II.5: Comparison of experimental and simulation result of dust removal efficiency:

(a) mass flow rate of liquid 0.13 kg. s⁻¹, (b) mass flow rate of liquid 0.16 kg .s⁻¹ [53].

M. M. Toledo-Melchor et al (2014) [55] performed a 3D simulation of fluid flows on five venturi geometries with inlet and throat diameters of 250 and 122.5 mm. The difference between them is in the angles of convergence and divergence. One simulation performed the two-phase simulation of single venturi geometry with liquid mass flow rates of 0.013 and 0.038 kg/s to study the effect of water flow on pressure drop. The results showed that the pressure drop depends largely on the gas flow rate and that the water flow rate has effects neither on the pressure drop nor on the maximum velocity of the liquid inside the scrubber (see Figures II.6-II.7).

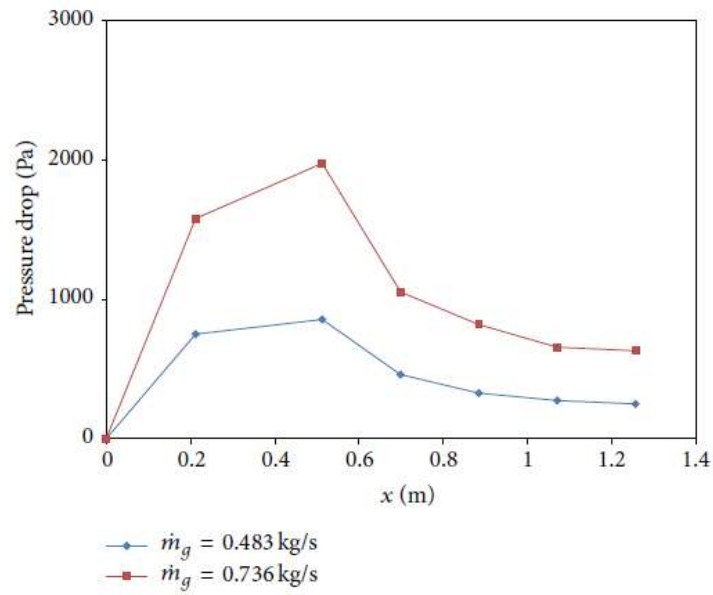


Figure II.6 : Numerical pressure drop results for water mass flow rate of 0.013 kg/s [55].

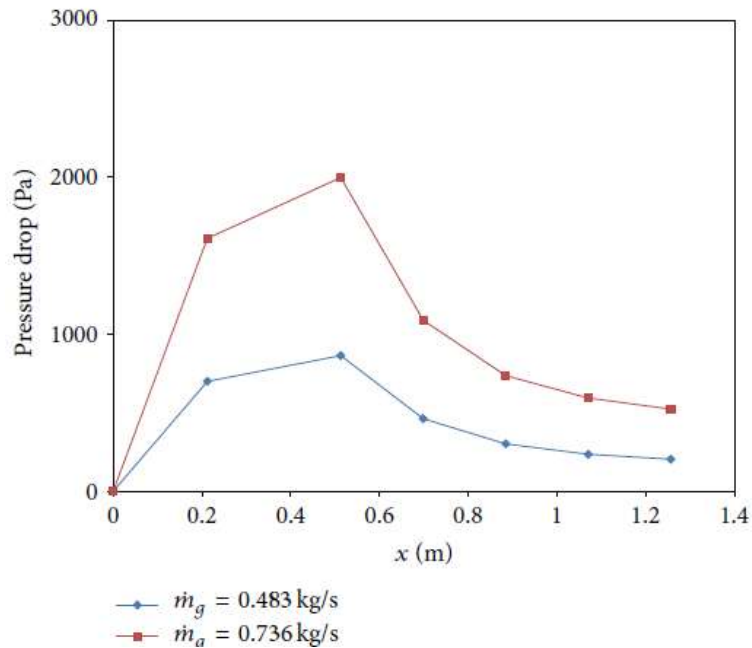


Figure II.7 : Pressure drop results for water mass flow rate of 0.038 kg/s [55].

By designing experiments on the venturi using Taguchi's L16 orthogonal, **S. Kousalya et al (2015)** [56] found that venturi with larger diameters and lower lengths decreases the pressure drop. To predict the velocity at which achieved, he made a three-dimensional simulation of the proposed design using CFD code.

S. A. Qamar et al (2017) [57] studied the effect of the number and position of orifices on the efficiency of dust collection in the venturi region by numerical simulation using ANSYS CFX. These simulations were based on the Eulerian-Lagrangian approach, a Cascade atomization and breakup model used to predict liquid dissociation in a scrubber and a k- ϵ turbulent model. The boundary conditions were gas flow 1 g/s, dust particles (TiO_2) of 1 diameter at the inlet, and liquid flow 6 g/s at the orifices (number the Orifices 2, 4, 6, and 8 orifices placed at the start of the throat). The results showed that placing the slots in a close section leads to maximum efficiency when using 8 Orifices. Using 8 Orifices in a narrow space will narrow the airflow resulting in more velocity and more negative pressure (see Figure II.8).

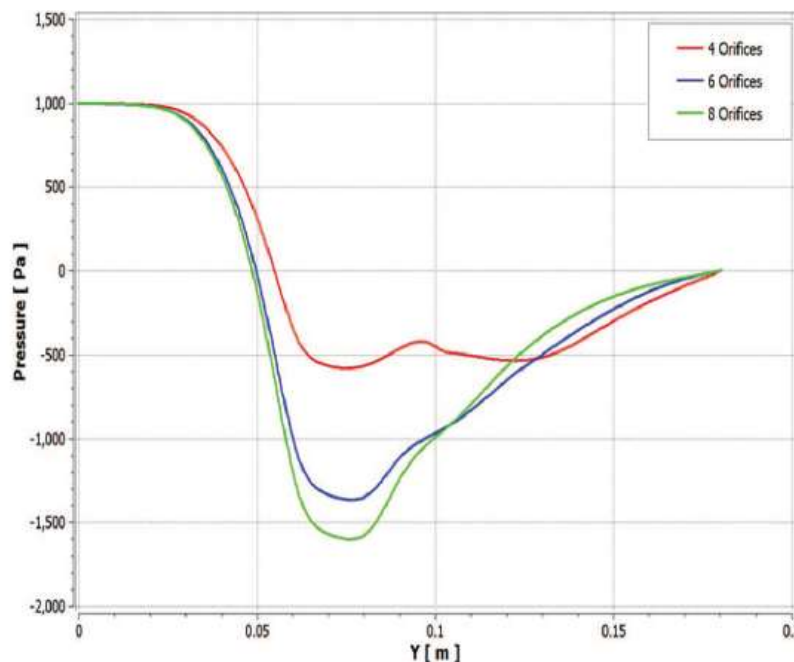


Figure II.8: Centerline pressure for different cases [57].

To improve the efficiency of tar removal from biomass gas, **Z. Luan et al (2017)** [58] performed a numerical simulation of the flow of biomass gas in a square-section venturi device with a diameter of 100 mm inlet and outlet and a diameter of 50 mm in the throat using the ANSYS-FLUENT CFD code. The gas was set as a continuous phase with an inlet velocity of 12 m/s, the outlet as free flow, non-slip wall conditions, and inlet and outlet temperatures 50 and 30 degrees Celsius, respectively. The velocity contours, pressure contours, and turbulent kinetic energy were examined and compared with the results of the

circular section venturi. The results show that the square section tube has advantages such as large pulsation velocity, large pressure loss, large turbulent kinetic energy, and has high tar removal efficiency (see Figure II.9).

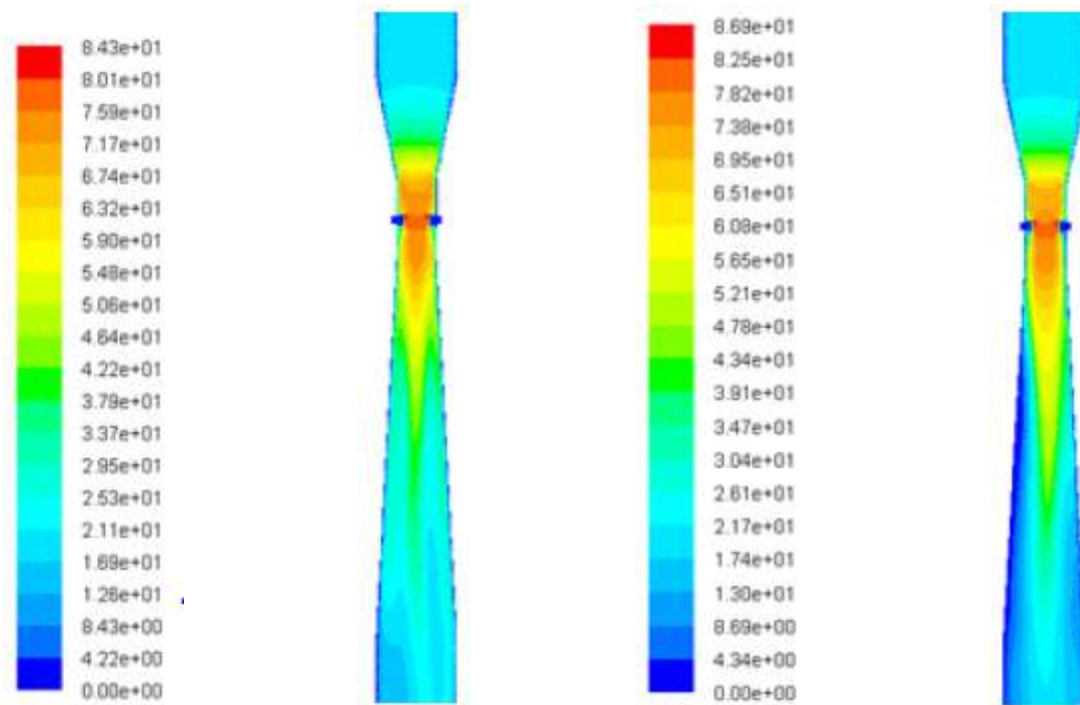


Figure II.9: The velocity contours of square tube and circular tube [58].

M. Bal and B. C. Meikap (2017) [59] performed a three-dimensional simulation of flow fluid in a venturi scrubber by CFD. For studying the effects of throat gas velocity, liquid mass flow rate, and liquid the gas ratio on the pressure drop. This simulation used the k- ϵ turbulence model and the volume of the fluid model. The results showed that the maximum pressure drop of 2064.34 Pa was at throat gas velocity 60 m/s and liquid flow rate 0.033 kg/s, and the lowest pressure drop of 373.51 Pa was at throat gas velocity 24 m/s and liquid flow rate 0.016 kg/s (see Figure II.10).

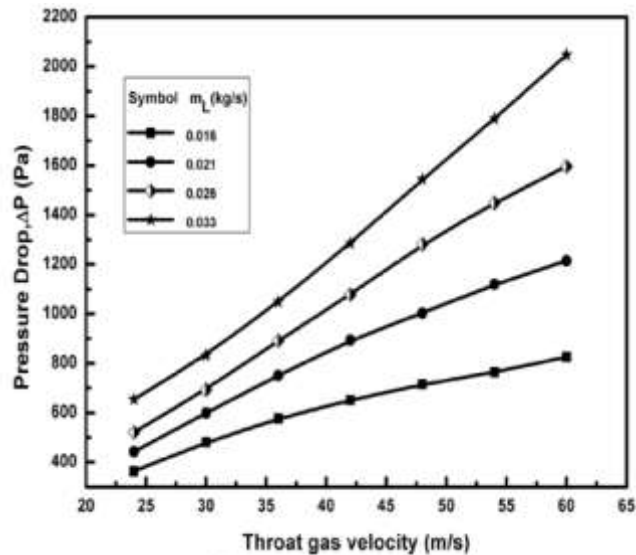


Figure II.10: The effect of throat gas velocity on the pressure drop [59].

To examine the effect of the liquid to the gas ratio on the collection efficiency of The potassium oxide particles in venturi, **I. Safdar et al (2017)** [60] made a 3D simulation using CFX code for different streams of gas and liquid. The results showed that the increase in the particle removal efficiency was due to the increase in the mass flow rate of the gas and the ratio of liquid to gas (see Figure II.11).

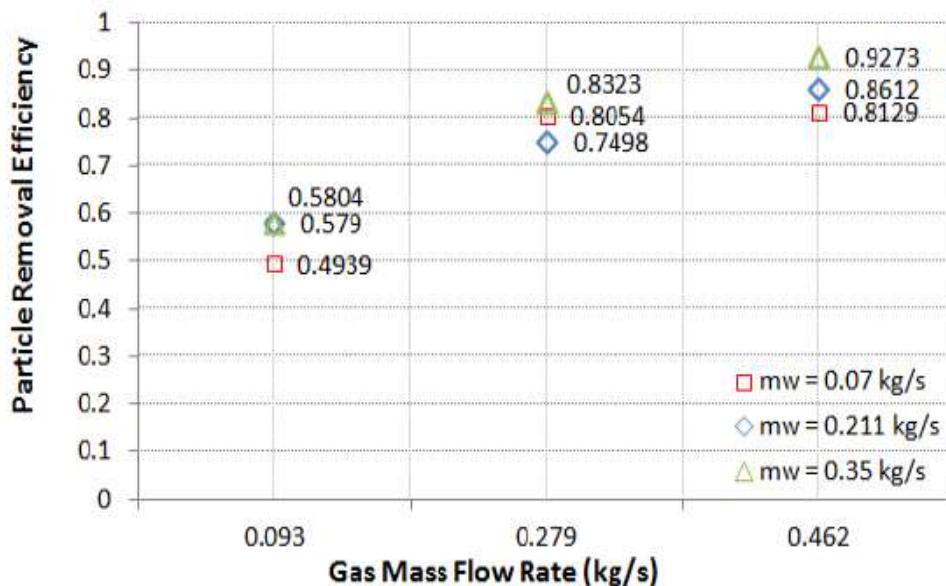


Figure II.11: Particulate collection efficiency at specific gas and liquid mass flow rates [60].

To investigate the effect of ring baffles, thickness, and opening area ratio on fluid flow rate and pressure drop, **S. Yang (2019)** [61] performed a numerical simulation using the CFD code of self-priming venturi device with ring baffle as shown in Fig. In this simulation, the gas velocity ranged between 7.5 and 18.75 m/s. Water is injected into the venturi due to the pressure difference between the throat and the ambient pressure. The results showed that the use of a ring baffle near the throat results in a large pressure loss and a decrease in the injection flow rate. The best placement of the ring baffles about 7/16 of the length of the diffuser above the throat, with a thickness of 5 mm (see Figure II.12).

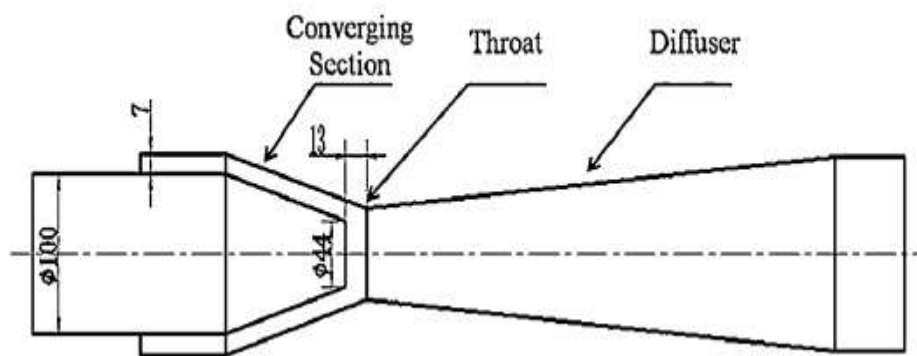


Figure II.12 : Structure of self-priming venturi scrubber [61].

To assess the efficiency of venturi's devices in removing iodine from gases produced by venting a portion of containment air in nuclear plants, **A. Ahmed et al (2020)** [62] performed a three-dimensional numerical simulation of venturi using ANSYS Fluent CFD code. The properties of iodine were introduced into the program, using water as a washing liquid. Eulerian-Eulerian of two-phase flow model used, the $k-\epsilon$ turbulent flow model, UDF was used to model the mass transfer of iodine from gas to liquid. Boundary conditions are the mass flow inlet at the air inlet, the pressure inlet at the openings, and the pressure at the outlet. The results of this simulation were compared to the experimental results (see Figure II.13).

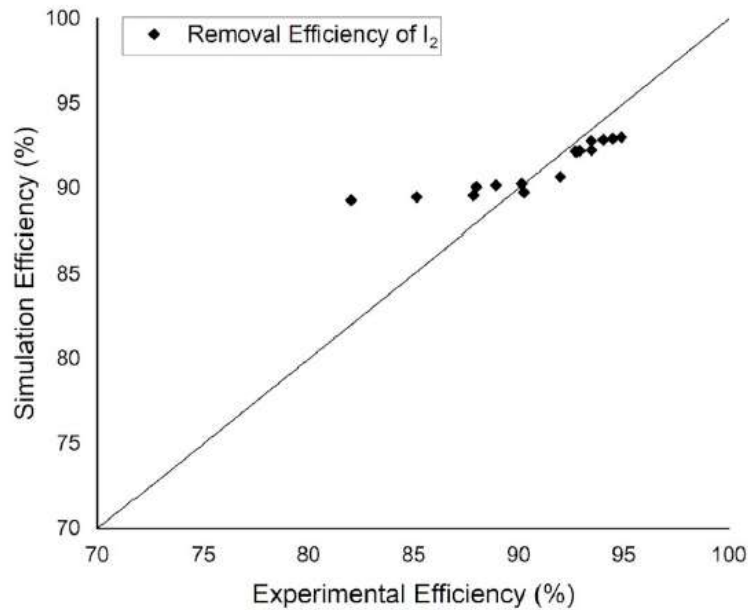


Figure II.13 : Comparison of numerical and experimental removal efficiency of iodine [62].

I.5 Conclusion

From the review of previous studies in this chapter, we found that most of the studies on venturi were focused on the dynamic behavior of flows in venturi, especially pressure drop. It also paid attention to improving the removal efficiency of the venturi scrubber. It neglected the phenomenon of thermal and mass transfer in venturi scrubber. The efficiency of venturi in the purification of gases resulting from gasification of biomass also has been neglected.

Chapter III:

Computational Models and Methods

III.1 Introduction

This chapter consists of two parts. The first part included a description of the physical model, the governing equations, the properties of the fluids used, the expressions of some parameters, and the boundary conditions. The second part included the solution methodology and mesh sensitivity study.

III.2 Computational models

III.2.1 Physical model

The physical system under study is two-dimensional and consists of two parts: The first part contains two orifices with a diameter of 0.001m to enter the liquid before the convergence section. The second part is the venturi scrubber consists of three sections: converging, throat, and diffuser (As shown in the Figure III.1). The table III.1 shows detailed dimensions of the venturi scrubber.

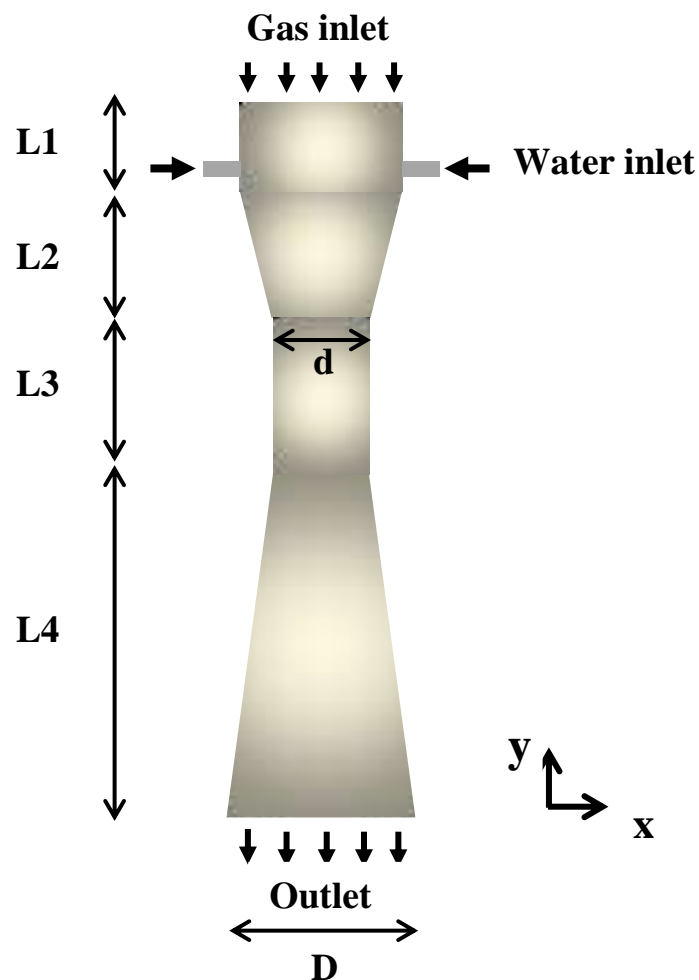


Figure III.1: Geometry description of venturi scrubber.

Table III.1: Physical characteristics of the venturi scrubber.

Physical characteristics of the venturi	
Converge diameter D [m]	0.075
Diffuser diameter D [m]	0.075
Throat diameter d [m]	0.027
Length L1 [m]	0.05
Length L2 [m]	0.13
Length L3 [m]	0.165
Length L4 [m]	0.34
Orifice [m]	0.001

III.2.2 Governing equations

CFD ANSYS-Fluent 16's code was used to perform a numerical simulation of the multiphase flow (liquid-gas) in a venturi scrubber for steady incompressible flow.

In this simulation, the gas is considered a continuous phase, the equations below express the mass conservation equation, the momentum conservation equation and the energy conservation equation:

❖ **Mass conservation equation**

$$\nabla \cdot u = 0 \tag{III.1}$$

❖ **Momentum conservation equation**

$$\rho(u \cdot \nabla u) = -\nabla p + \mu \nabla^2 u + \rho g \tag{III.2}$$

❖ **Energy conservation equation**

$$\rho c u \cdot \nabla T = \lambda \nabla^2 T \tag{III.3}$$

Where: u , ρ , P and μ represent respectively, the velocity, the density, the static pressure and dynamic viscosity.

And c , T , and λ represent specific heat capacity, temperature and conductivity, respectively.

III.2.3 The $k - \varepsilon$ Model

A model based on the turbulent kinetic energy equations and the turbulent dissipation to determine the turbulent viscosity. This model is the best known and most used in the engineering simulation of flows. The equations of the standard $k - \varepsilon$ model are written:

III.2.3.1 Turbulent kinetic energy equation k

$$\frac{\partial}{\partial x_i}(\rho k u_i) = \frac{\partial}{\partial x_j} \left[\left(\mu + \frac{\mu_t}{\sigma_k} \right) \frac{\partial k}{\partial x_j} \right] + G_k + G_b - \rho \varepsilon + S_k \quad (\text{III.4})$$

III.2.3.2 Equation of the dissipation rate ε of turbulent kinetic energy

$$\frac{\partial}{\partial x_i}(\rho \varepsilon u_i) = \frac{\partial}{\partial x_j} \left[\left(\mu + \frac{\mu_t}{\sigma_\varepsilon} \right) \frac{\partial \varepsilon}{\partial x_j} \right] + C_{1\varepsilon} \frac{\varepsilon}{k} (G_k + C_{3\varepsilon} G_b) - C_{2\varepsilon} \rho \frac{\varepsilon^2}{k} + S_\varepsilon \quad (\text{III.5})$$

The turbulent viscosity μ_t this computed by combining k and ε as follows:

$$\mu_t = \rho C_\mu \frac{k^2}{\varepsilon} \quad (\text{III.6})$$

$C_{1\varepsilon}$, $C_{2\varepsilon}$, C_μ , σ_k , and σ_ε value constants:

$$C_{1\varepsilon} = 1.44, C_{2\varepsilon} = 1.92, C_\mu = 0.09, \sigma_k = 1, \sigma_\varepsilon = 1.3$$

σ_k and σ_ε are turbulent numbers Prandtl for k and ε , respectively.

G_k : represents the production of kinetic energy of turbulence due to velocity gradients.

G_b : is the kinetic energy production of turbulence due to buoyancy;

S_k and S_ϵ are source terms.

III.2.4 Species transport model expression

ANSYS Fluent can model the transfer of species by solving conservation equations that describe convection and diffusion for each constituent species wherever the sum of the mass fractions of all species equals 1 through the species transport model which is also applied on multiphase flows. ANSYS Fluent can predict the local mass fraction C_i for each species by solving the mass and diffusion equation for the species with the following general form:

$$\nabla \cdot (\rho u c_i) = -\nabla \cdot J_i \quad (\text{III.7})$$

J_i is the diffusion flux of species , which arises due to gradients of concentration and temperature. By default, ANSYS Fluent uses the dilute approximation (also called Fick's law) to model mass diffusion due to concentration gradients, under which the diffusion flux in turbulent flows can be written as:

$$J_i = -\left(\rho D_{i,m} + \frac{\mu_t}{Sc_t} \right) \nabla c_i - D_{T,i} \frac{\nabla T}{T} \quad (\text{III.8})$$

$$Sc_t = \frac{\mu_t}{\rho D_t} \quad (\text{III.9})$$

Sc_t is the turbulent Schmidt number, $D_{i,m}$ is the mass diffusion coefficient for species i, $D_{T,i}$ is the thermal diffusion coefficient and D_t is the turbulent diffusivity.

III.2.5 Reynolds number expression

Reynolds is an important dimensionless number used to determine the regime of flows; its expression is given as follows:

$$\text{Re} = \frac{\rho u D_h}{\mu} \quad (\text{III.10})$$

Reynolds values in this study between 20000 and 400000.

III.2.6 Nusselt number expression

Nusselt is the dimensionless number that represented the Ratio of convection to conduction heat transfer; its expression is given as follows, its formulation is given as follows:

$$\text{Nu} = \frac{h \cdot D_h}{\lambda} \quad (\text{III.11})$$

h is the convection coefficient, D_h hydraulic diameter.

III.2.7 Probability density function PDF

The probability density function PDF (α) is the probability (in %) of the scalar mass fraction C to be present between two values; the PDF (α) in an interval $[\alpha_a, \alpha_b]$ at the default-interior is equal to the number of mesh cells in which α values are within $[\alpha_a, \alpha_b]$ divided by the total number of cells on the default-interior. Based on the distribution F_α function of a scalar field α , the density of probability function is defined as follows:

$$f_\alpha = \frac{\partial F_\alpha}{\partial \alpha} \quad (\text{III.12})$$

III.2.8 The removal efficiency

Collection efficiency in venturi scrubber gives the following relationships:

$$E_R = \frac{C_{in} - C_0}{C_{in}} \quad (III.13)$$

C_{in} is the water mass fraction at water inlet; C_0 is water mass fraction at outlet.

III.2.9 The Removal Energy Cost

The pressure drop must be taken into account with the removal efficiency and the flow rate when evaluating the overall performances of the cleaning venturi reliability. For this, it's important to present the Removal Energy Cost "REC" which is expressed by:

$$REC = \frac{Q \cdot \Delta p}{E_R} \quad (III.14)$$

Where Q is the flow rate (m^3/s), ΔP is the pressure drop along the venturi and E_R is the removal efficiency of the proposed venturi.

III.2.10 Fluid properties

In this study, two liquids were used, the first fluid is the gas that is cleaned, which is the product gas (PG) generated from biomass through the thermochemical gasification process, and the liquid used to clean the gas is water. The properties of both liquids are shown in Tables III.2 and Tables III.3.

Table III.2: Properties of gas generated from biomass [63].

Parameters	Symbol	Units	Value
Chemical composition of PG:			
Carbon monoxide	CO	Vol %	16
Hydrogen	H ₂	Vol %	17
Methane	CH ₄	Vol %	1
Carbon dioxide	CO ₂	Vol %	13
Nitrogen	N ₂	Vol %	49
Water vapour	H ₂ O	Vol %	4
Molar mass	M _m	kg/kmol	25.14
Lower Heating Value	LHV _m	kJ/m ³	4042
Specific gravity at NTP	SG	-	0.87
Wobbe Index	WI	kJ/m ³	4171
Stoichiometric air-PG ratio	(A/F) _{stoic}	kg air/kg PG	1.01
Adiabatic Flame Temperature	T _{adfl}	K	1770
Laminar burning velocity	S _L	m/s	0.45
Molar specific heat capacity at constant pressure at NTP	\bar{c}_{Pm}	kJ/(kmol.K)	30.36
Molar specific heat capacity at constant volume at NTP	\bar{c}_{Pv}	kJ/(kmol.K)	22.05
Absolute entropy of PG	\bar{s}_m°	kJ/(kmol.K)	196.44
Reversible Work	W _{rev}	kJ/kmol	88021
Mass density at NTP	ρ	kg/m ³	1.03
Absolute viscosity	μ_m	kg/(m.s)	1.57263x10 ⁻⁵
Thermal conductivity	K _m	W/(m.K)	0.0344
Diffusion coefficient	D _{air-mixt}	m ² /s	0.209x10 ⁻⁴

Table III.3: Properties of water liquid.

Properties of water	Value	Units
Density	998.2	kg/m ³
specific heat	4182	J/(kg.K)
viscosity	0.001003	kg/(m.s)
Thermal conductivity	0.6	W/(m.K)
Diffusion coefficient	0.299x10 ⁻⁹ [64]	m ² /s

III.2.11 The boundary conditions

The boundary conditions are:

- **At gas inlet:** Impose velocity of gas constant with a temperature equal to 310 K, water mass fraction equal to 0.
- **At liquid inlet:** Impose mass flow rate of water constant with a temperature equal to 300 K, water mass fraction equal to 1.
- **At outlet:** Pressure equal to 0 Pa is applied.
- **At wall:** A no-slip velocity condition imposed with a temperature equal to 300 K.

III.3 Numerical methodology

III.3.1 Solution methodology

Numerical simulations of gas and water flow in venturi scrubber are performed using CFD code. The multiphase flow is processed using the species transport model. The Simple algorithm for pressure-velocity coupling applied. Second-order upwind approximation scheme used to discretize the convective terms of the mass conservation equation, momentum conservation equation, energy conservation equation.

III.3.2 Grid independency tests

The grid independency tests have an essential role in the CFD simulation to obtain good results using optimal mesh, so choosing the best mesh is very important. The simulations have been carried out of fluid flows in four meshes with a velocity gas of 20 m /s and a mass flow rate of 0.02 kg / s. The structural elements used were a quadrilateral grid generated using ‘GAMBIT’ as shown in Figure III.2.

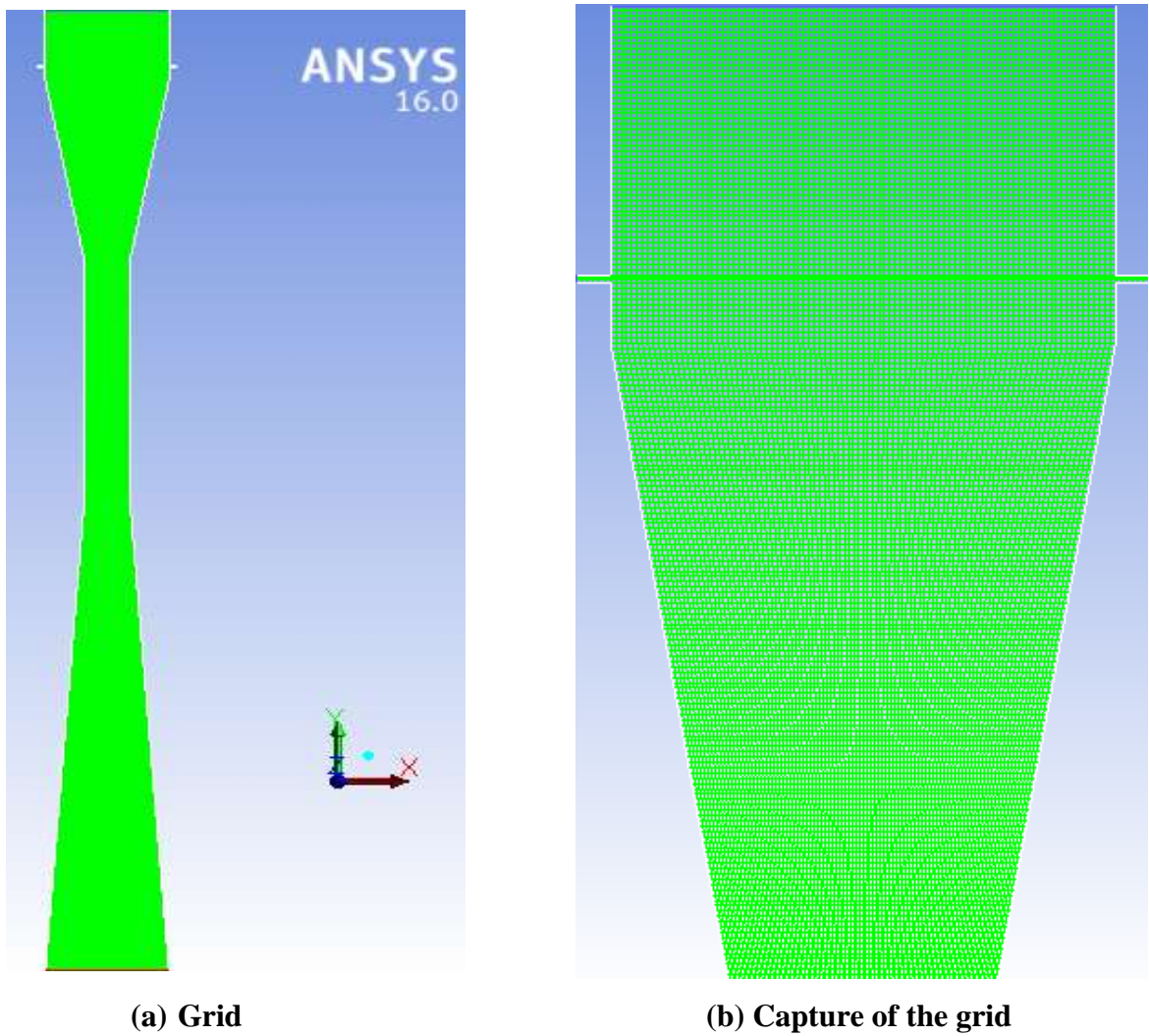


Figure III.2: Grid sensitivity study.

The nodes number in these models is as follows: 13557, 31345, 81938 and 144696 elements. The velocity variations is evaluated for increasing nodes as shown in Figure III.3 as we note, there is no significant difference between the different mesh results. Therefore, the mesh which includes 81938 elements adopted as a suitable mesh for investigation.

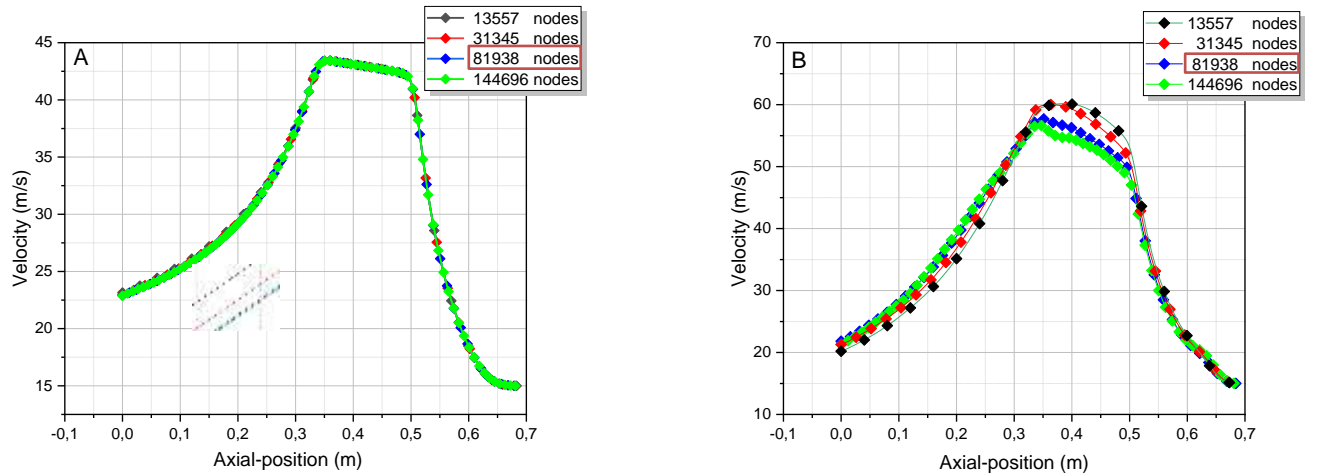


Figure III.3: Mesh study for : **A-** Single phase(gas) , **B-** Two phases(gas-water).

III.4 Conclusion

In this chapter, the description of the physical model of venturi scrubber used in this study is addressed; the governing equations, the applied models, the expressions of Reynolds number and Nusselt number, the removal efficiency, the adopted numerical solution method, and the grid independency tests.

Chapter IV

Flows Behavior in Venturi Scrubber

IV.1 Introduction

The object of this chapter is: to understand the flow behavior in the venturi scrubber, which contains contours of velocity, pressure (static, dynamic), turbulent kinetic energy, and turbulent dissipation rate. It also shows the effect of changing gas velocity and liquid flow at inlets on these parameters.

IV.2 Validation

A validation test performs to check the numerical results obtained with the presently used solver. The numerical simulation that Silva [65] carried out on venturi achieved with conditions represented by the gas velocity at the throat at 70 m/s and the fluid mass flow at 0.075 kg/s and compared the results of axial velocity. The curves show that the simulation results were satisfactory (see Figure IV.1).

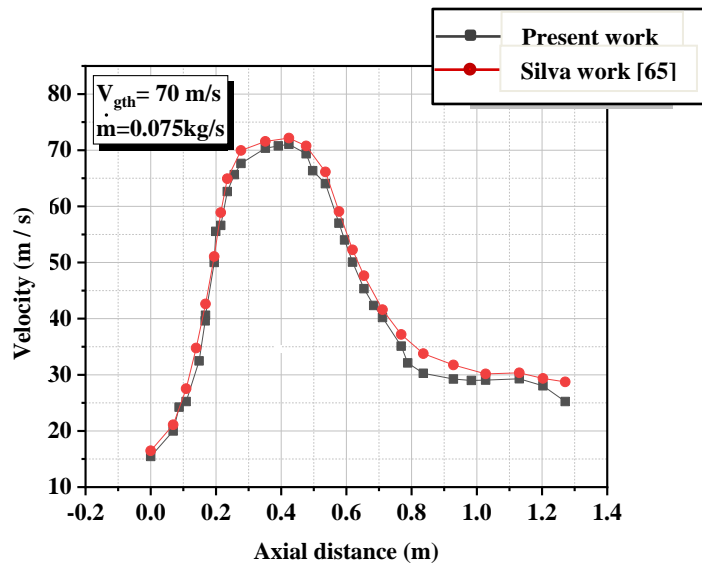


Figure IV.1: Validation using CFD code.

IV.3 The velocity evolution

Figure IV.2 shows the evolution of velocity in venturi scrubber with mass flow rate equals 0.06 kg/s and different gas velocities.

From the curves, we see that the velocity increases in the convergent section due to the decrease in the diameter, and it arrives at its maximum value in the throat section, and then the increase in the diameter leads to a decreasing its value.

We note that the maximum values increase with the increasing the gas velocities at the inlet.

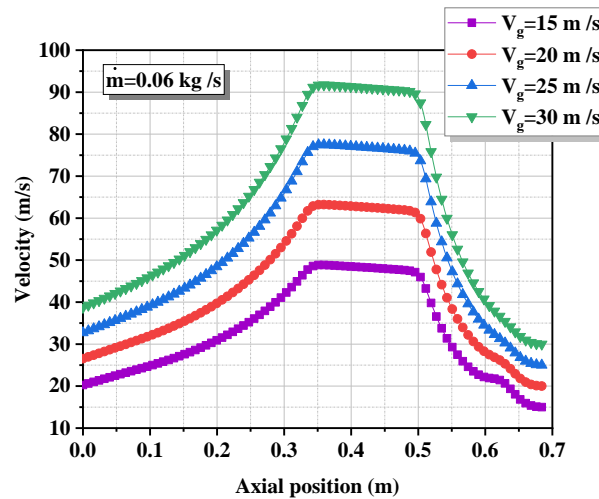


Figure IV.2: Evolution of velocity in venturi scrubber with mass flow rate equals 0.06 kg/s and different gas velocities.

Figures IV.3- IV.6 and Figure IV. 7 represent the contours and the graphs of the velocity in the venture scrubber for different liquid mass flow rates with a constant gas velocity.

We note that the maximum values increase little with the increasing liquid mass flow rate. We see its values reach about 45, 47, and 48 m/s at the gas velocity of 15 m / s with the water mass flow of 0.02, 0.04, and 0.06 kg/s, respectively. It arrives at about 59, 61, and 63 m/s at the gas inlet velocity of 20 m / s at the inlet water mass flow of 0.02, 0.04, and 0.06 kg/s, respectively. They arrive at about 73, 75, and 77 m/s at the gas inlet velocity of 25 m / s at inlet water mass flow of 0.02, 0.04, and 0.06 kg/s, respectively. It arrives at about 87, 89, and 91 m/s at the gas inlet velocity of 30 m / s at inlet water mass flow of 0.02, 0.04, and 0.06 kg/s, respectively.

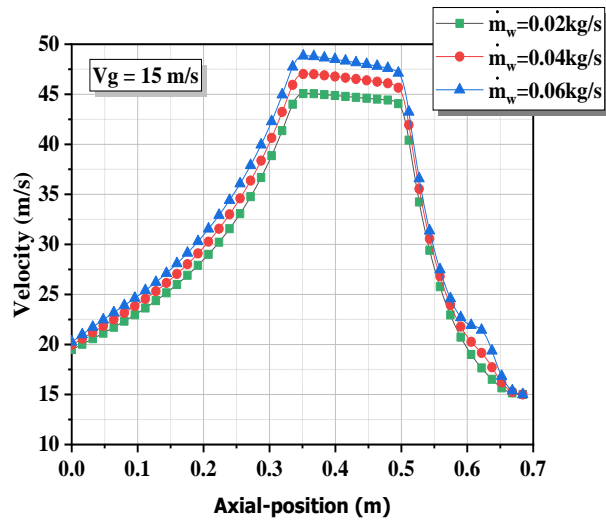


Figure IV.3: Velocity profiles for different mass flow rate at the middle of the venturi with gas velocity of 15 (m/s).

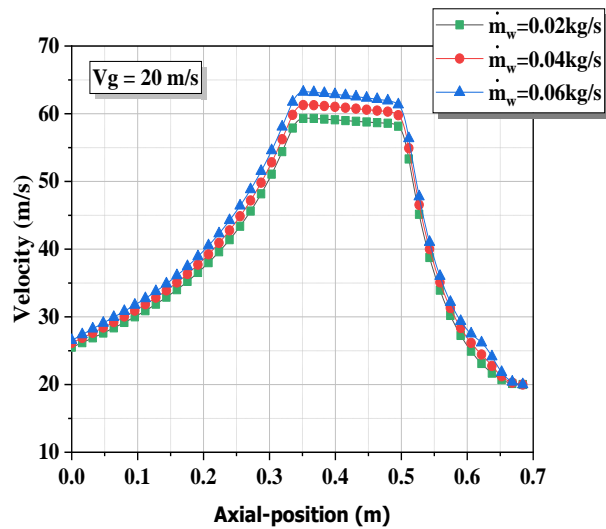


Figure IV.4: Velocity profiles for different mass flow rate at the middle of the venturi with gas velocity of 20 (m/s).

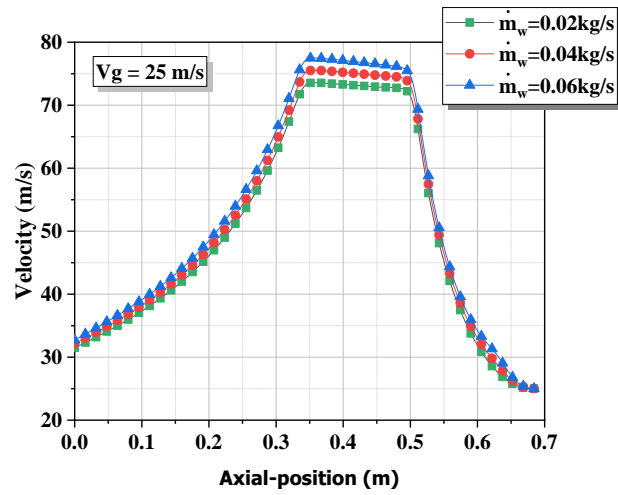


Figure IV.5: Velocity profiles for different mass flow rate at the middle of the venturi with gas velocity of 25 (m/s).

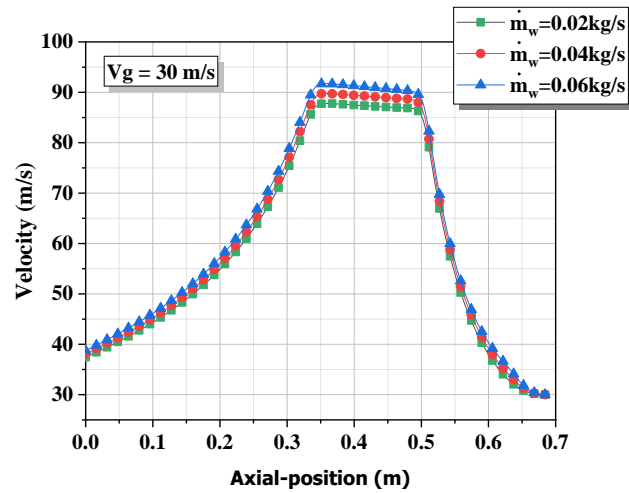
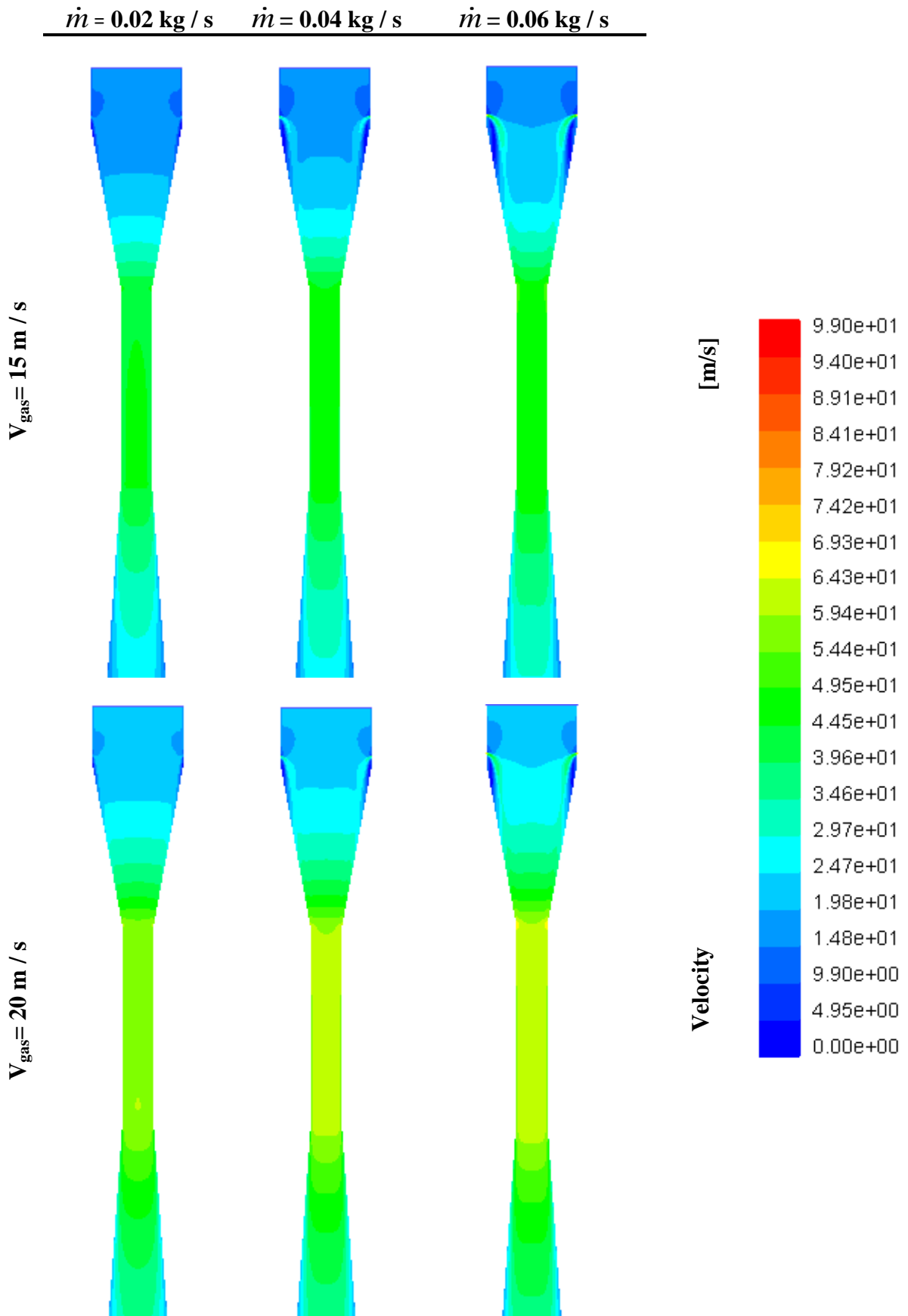


Figure IV.6: Velocity profiles for different mass flow rate at the middle of the venturi with gas velocity of 30 (m/s).



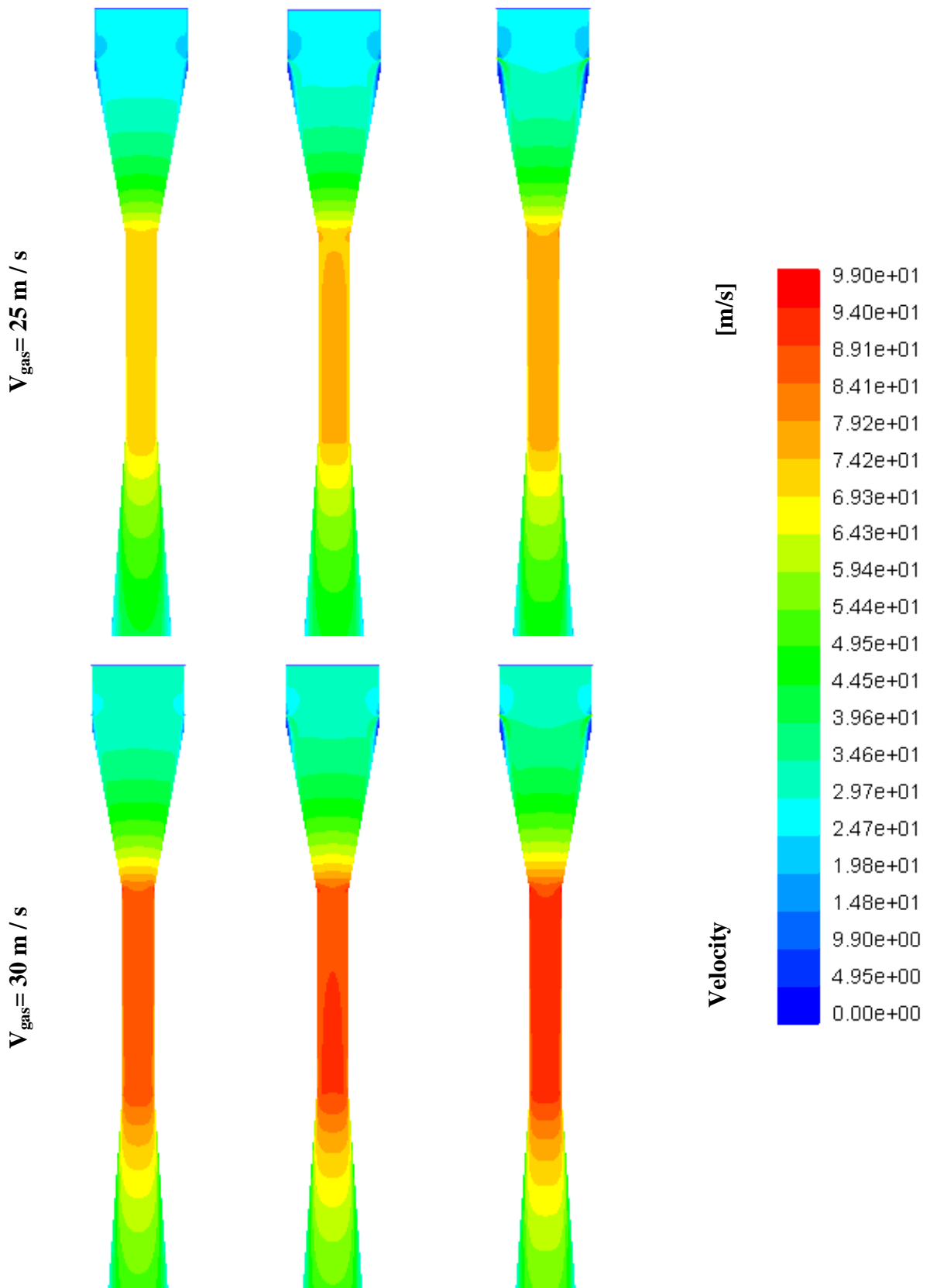
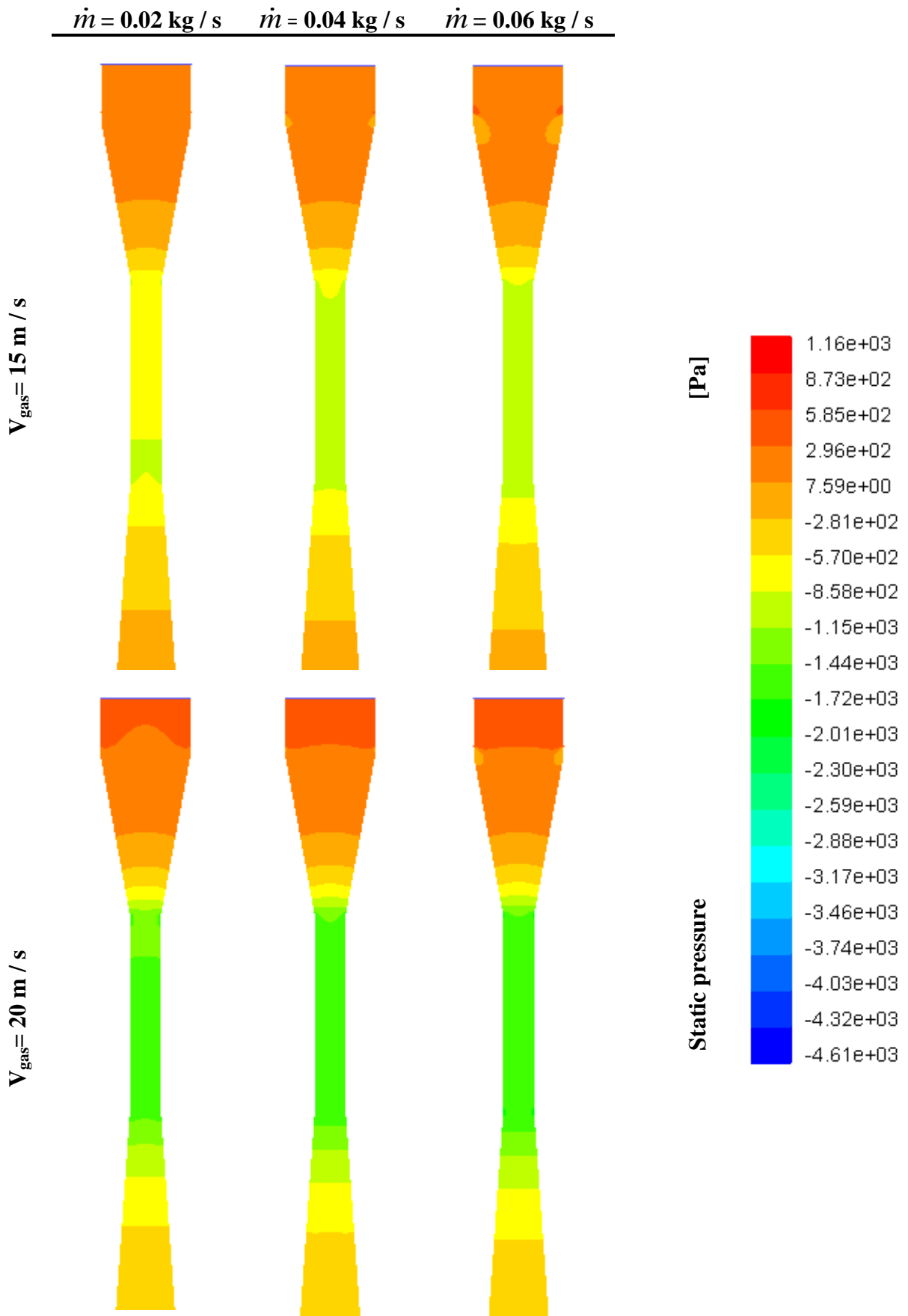


Figure IV.7: Contours of velocity magnitude.

IV.4 The evolution of pressure

Figure IV.8 indicates the contour of static pressure in the venturi. The static pressure is high at the beginning of the venturi. It begins to decrease in the convergent section due to the conversion of static pressure into kinetic energy. There is a sharp drop of static pressure due to friction in the throat. Part of the pressure recovers in the diffuser due to the conversion of kinetic energy into pressure.

The results of the comparison of static pressure with mass flow difference for inlet water mass flow and static gas velocity inlet are represented in Figure IV.9 where we note, at the gas velocity inlet of 15 m / s and the inlet water mass flow 0.02, 0.04, and 0.06 kg/s, static pressure approximate values at the beginning of the venturi were 175.958, 199.426, and 217.512 (Pa), respectively. The minimum value of static pressure at the throat is approximately -966.185 (Pa) for the three mass flows at the water inlet. For gas velocity inlet of 20 m / s and the inlet water mass flow 0.02, 0.04, and 0.06 kg/s, static pressure approximate values at the beginning of the venturi were 288.398, 312.168, and 348.976 (Pa), respectively. The minimum value of static pressure at the throat is approximately -1633.55 (Pa) for the three velocities of water at the inlet. For gas velocity inlet of 25 m / s and the inlet water mass flow 0.02, 0.04, and 0.06 kg/s, static pressure approximate values at the beginning of the venturi were 425.49, 464.887, and 502.941 (Pa), respectively. The minimum value of static pressure at the throat is approximately -2478.06 (Pa) for the three velocities of water at the inlet. Also, for gas velocity inlet of 30 m / s and the inlet water mass flow 0.02, 0.04, and 0.06 kg/s, static pressure approximate values at the beginning of the venturi were 586.422, 633.839, and 679.404 (Pa), respectively. The minimum value of static pressure at the throat is approximately -3500 (Pa) for the three velocities of water at the inlet.



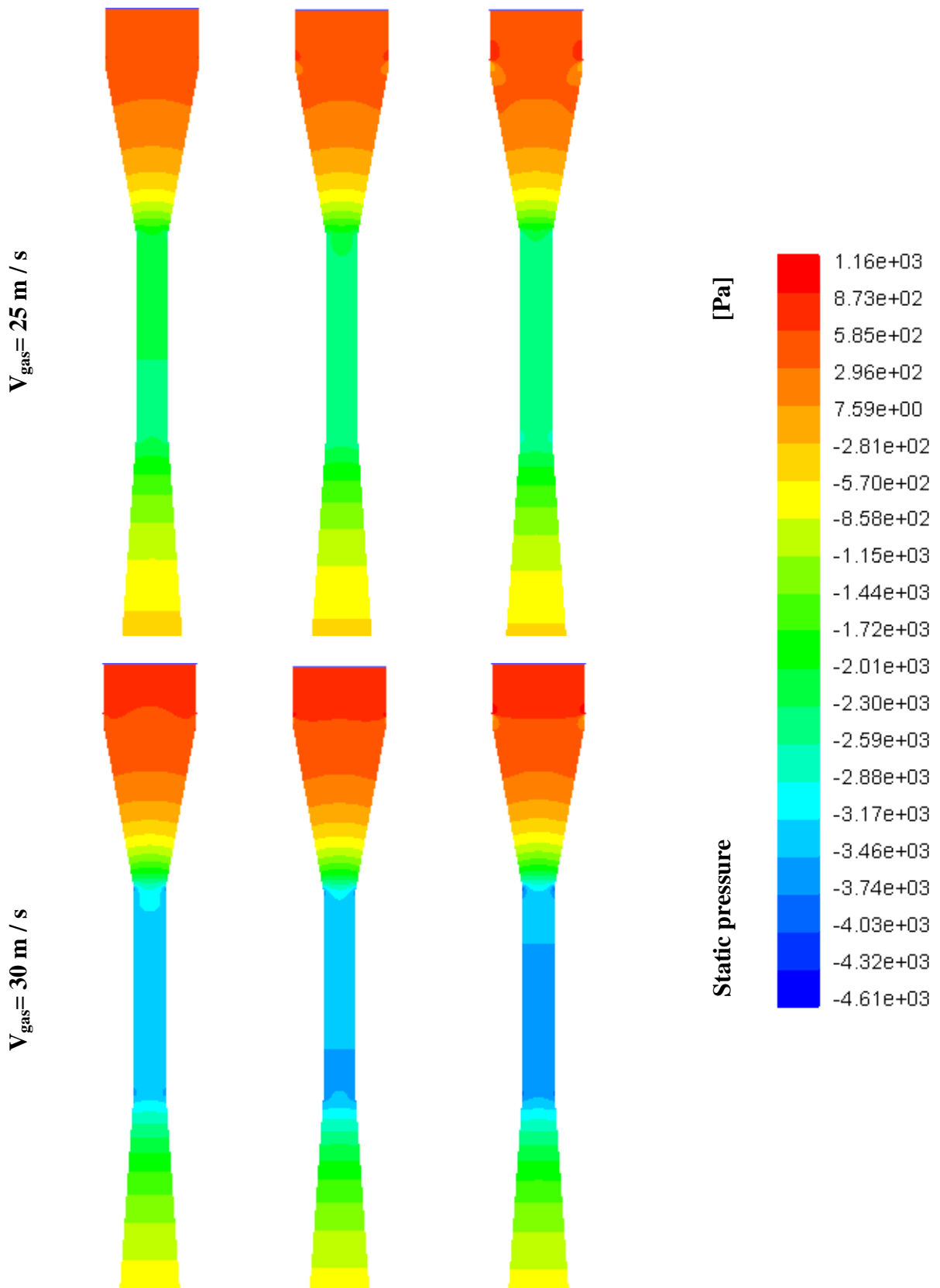


Figure IV.8: Contours of static pressure.

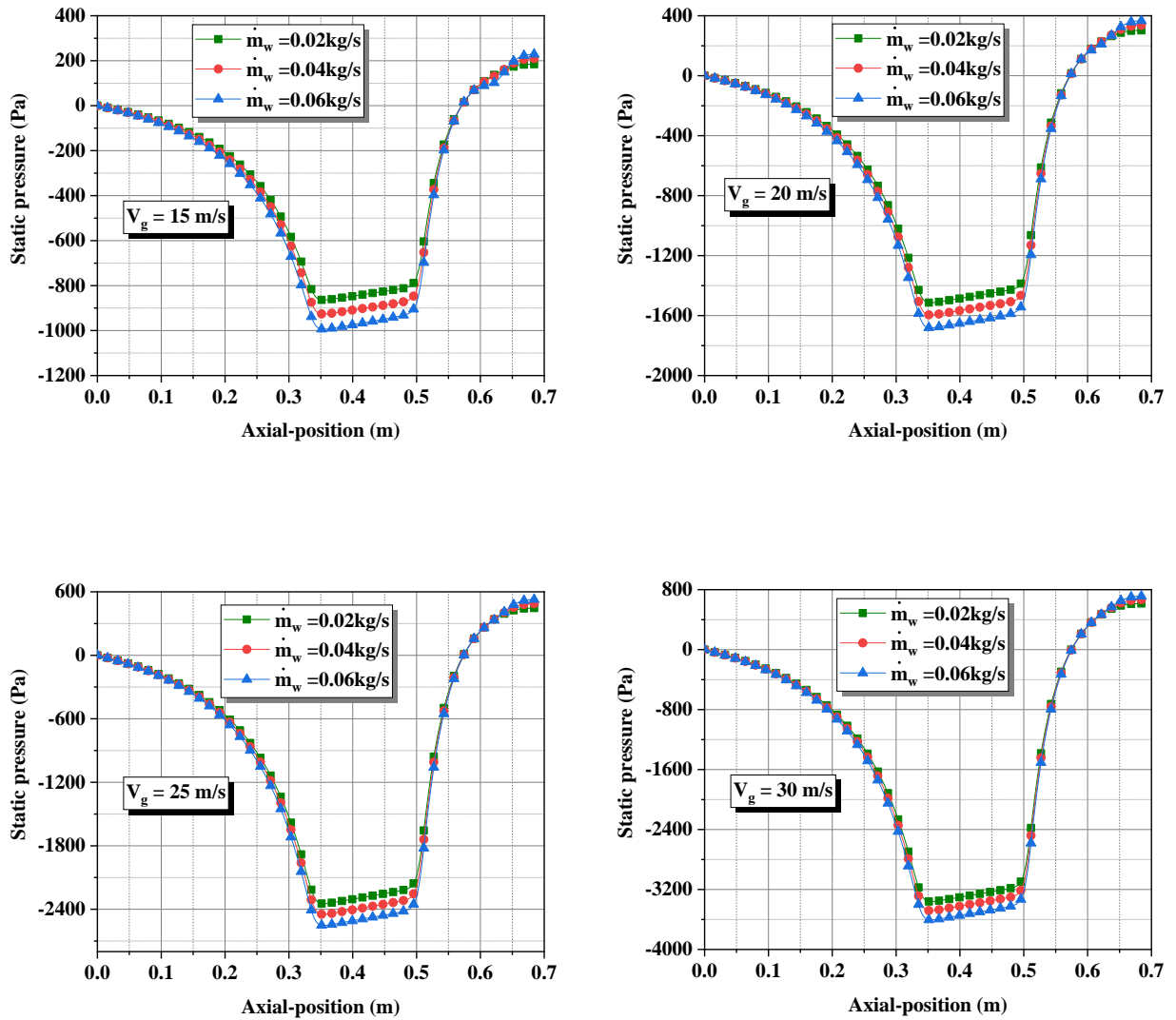


Figure IV.9: The comparison of static pressure values for different gas velocities.

Figure IV.10 include a comparison of dynamic pressure results with the mass flow difference of mass flow inlet and a constant gas velocity inlet. Through the curves, notice that the dynamic pressure behaves the same as velocity because its value is related to the square of velocity. The dynamic pressure also increases with the increase of velocity water inlet.

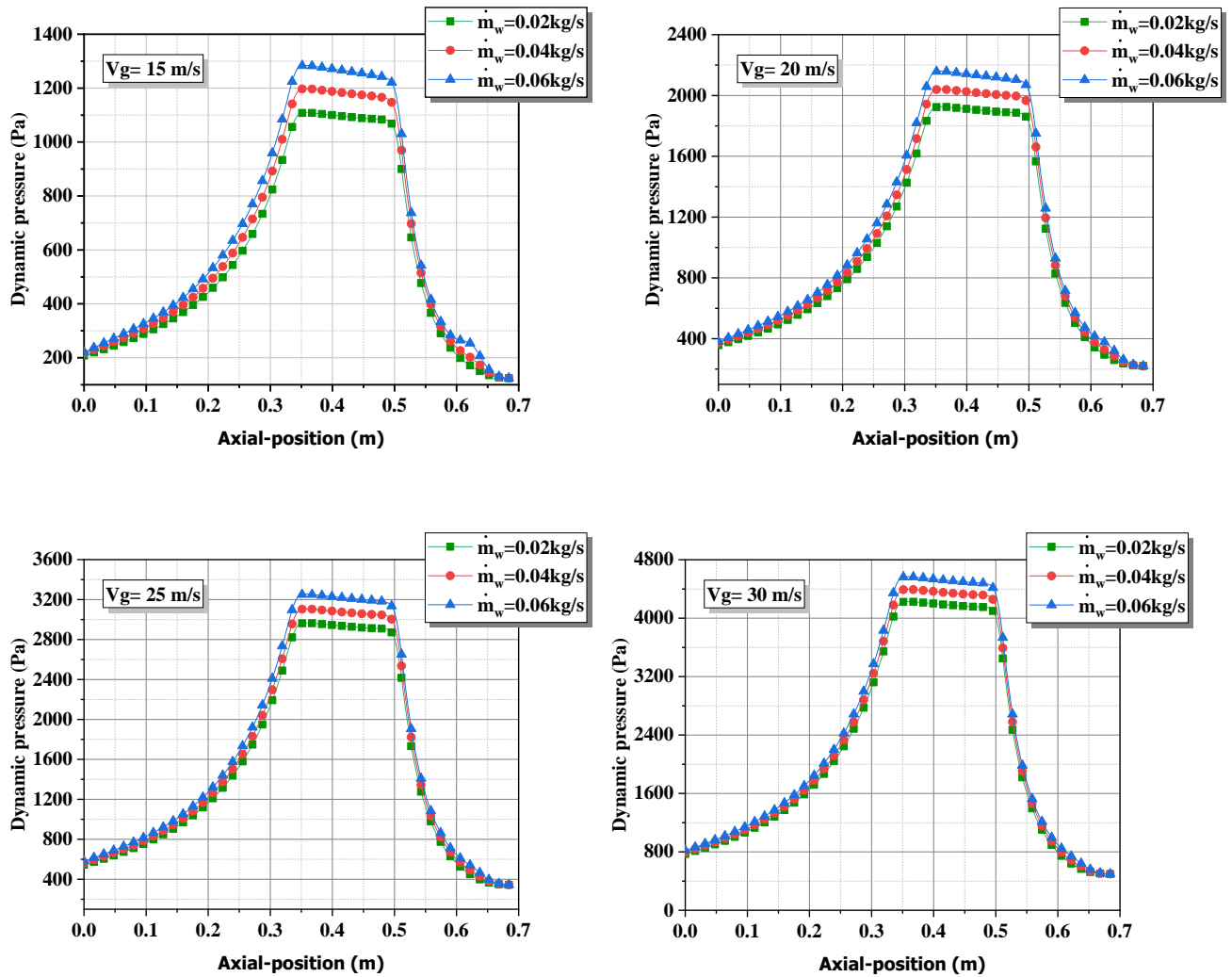
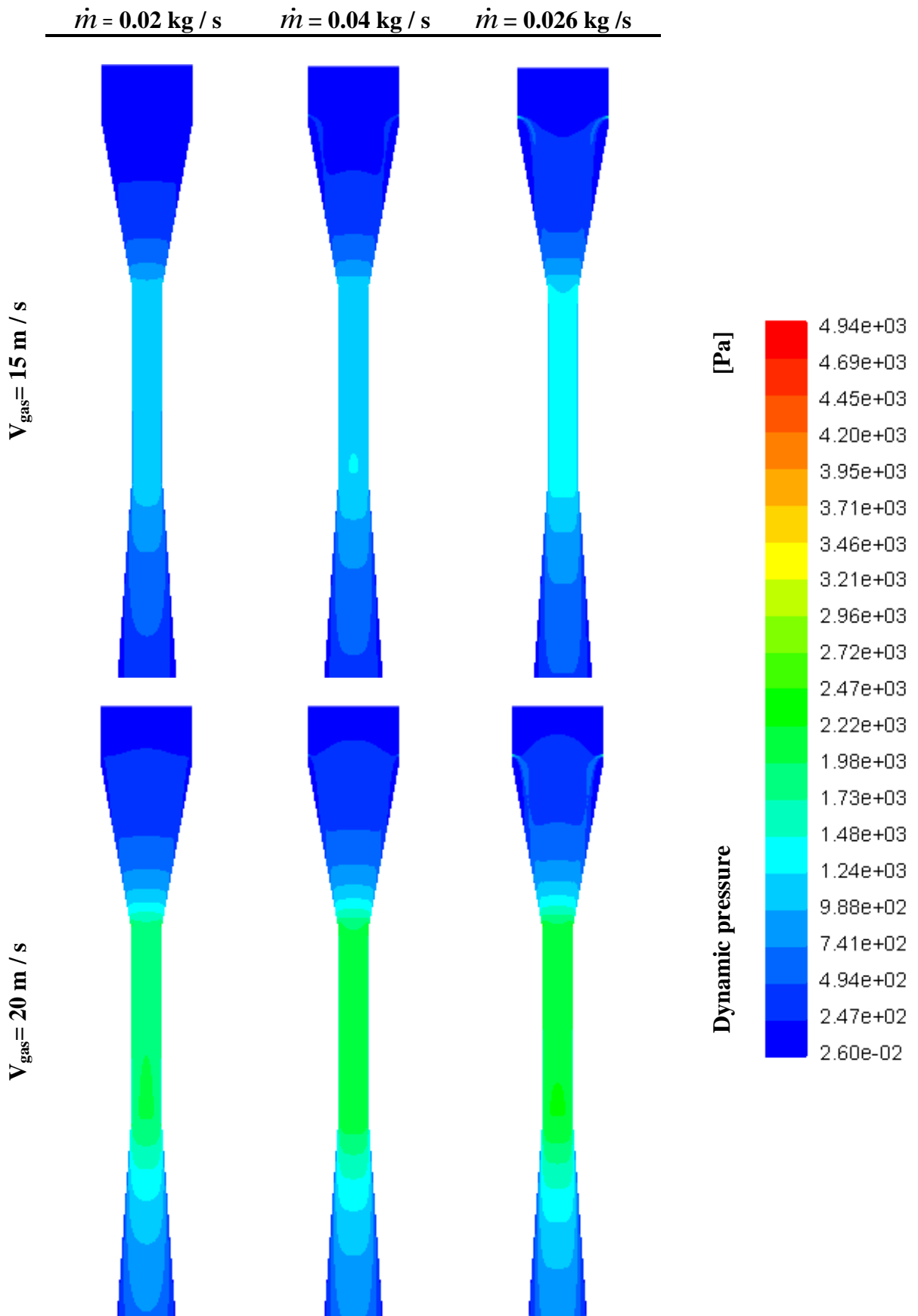


Figure IV.10: The comparison of dynamic pressure values for different gas velocities.

The contour of dynamic pressure is shown in Figure IV.11. The dynamic pressure increases in the convergent section and arrives at its high values in the throat. In the diffuser section, the dynamic pressure decreases.



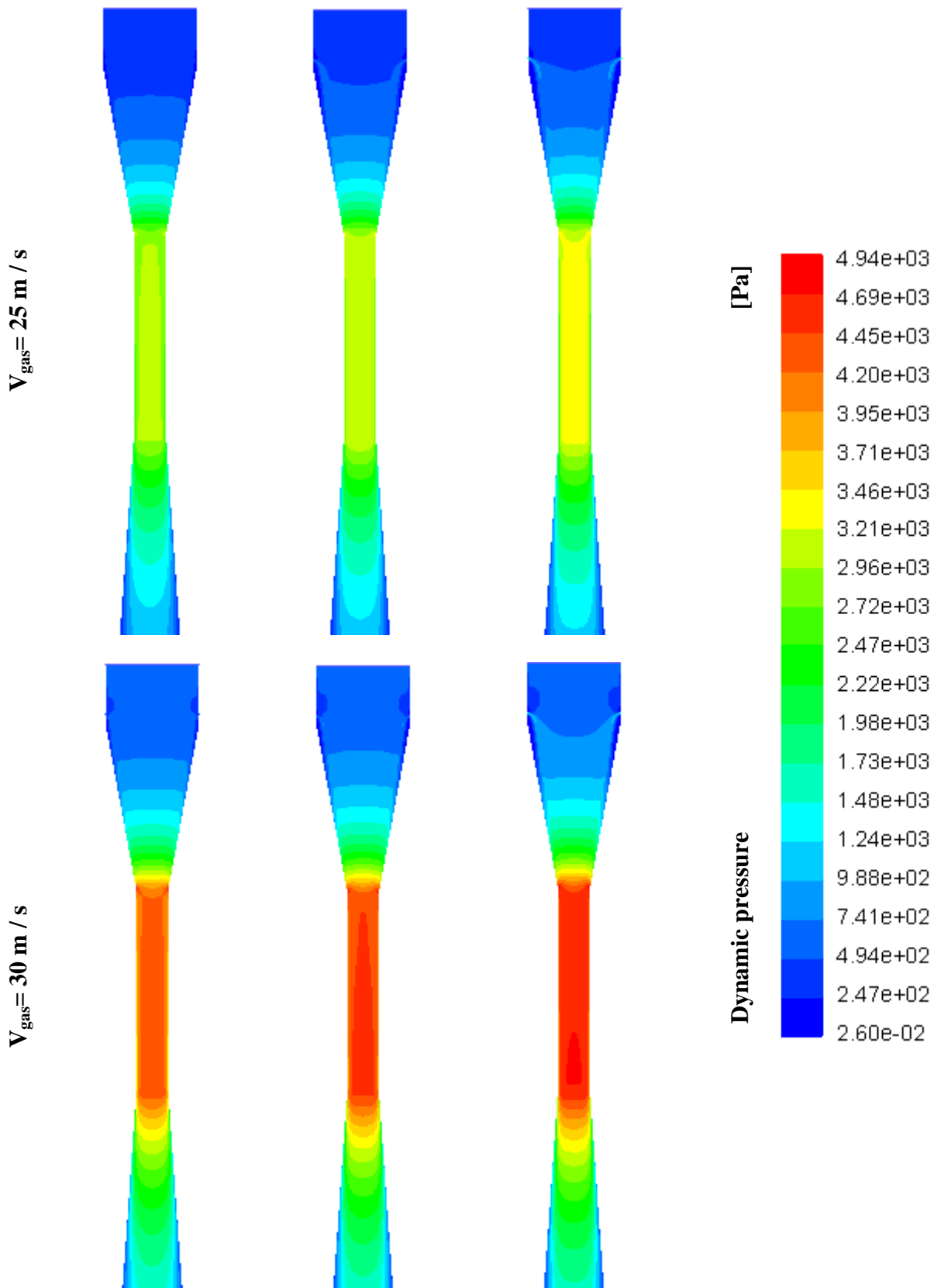


Figure IV.11: Contours of dynamic pressure.

IV.5 Pressure drops assessment

Figures IV.12 - IV.13 include the effect of inlet gas velocity and inlet water mass flow on pressure drop. We observe from Figure IV.12 that an increase in gas velocity leads to an increase in pressure drop, and Figure IV.13 shows that the increase in the flow of liquid also increases the pressure drop, but with a lesser increase than the increase in the velocity of the gas.

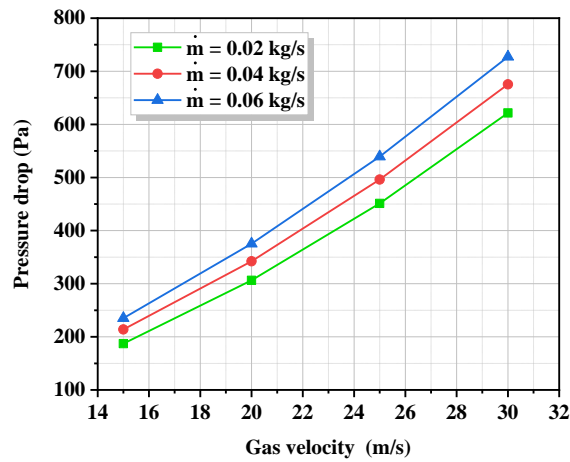


Figure IV.12: Effect of inlet gas velocity on pressure drop.

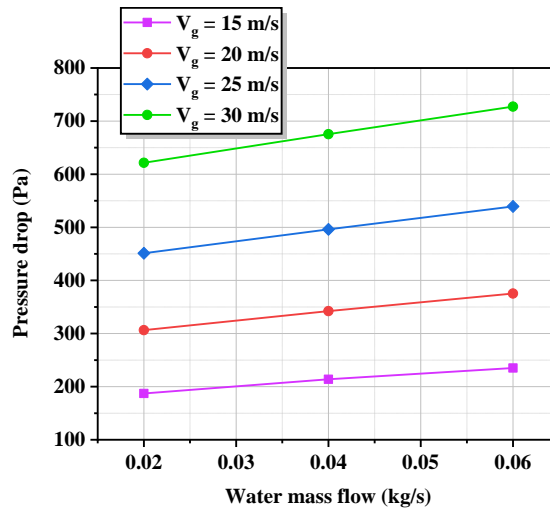


Figure IV. 13: Effect of inlet water mass flow rate on pressure drop.

IV.6 The evolution of turbulent kinetic energy

Figure IV.14 shows the contour of the evolution of turbulent kinetic energy in venturi. The kinetic energy increases in the throat, and maximum values are near the wall at the throat.

The evolution of turbulent kinetic energy in the position axial of the venturi scrubber is shown in Figure IV.15. The turbulent kinetic energy increases in convergence (conversion of potential energy into kinetic energy) until it reaches its highest value in the throat (Because of the high-velocity values) and decreases in the diffuser (conversion of kinetic energy into potential energy). The value of the turbulent kinetic energy increases with the increase in the velocity at the inlet, reaching its highest value of $60 \text{ m}^2/\text{s}^2$ with the inlet gas being 30 m/s and mass flow 0.02 kg/s . The turbulent kinetic energy value decreases with the increasing liquid mass flow rate.

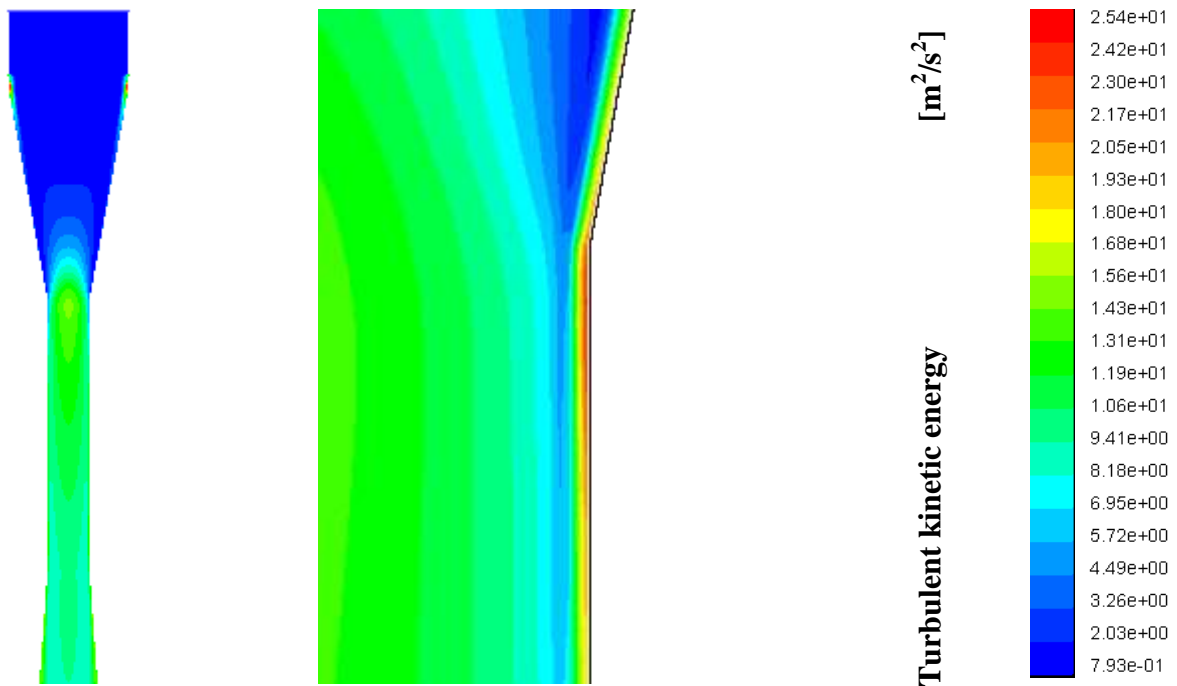


Figure III.14: Contours of turbulent kinetic energy in the throat near the wall.

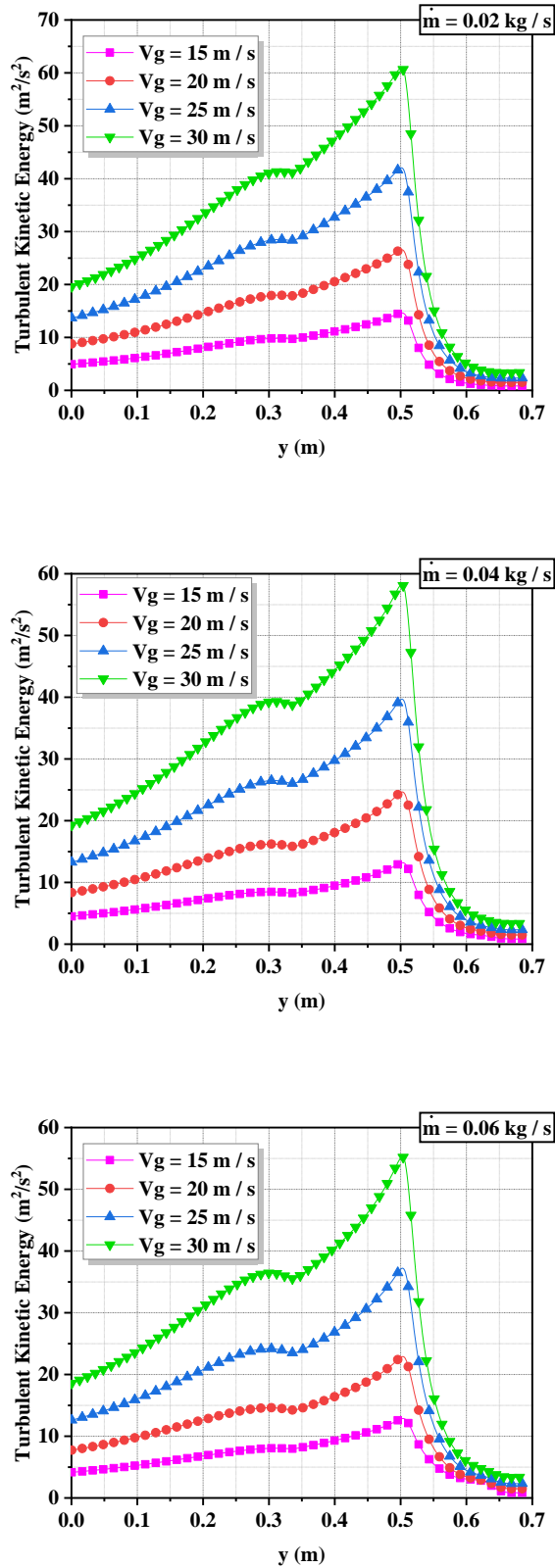


Figure IV.15: The evolution of turbulent kinetic energy in the axial position.

IV.7 The evolution of turbulent dissipation rate

Figure IV.16 shows the contour of the turbulent dissipation rate in the venturi. The kinetic energy increases in the throat, and maximum values are near the wall at the throat.

The evolution of the turbulent dissipation rate in the axial position of the venturi scrubber is shown in Figure IV.17. The turbulent dissipation rate increases in convergence (the increase in the velocity) until it reaches its highest value at the end of the throat and decreases in the diffuser (the decrease in the velocity). The turbulent dissipation rate increases with the increase in the velocity at the inlet, reaching its highest value of $7000 \text{ m}^2/\text{s}^3$ with the inlet gas being 30 m/s and mass flow of water 0.02 kg/s . The turbulent dissipation rate value decreases with the increasing liquid mass flow rate.

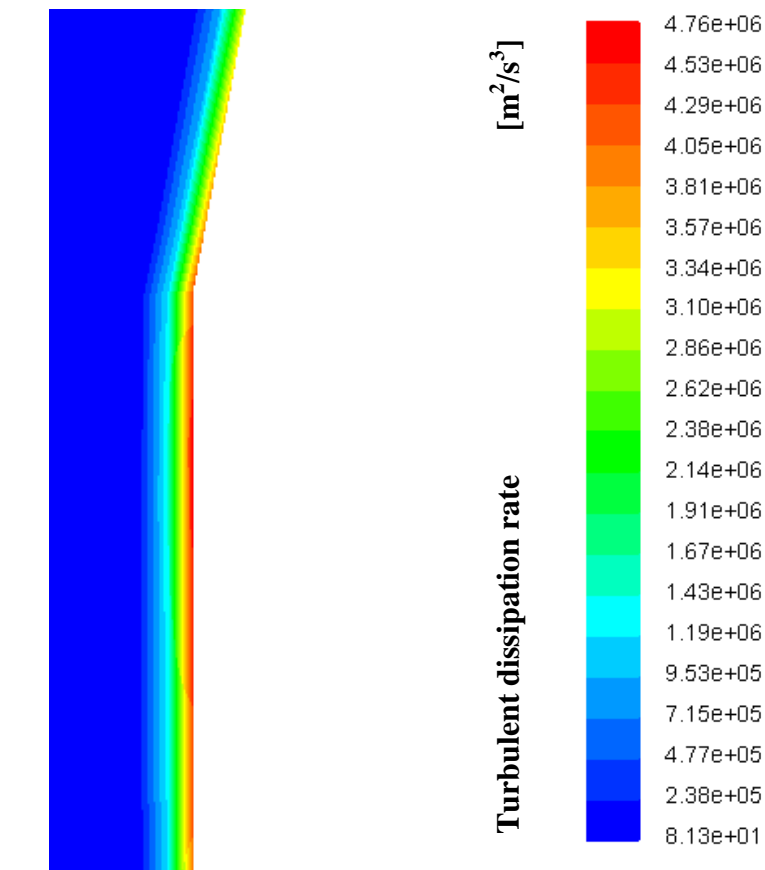


Figure IV.16: Contours of turbulent dissipation rate in the throat near the wall.

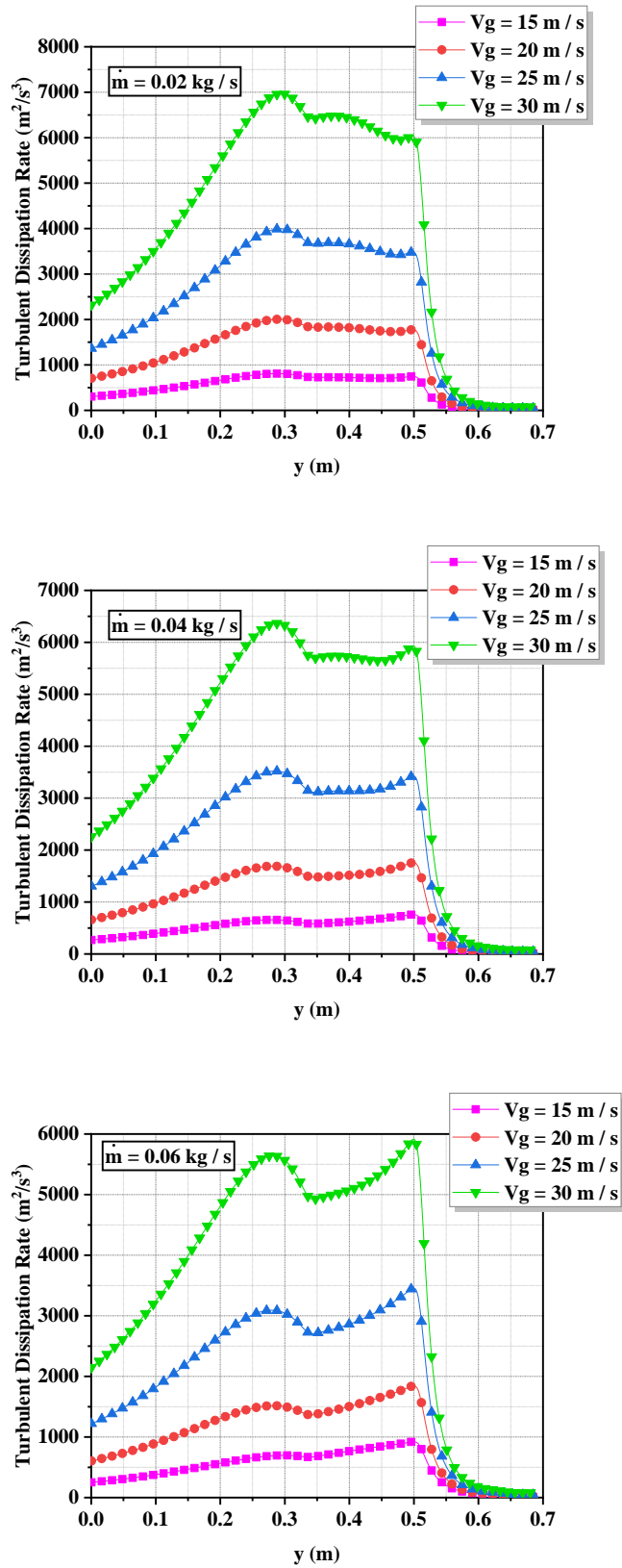


Figure IV.17: The evolution of turbulent dissipation rate in the axial position.

IV.8 Turbulent viscosity

Figures IV.18 - IV.21 represent the local turbulent viscosity evolution on the X-axis in different sections of the venturi scrubber (convergence, throat, and diffuser) with gas velocities and water mass flow differences. The turbulent viscosity at the wall is equal to zero, and its maximum values are in the center of the three sections because the maximum velocity values are in this position and null at the wall. The maximum value was in the throat section, then the convergence, and then the diffuser. Also, the increase in gas velocity increases the value of the turbulent viscosity, and the increase in the flow of liquid decreases its value.

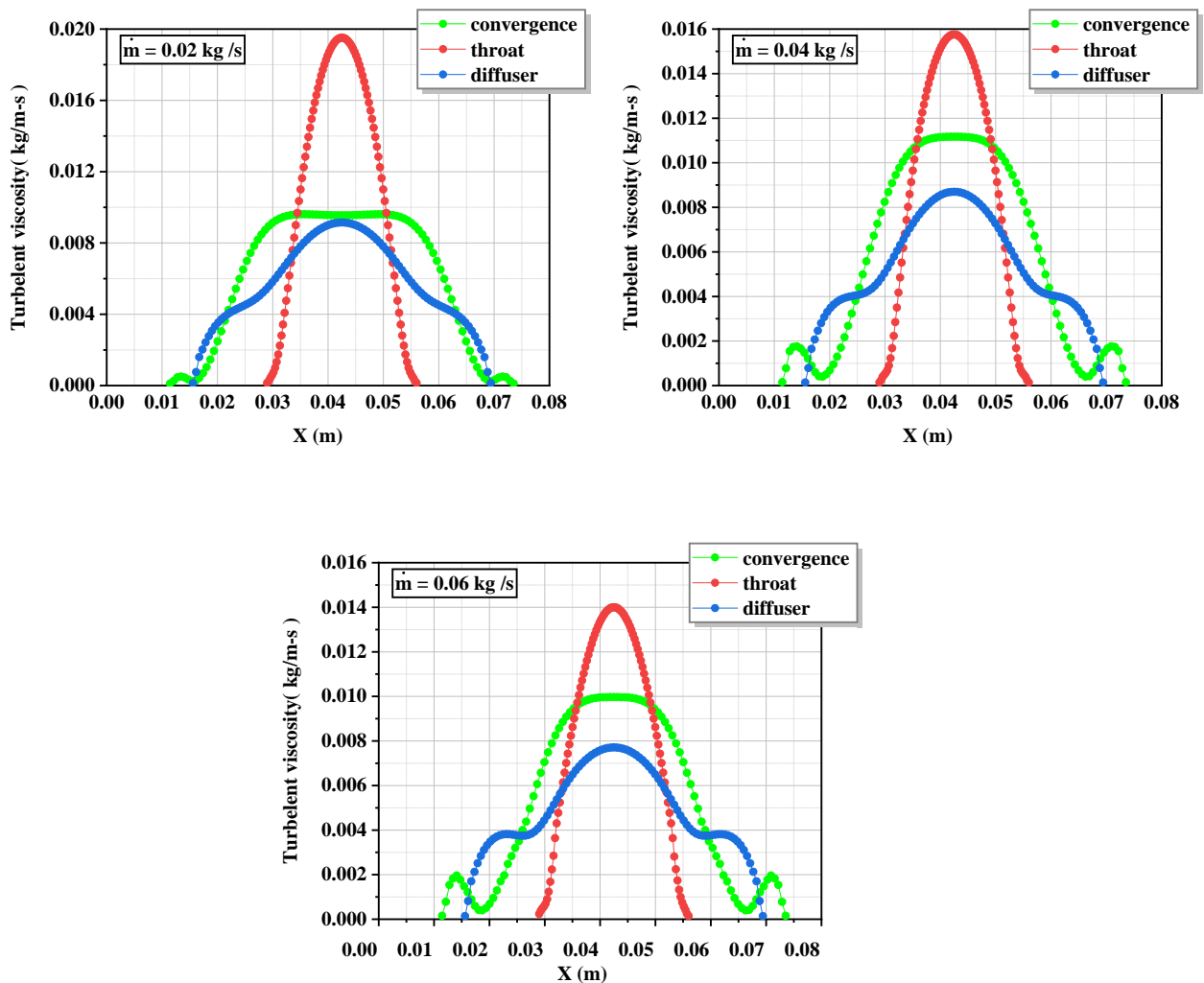


Figure IV.18: Evolution of turbulent viscosity in different sections of the venturi with gas velocity of 15 m / s for different water mass flow rates.

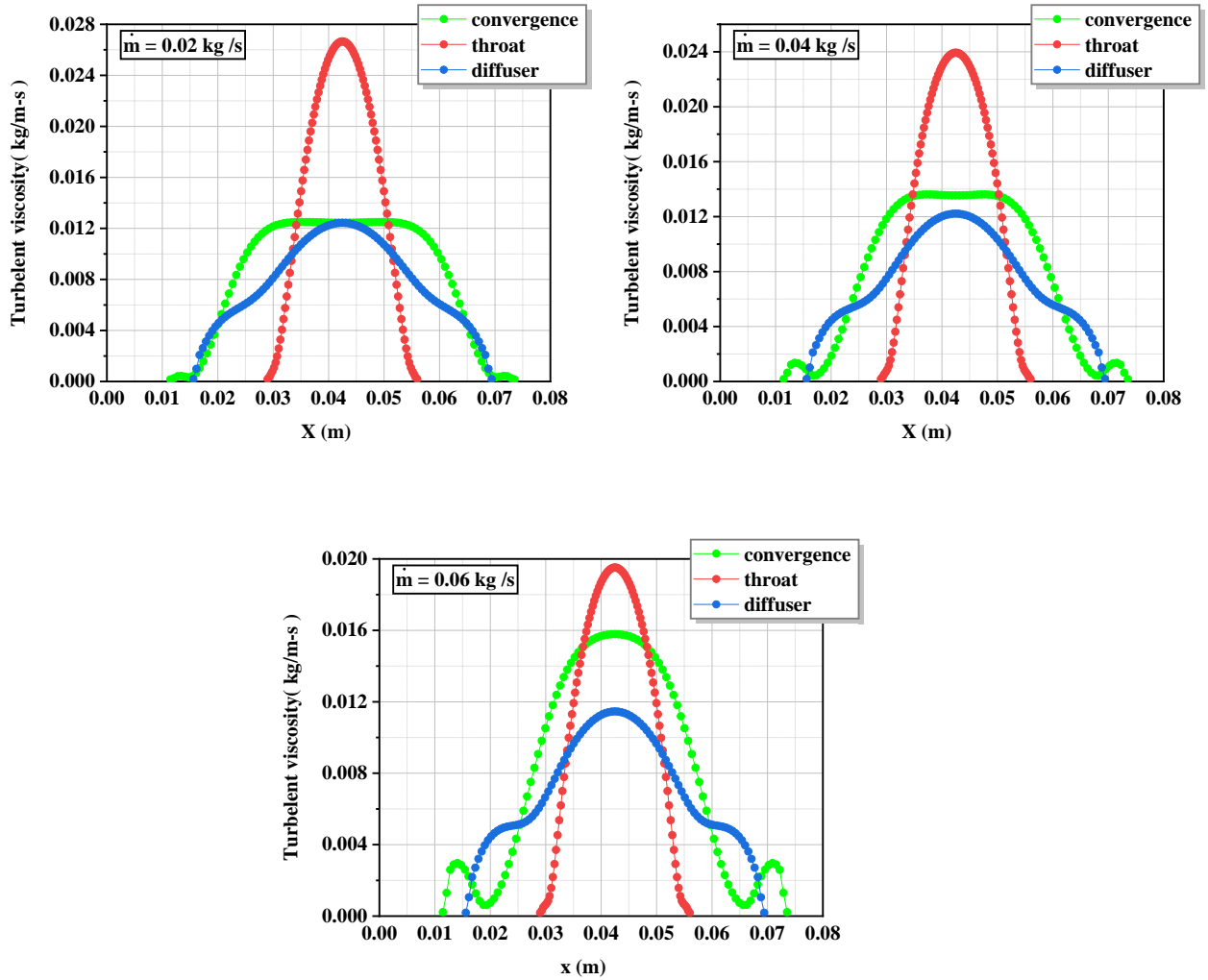


Figure IV.19: Evolution of turbulent viscosity in different sections of the venturi with gas velocity of 20 m / s for different water mass flow rates.

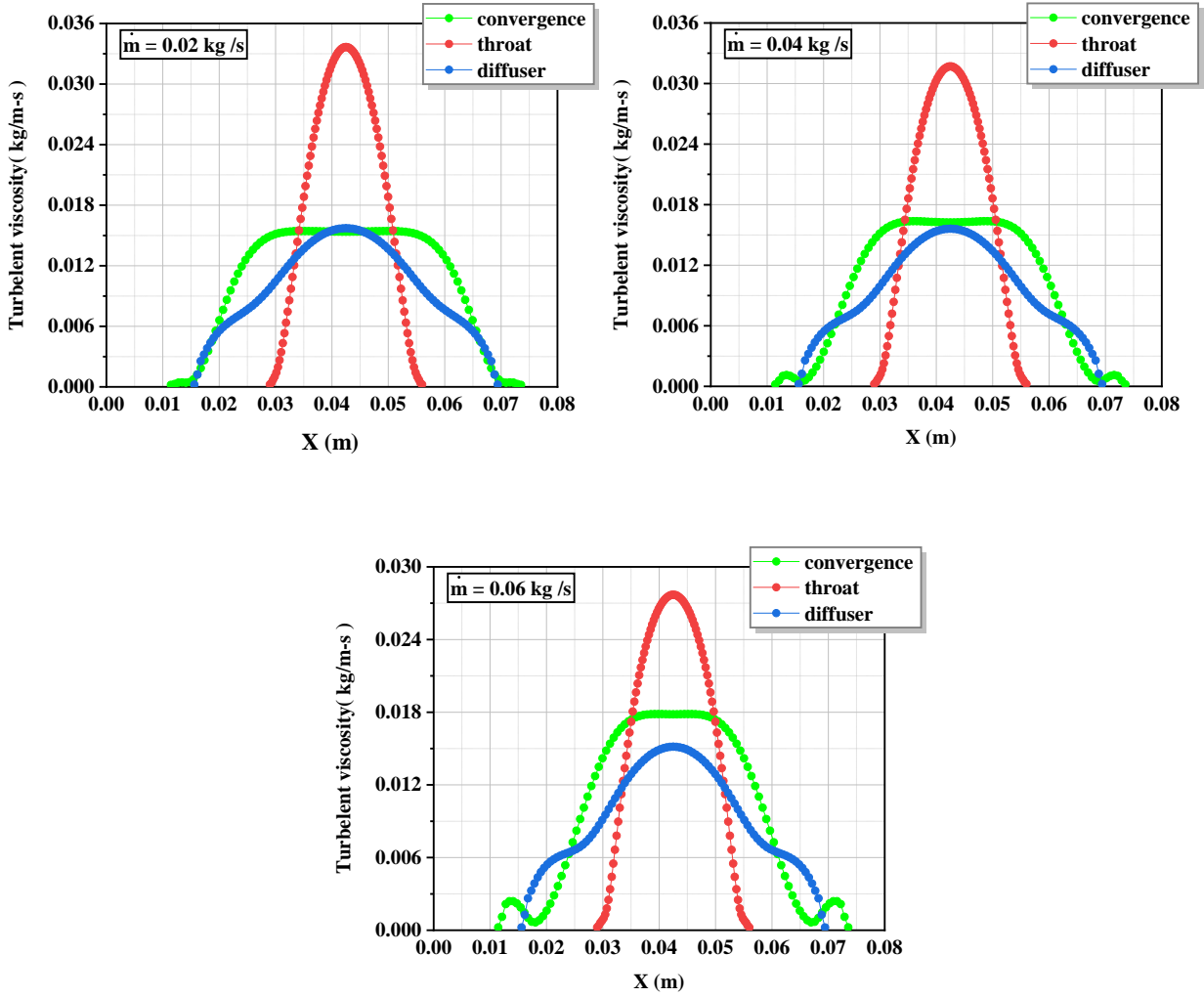


Figure IV.20: Evolution of turbulent viscosity in different sections of the venturi with gas velocity of 25 m / s for different water mass flow rates.

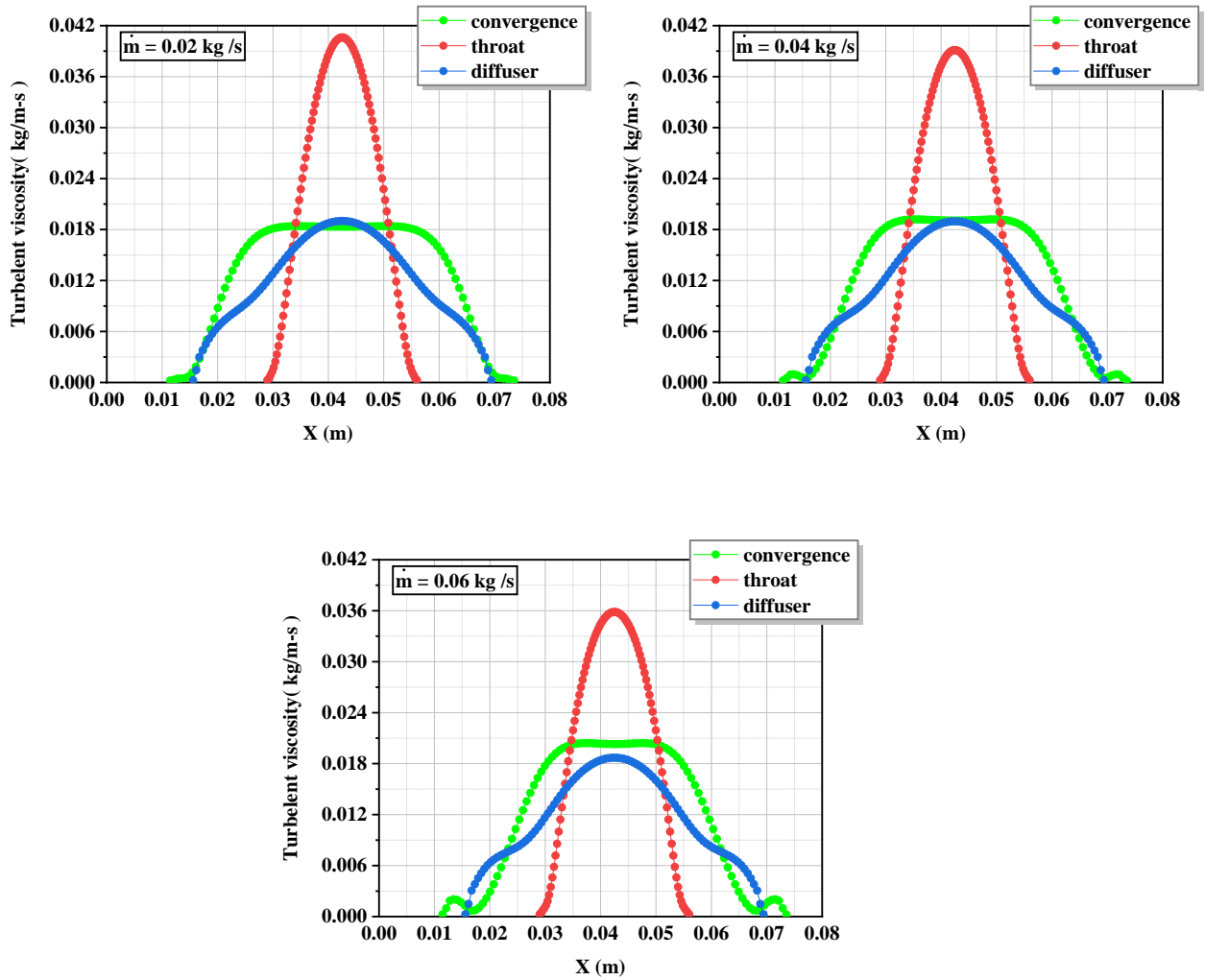


Figure IV. 21: Evolution of turbulent viscosity in different sections of the venturi with gas velocity of 30 m / s for different water mass flow rates.

IV.9 Conclusion

This chapter studied the behavior of flows in venturi by examining the most important parameters of velocity, pressure, turbulent kinetic energy, turbulent dissipation rate, pressure drop, and turbulent viscosity .as well as focusing on the effect of gas velocity and mass of liquid flow.

Chapter V:

Heat and Mass Transfer in venturi

V.1 Introduction

The objective of this chapter is to present the results of the heat and mass transfer in venturi. The results represent the contour of the temperature distribution, the contours of mass fraction, the temperature evolution curves, and mass fraction for gas and liquid and display the results of the Nusselt number, the PDF probability density function, removal efficiency, and the removal energy cost.

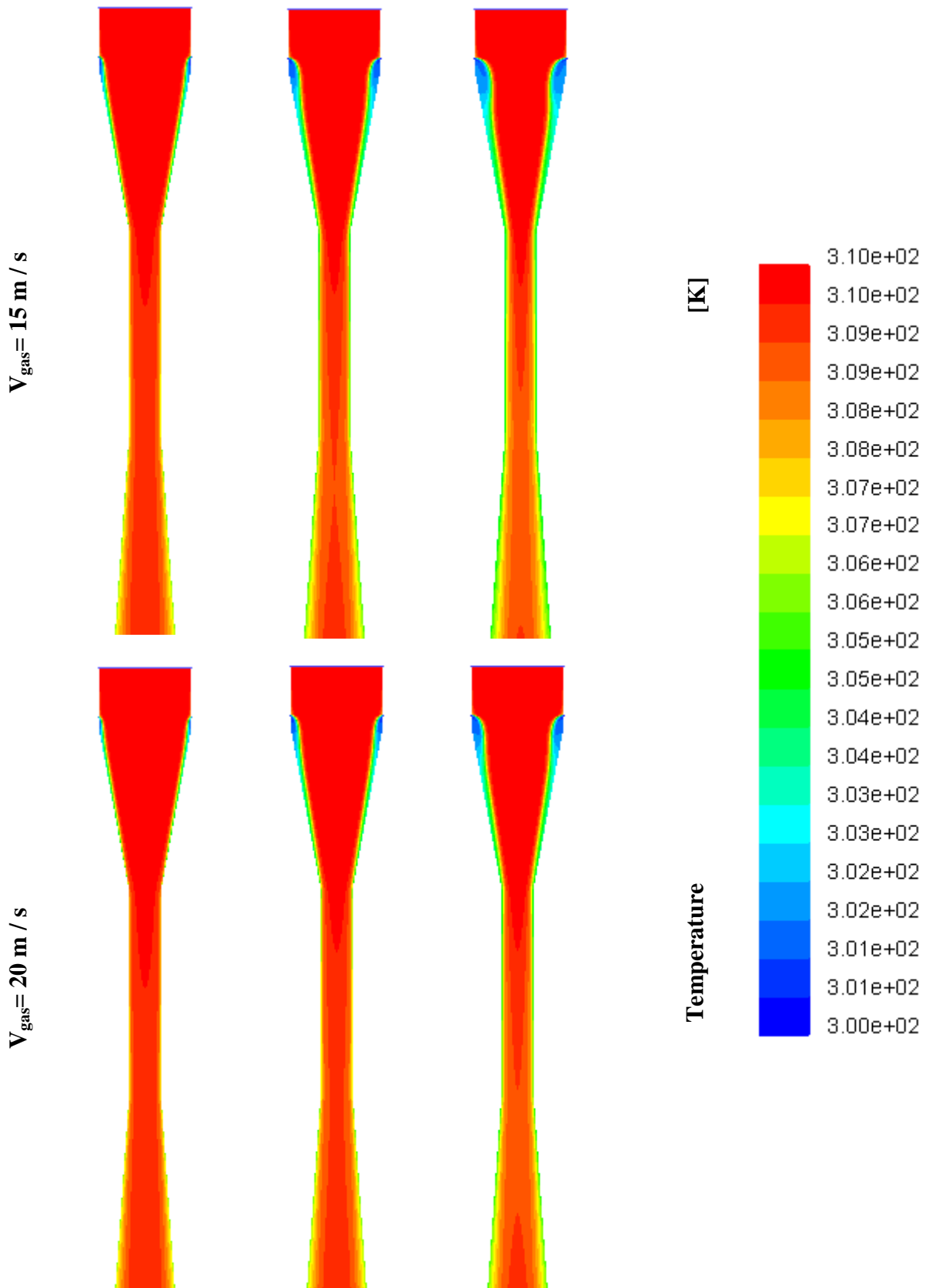
V.2 Evolution of temperature

The contour of temperature in venturi scrubber represents in Figure V.1. In all cases, the temperature decreases at the water inlet and near the wall.

Figure V.2 represents temperature profiles as a function of different gas velocities at the middle vertical line of the venturi with inlet water mass flow 0.02, 0.04, and 0.06 kg /s. From the figure, it is clear that the temperature is constant and when the liquid enters decreases a little and then increases. In all cases, the velocities of the gas have little effect on the temperature. The temperature decreases more with the gas velocity of 15 m/s. Also, the fluid mass flow has little effect on the temperature, as the temperature decreases more with the mass flow of water 0.06 kg/s.

HEAT AND MASS TRANSFER IN VENTURI SCRUBBER

$\dot{m} = 0.02 \text{ kg / s}$ $\dot{m} = 0.04 \text{ kg / s}$ $\dot{m} = 0.06 \text{ kg / s}$



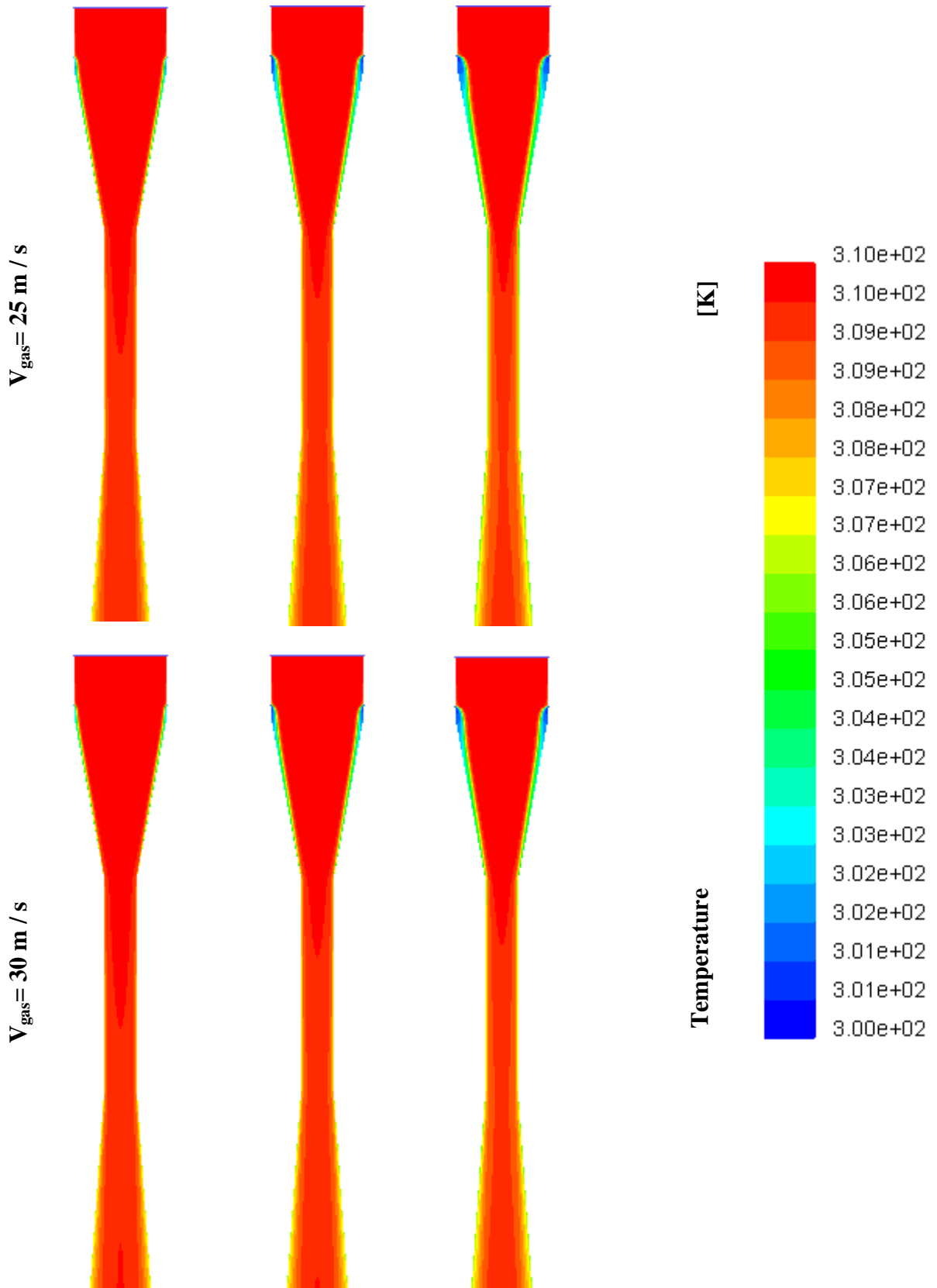


Figure V.1: Contours of temperature.

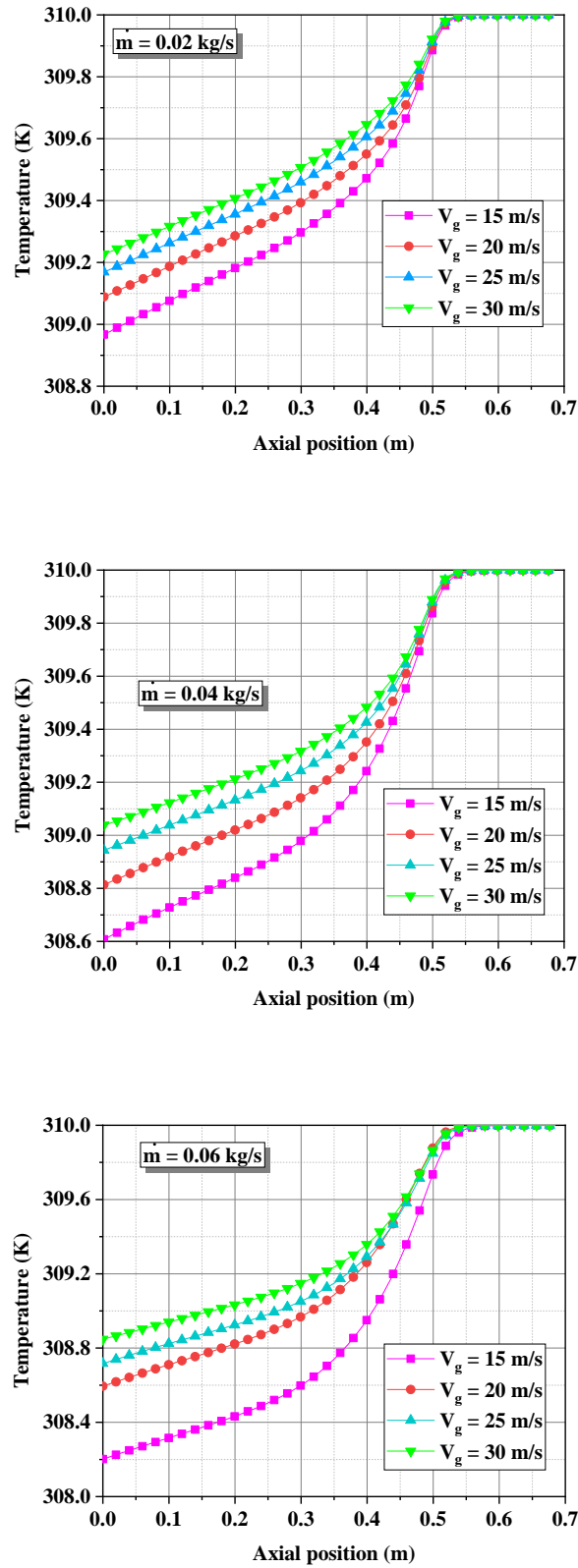


Figure V.2: Temperature profiles in the axial position with different gas velocities for different water mass flow rates.

V.3 The local Nusselt number evolution

Figures V.3-V.6 show the evolution of the local Nusselt number on the length of venturi. We note that the heat transfer increases in the convergent (conversion of potential energy into kinetic energy), this increase leads to an increase in heat exchange between the wall and the flow. Heat transfer reaches maximum values in the throat, and then decreases when crossing the divergent to tend asymptotically towards a constant value at the outlet of the venturi because the flow velocity decreases in this section due to the increase in the diameter of the venturi, which leads to a decrease in convection and heat transfer. Increasing the liquid mass flow rate decreases the heat flux transfer causing a decrease in the local Nusselt number.

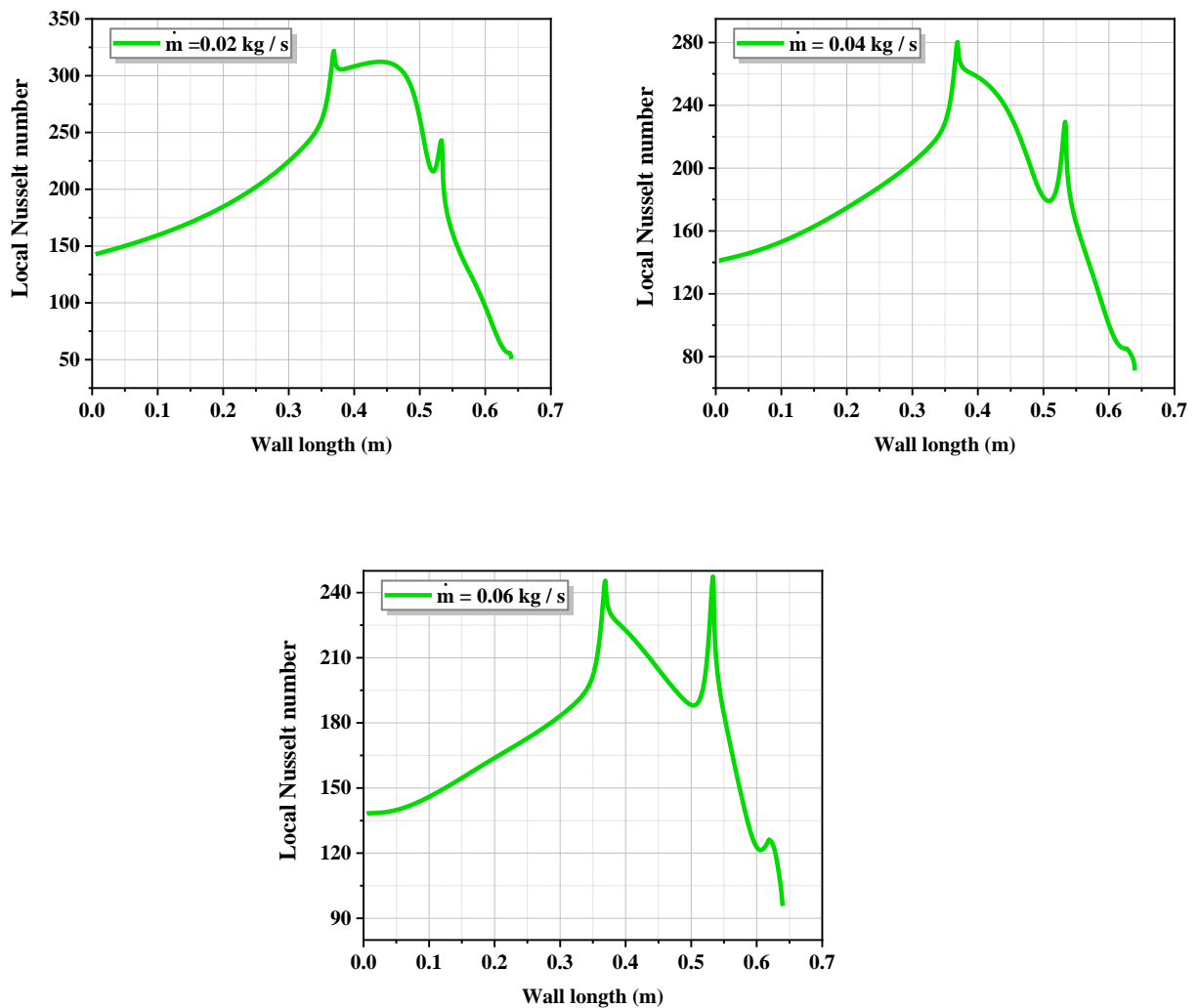


Figure V.3: The evolution of the local Nusselt number on the length of venturi with gas velocity of 15 m/s.

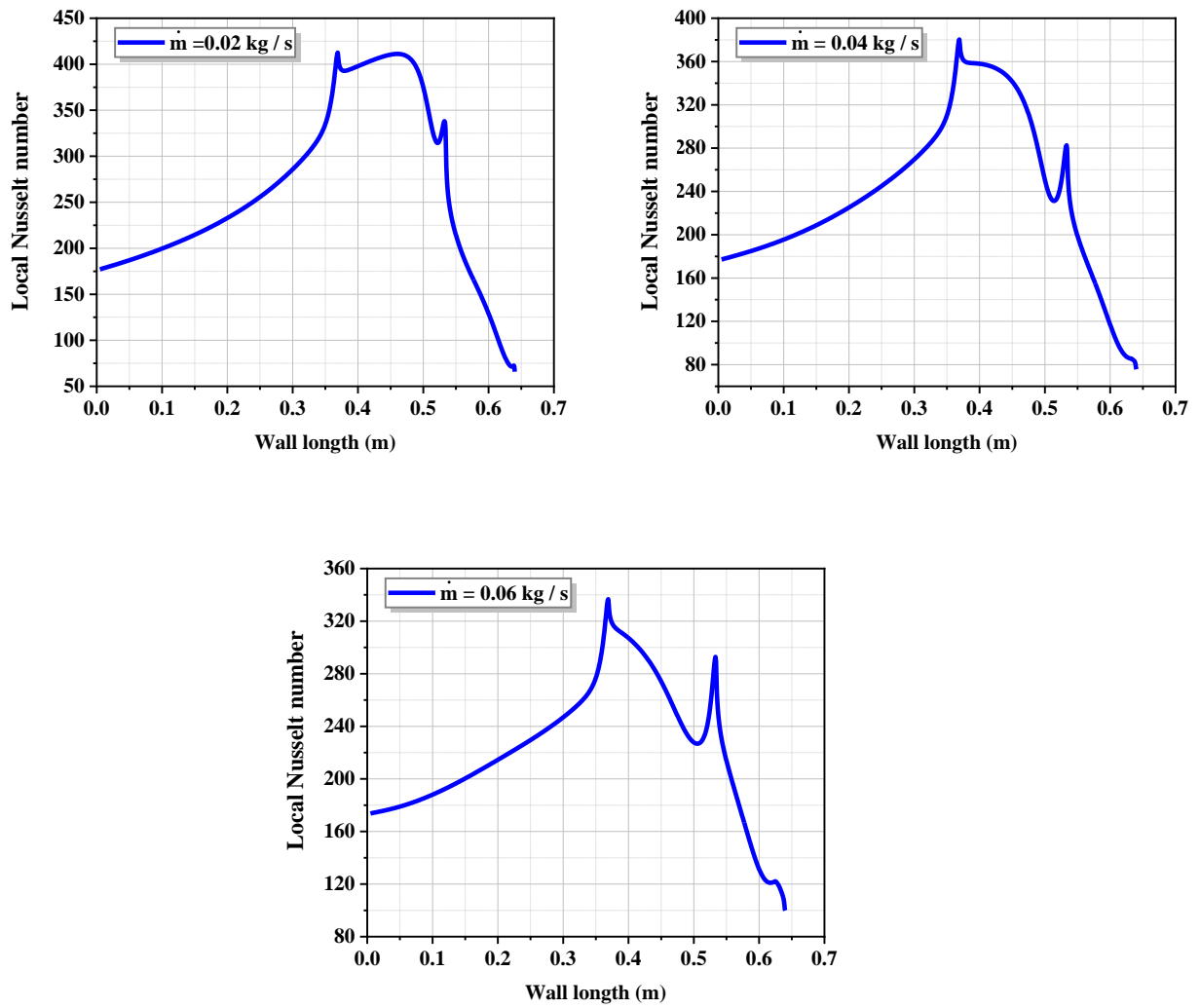


Figure V.4: The evolution of the local Nusselt number on the length of venturi with gas velocity of 20 m/s.

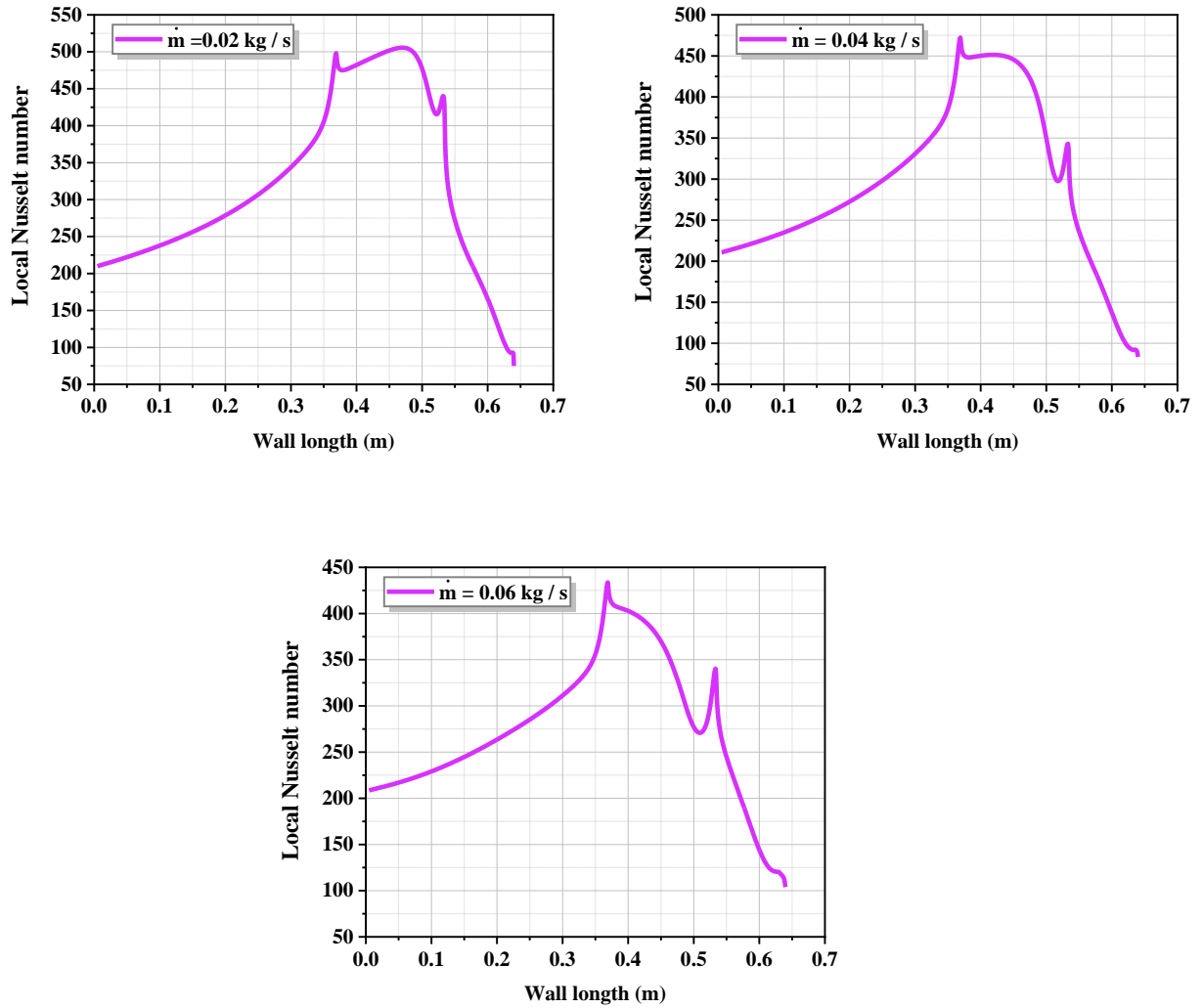


Figure V.5: The evolution of the local Nusselt number on the length of venturi with gas velocity of 25 m/s.

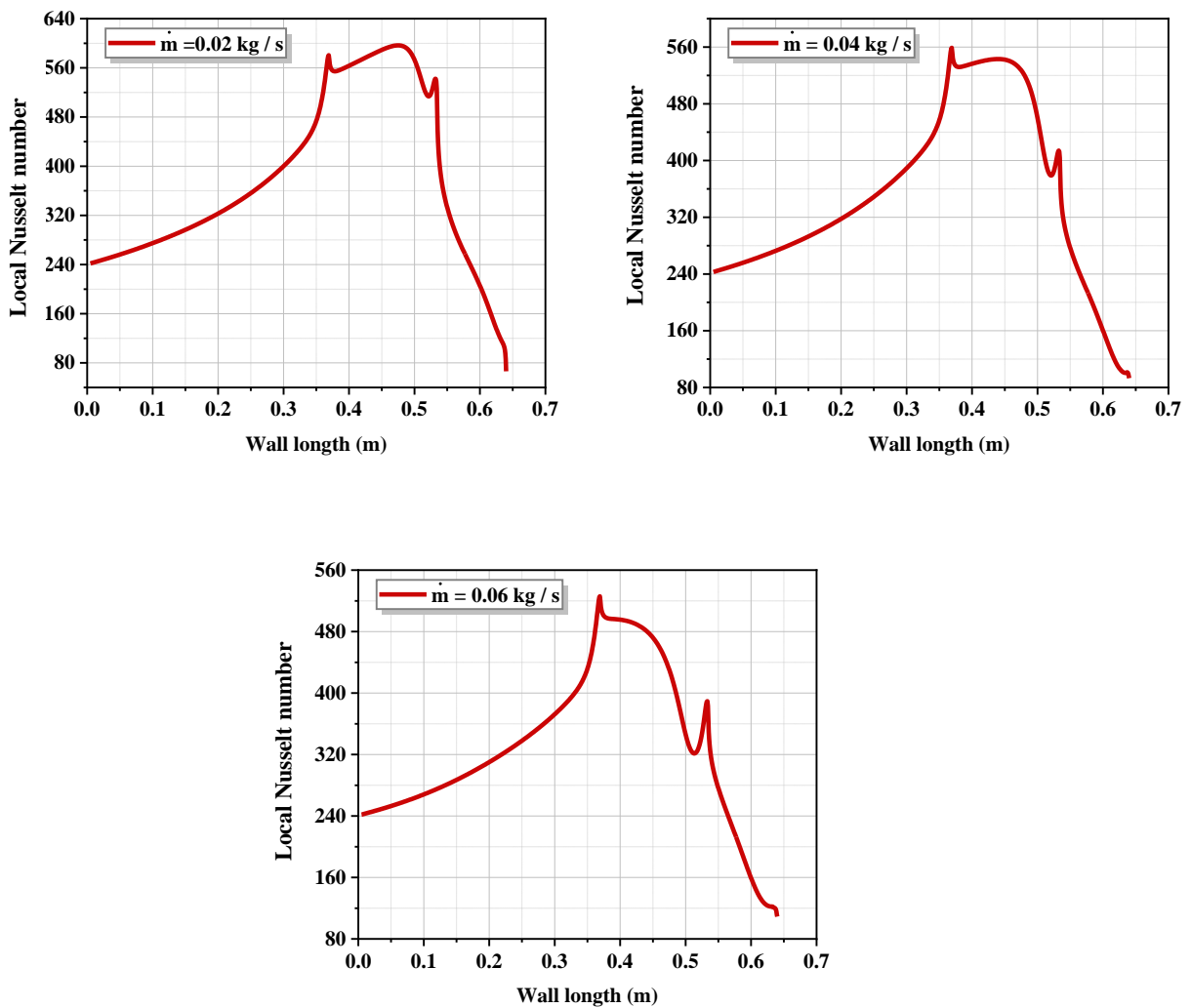
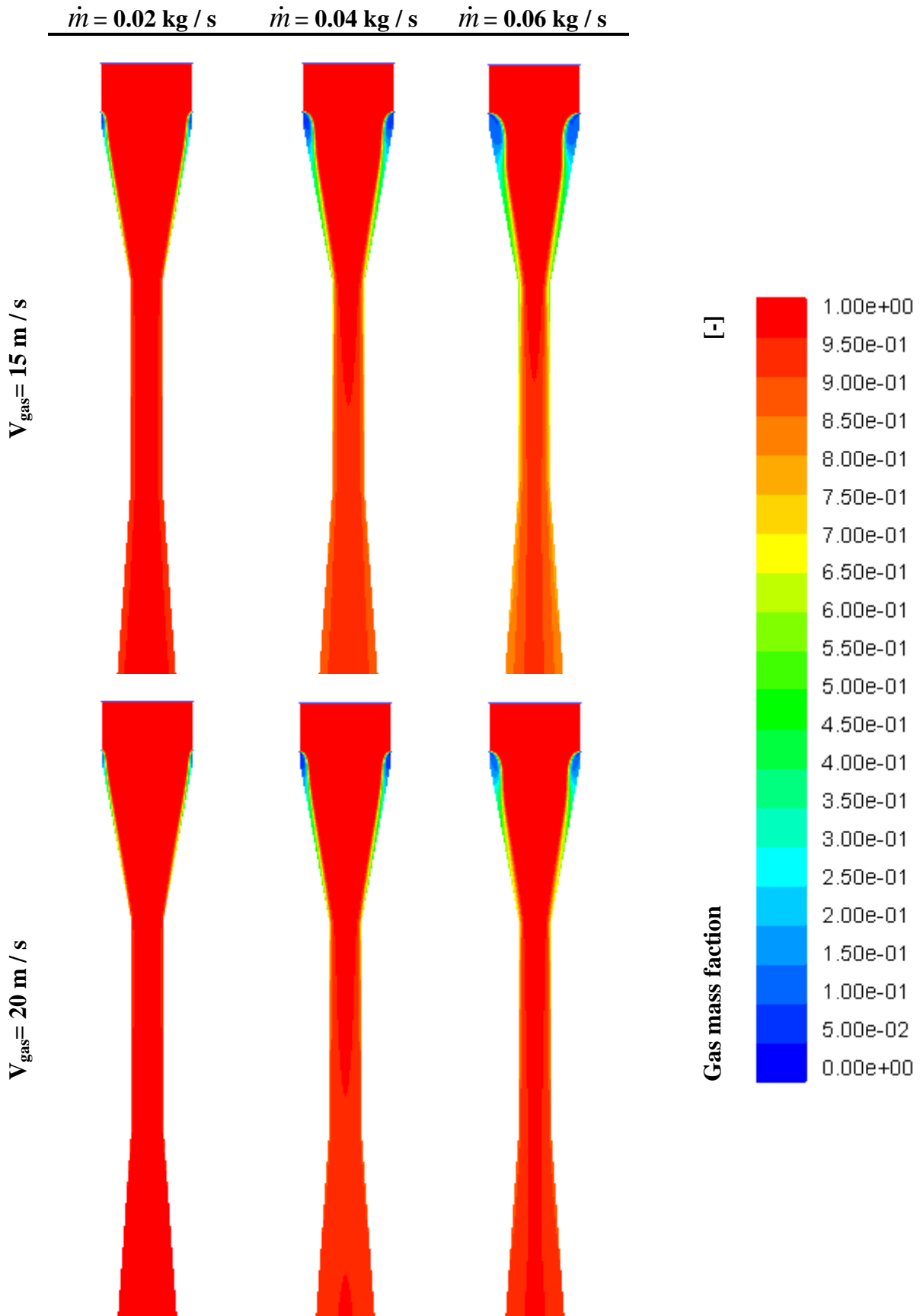


Figure V.6: The evolution of the local Nusselt number on the length of venturi with gas velocity of 30 m/s.

V.4 Mass fraction variations

V.4.1 Mass fraction of gas

The mass fraction of the gas contour represents in Figure V.7. In all cases, the mass fraction is high as it covers almost every venturi and is low at the water inlet and near the wall, especially with a mass water flow of 0.06 kg/s.



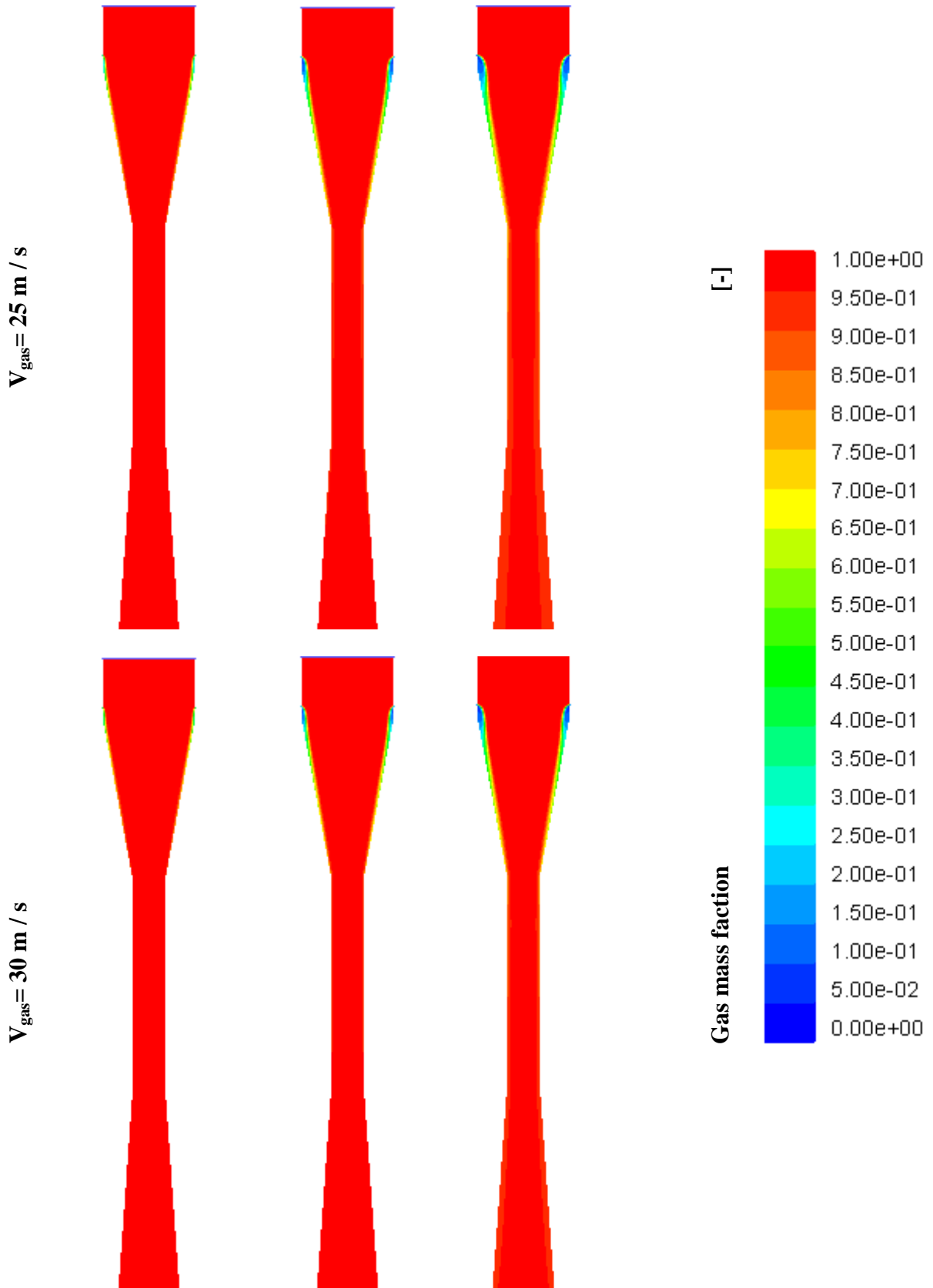


Figure V.7: Contours of the gas mass fraction.

Figure V.8 represented mass fraction evolution of gas at along the venturi scrubber axis. In the different cases, the mass fraction is at its maximum value before the water inlet. At the inlet of the water, the gas mass fraction decreases until it reaches a constant value at the outlet. Gas mass fraction decreases more in the case of the gas velocity of 15 m/s and the water mass flow rate of 0.06 kg/s.

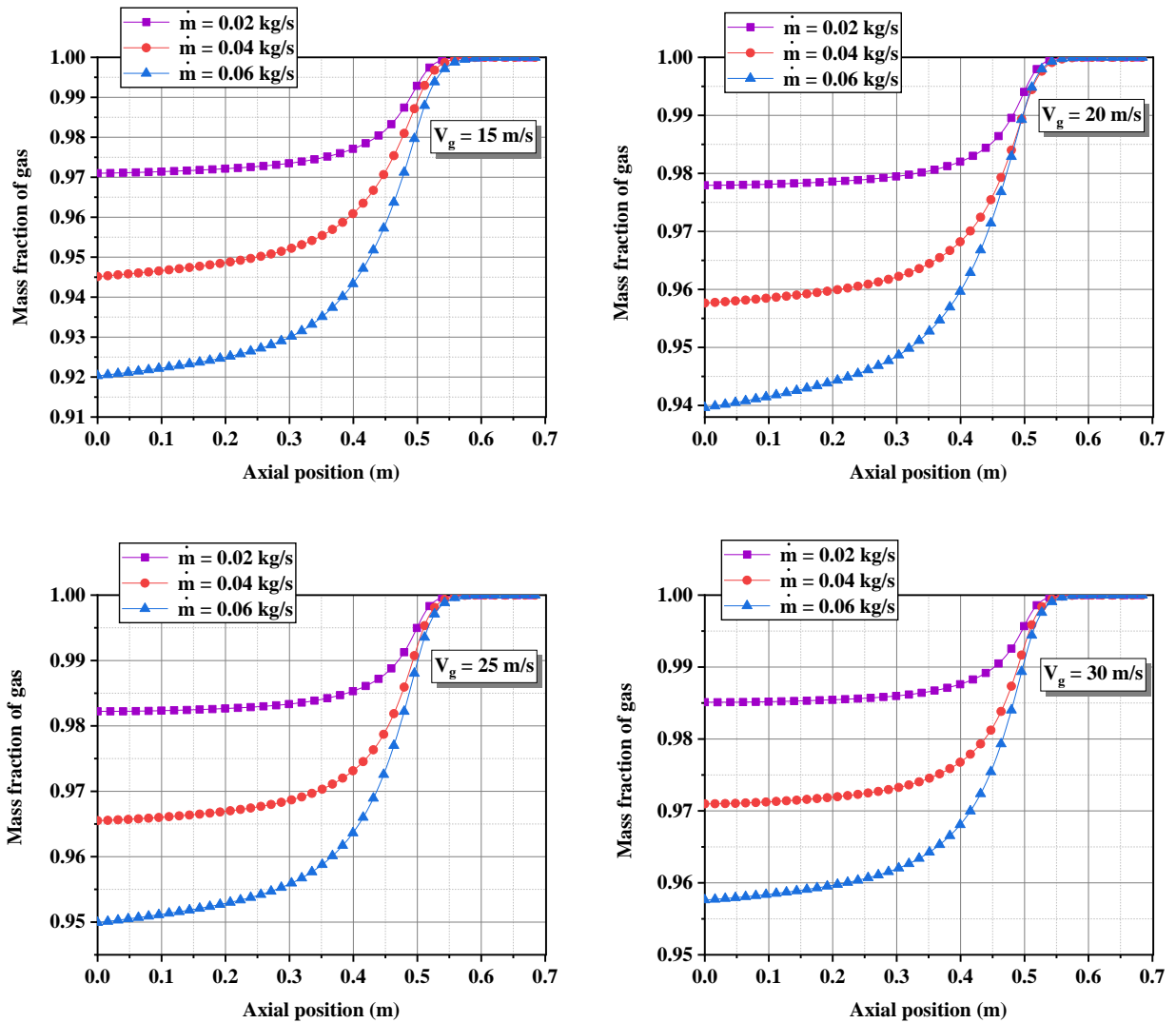


Figure V.8: Mass fraction evolution of gas at along the venturi scrubber axis.

Figure V.9 shows the mass transfer for the different gas velocity inlet cases in the venturi's throat. It observed that the gas mass fraction is high in the center of the throat and lowered at the wall of a venturi scrubber for all cases of water mass flow. The mass flow of liquid affects the mass fraction of the gas, as the increase in the mass flow of the liquid decreases the value of the

gas mass fraction, and the gas velocity also affects it, the higher the gas velocity, the higher the value of the gas mass fraction.

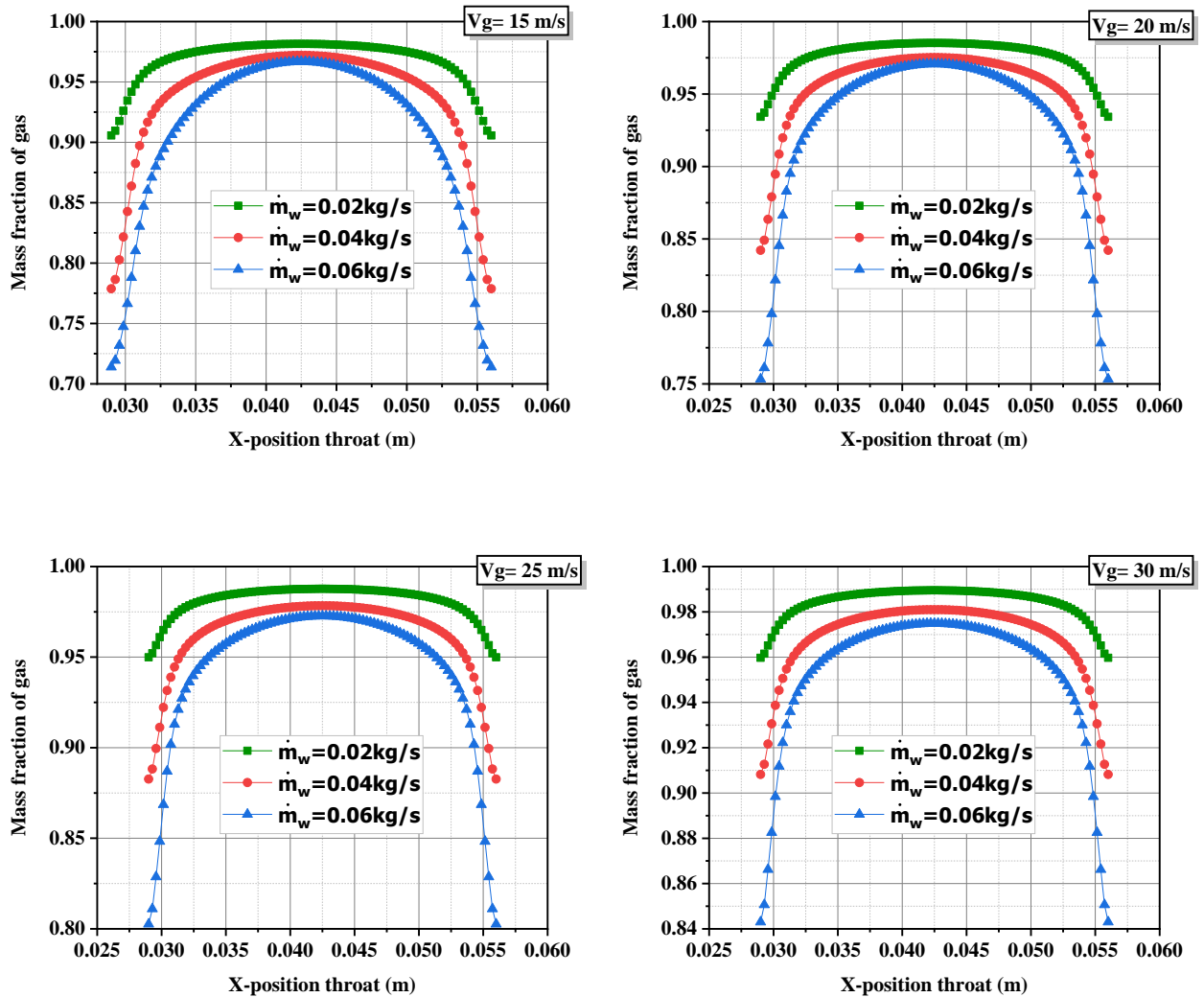
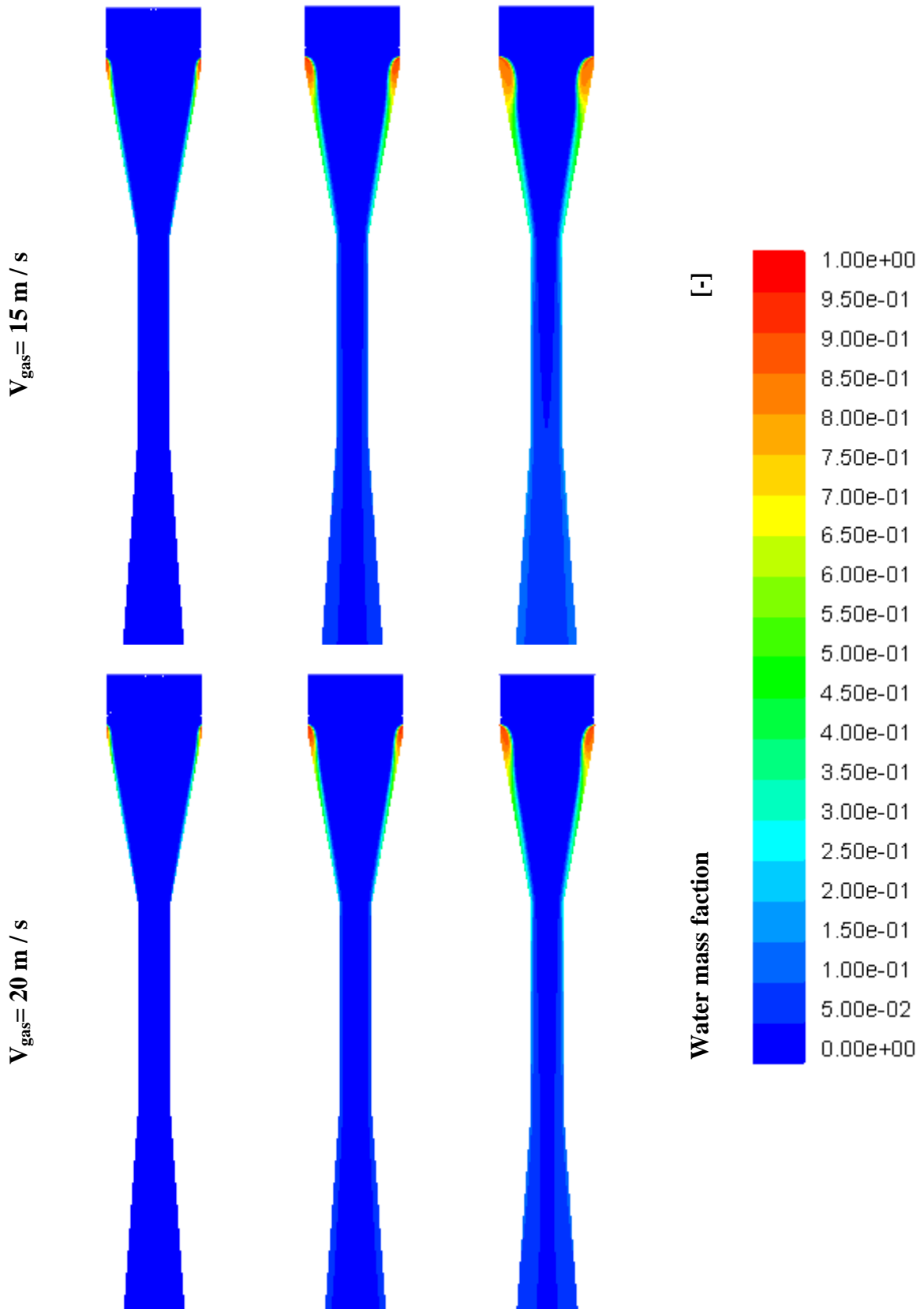


Figure V.9: Mass fraction of gas at X-position in the venturi throat.

V.4.2 Mass fraction of water

The mass fraction of the water contour represents in Figure V.10. In all cases, the mass fraction is high at the water inlet, especially with the mass flow water inlet 0.06 kg/s then concentrates on the wall under the influence of the high velocity of the gas.

$\dot{m} = 0.02 \text{ kg / s}$ $\dot{m} = 0.04 \text{ kg / s}$ $\dot{m} = 0.06 \text{ kg / s}$



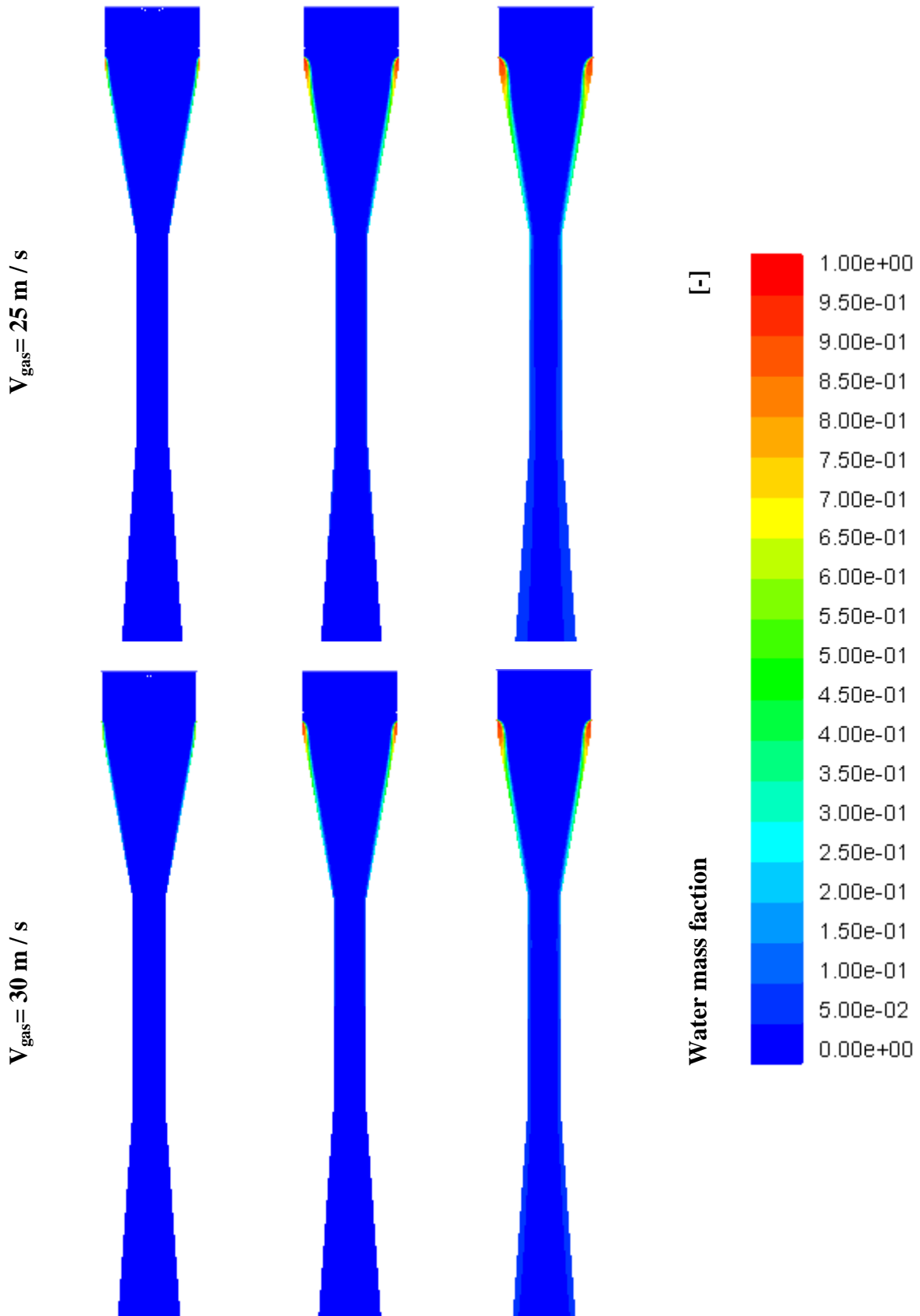


Figure V.10: Contours of water mass fraction.

Figure V.11 represented mass fraction evolution of water at along the venturi scrubber axis. In the different cases, the mass fraction is null before the water inlet. At the inlet of the water, the water mass fraction increases until it reaches a constant value at the outlet. Water mass fraction increases more in the case of the gas velocity of 15 m/s and the water mass flow rate of 0.06 kg/s.

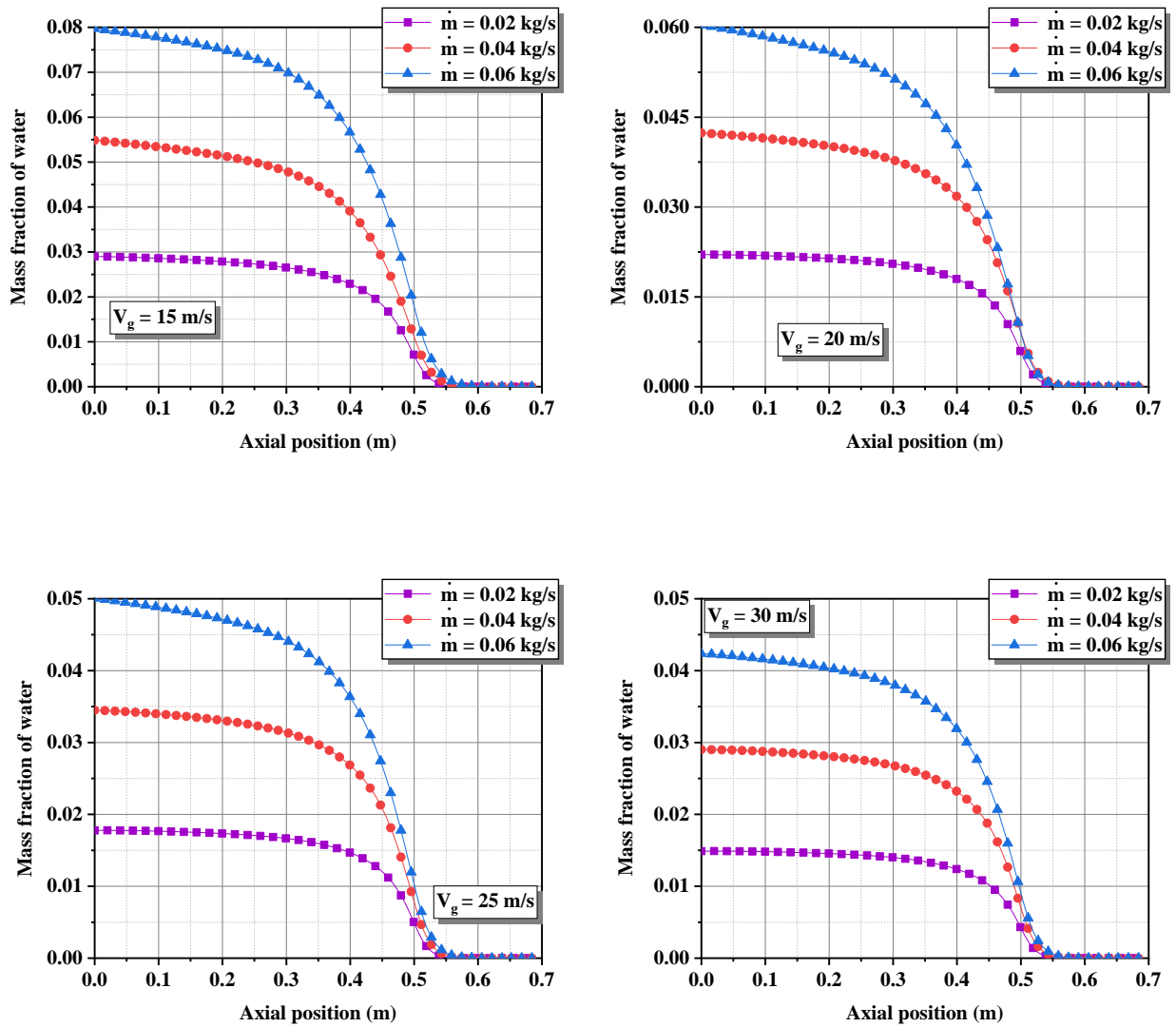


Figure V.11: Mass fraction evolution of water at along the venturi scrubber axis.

Figure V.12 shows the mass transfer for the different gas velocity inlet cases in the venturi's throat. We observed that the water mass fraction is Low in the center of the throat and high at the wall of a venturi scrubber for all cases of water mass flow. The mass flow of liquid affects the mass fraction of the water, as the increase in the mass flow of the liquid increases the value of the water mass fraction, and the gas velocity also affects it, the higher the gas velocity, the lower the value of the water mass fraction.

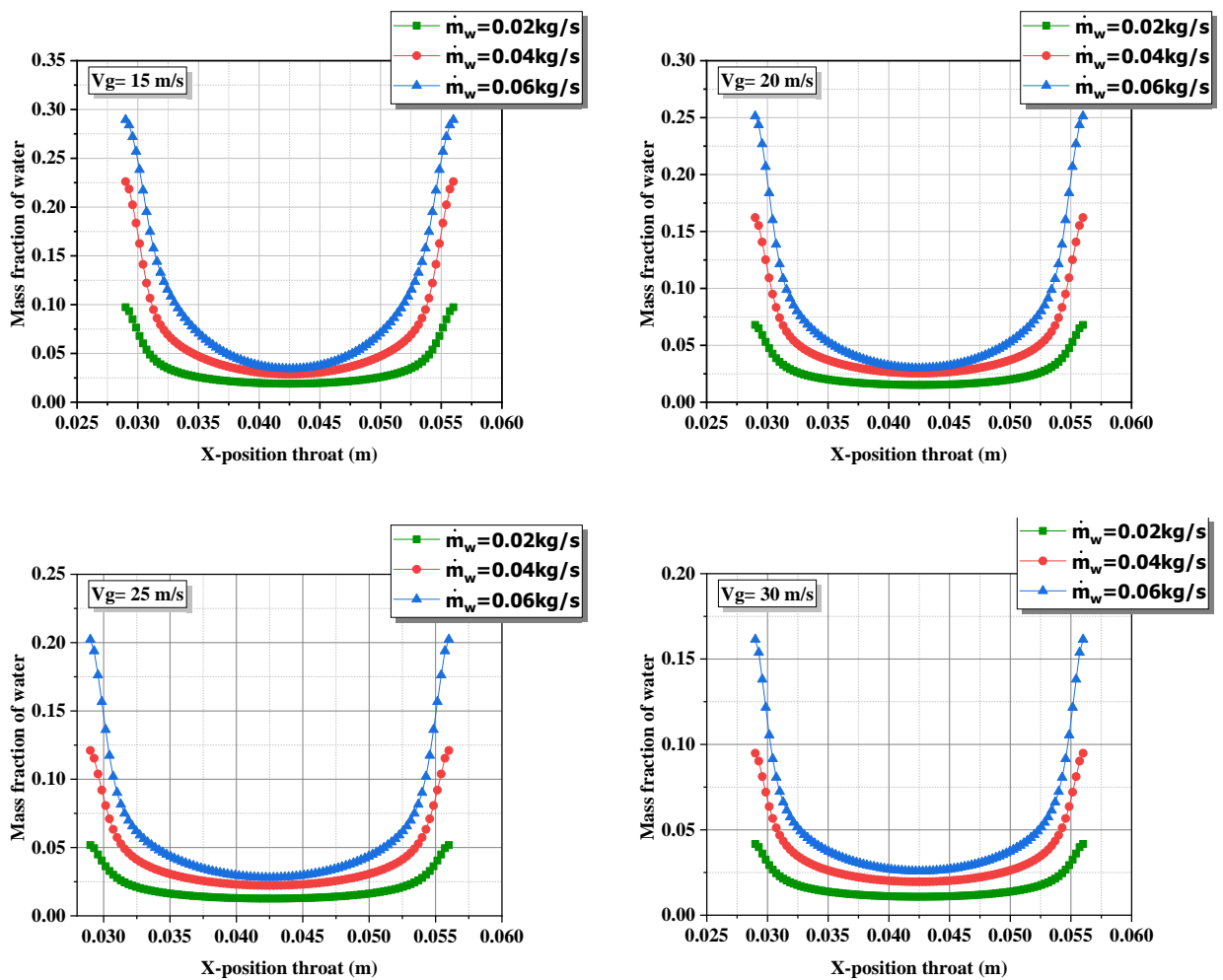


Figure V.12: Mass fraction of water at X-position in venturi throat.

V.5 The probability density function (PDF)

Figure IV.13 express the probability density function for the mass fraction of water with the velocity difference of water mass flow inlet and a constant gas velocity inlet in a venturi. We see that the large percentages of PDF were with a volume fraction less than 0.1 for all cases. This result indicates that the mass transfer in the venturi scrubber is weak.

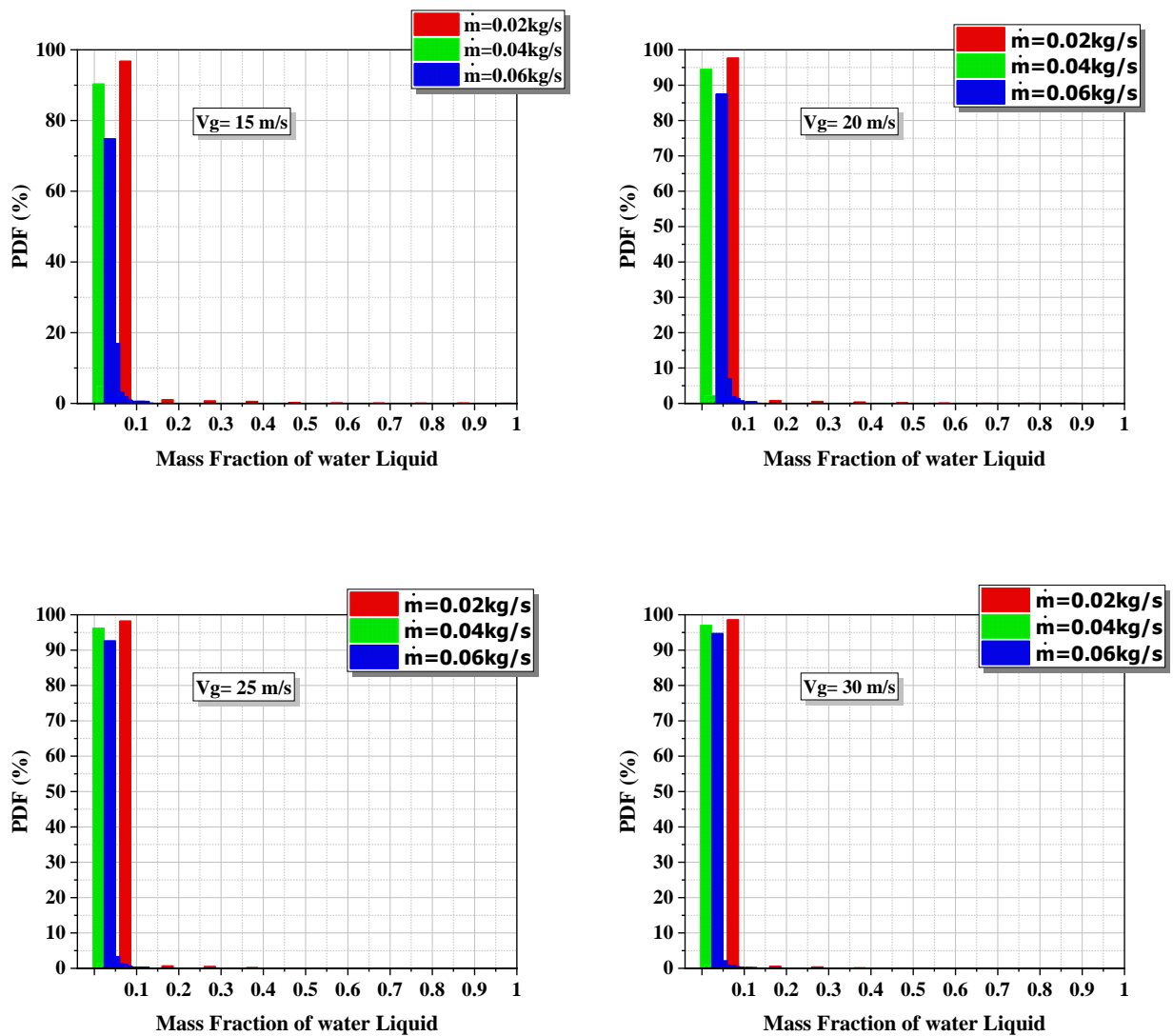


Figure V.13: The probability density functions of water mass fraction.

The temperature distribution inside the venturi is affected by gas velocity and liquid mass flow rate as shown in the probability density function in Figure V.14.

We note that the large percentages of the probability density function with the temperature are 310 K in the case of gas velocity m/sec and liquid flow 0.02 Kg / s. This result indicates that the heat transfer is better with height gas velocity and lowest water mass flow rate.

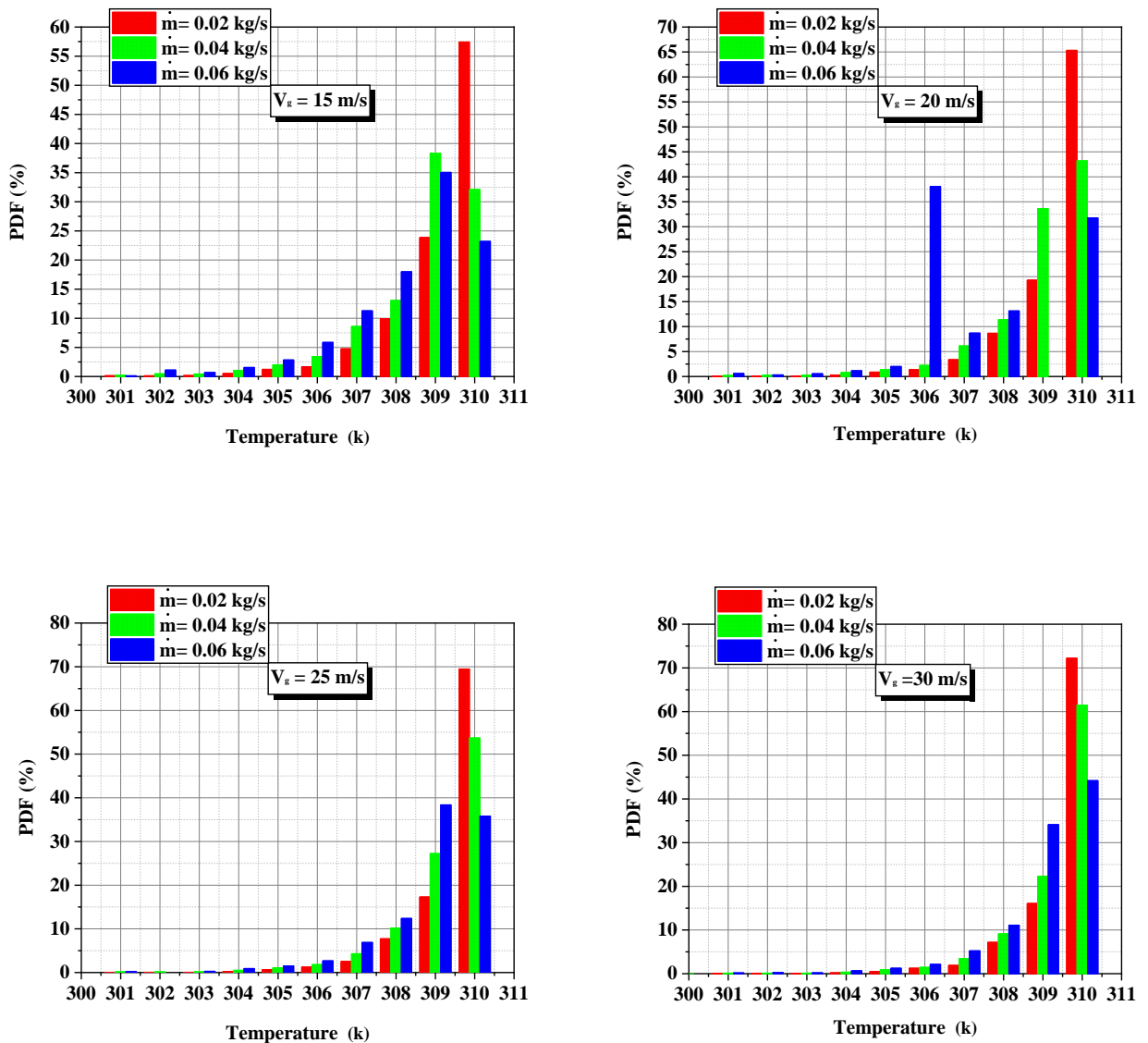


Figure V.14: The probability density function of temperature.

V-5 Removal efficiency and the removal energy cost

Figure V.15 shows the difference in removal efficiency at different mass flow rates. We observed that the removal efficiency of the venturi scrubber increases with a decrease in the liquid flow rate and an increase in the gas velocity.

Figure V.16 represents the effect of the temperature on the removal efficiency of venturi with gas velocity 30 m/s and different water mass flow. The figure shows the temperature does not affect the removal efficiency. That is, heat transfer has a weak effect on the removal efficiency.

Figure V.17 illustrates the evolution of the cost of removal energy of the venturi system for various cases of inlet mass flow rates. The removal energy cost increases with increasing water flow rate and the increase in the gas velocity.

The best case to use is the case where less energy with greater removal efficiency, as shown from the curves in the case of low liquid flow rate, the removal energy cost is less.

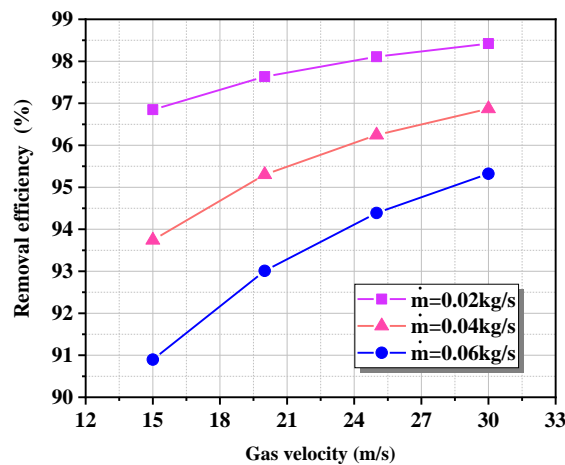


Figure V.15: Removal Efficiency of venturi scrubber at different fluid flow rates.

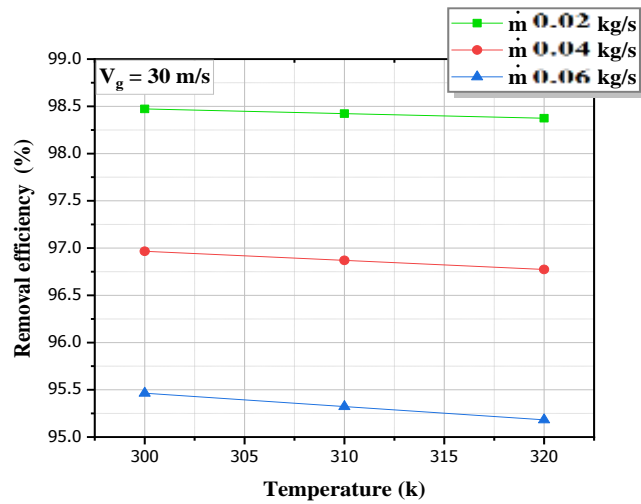


Figure V.16 : Effect the temperature on the Removal Efficiency.

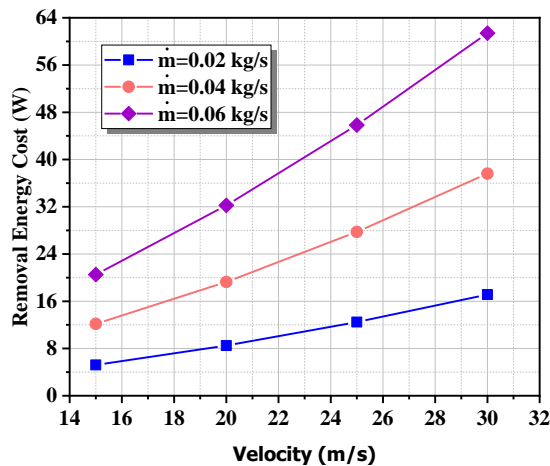


Figure V.17: Removal Efficiency Cost of venturi scrubber at different fluid flow rates.

V.7 Conclusion

This chapter included the results of thermal and mass transfer at venturi. By observing the contour of temperature, mass fraction, evolution curves Nusselt number curves, and the PDF probability density function. The heat and mass transfer have little effect on venturi devices, and the use of venturi devices in cleaning gases resulting from biomass gasification gives good collection efficiency.

General Conclusion

VI.1 General conclusion

We have conducted a numerical study to examine the cleaning of gas produced from biomass using venturi scrubber and the heat and mass transfer. The study investigated a two-dimensional numerical simulation using ANSYS Fluent code. We used the species transport model for the multiphase flow and the model $k - \varepsilon$ for the turbulent model.

This study considered the evolution of velocity, pressure, and pressure drop. The turbulent forced convection and mass transfer are studied. Evaluated the efficiency of the venturi scrubber is in cleaning the gas produced from biomass. The most important results are as follows:

- ❖ The velocity increase reached its maximum value with the highest gas velocity and the highest liquid rate at the entrances.
- ❖ The static pressure reached its minimum value with the highest gas velocity and the highest liquid rate at the entrances.
- ❖ The dynamic pressure reached its maximum value with the highest gas velocity and the highest liquid rate at the entrances.
- ❖ The pressure drop increases with increasing velocity and fluid flow.
- ❖ The turbulent kinetic energy and turbulent dissipation rate have the maximum values near the wall in the throat. They increase by the increase in the velocity of the gas and decrease by increasing the liquid flow rate.
- ❖ The turbulent viscosity increases with the increase in the velocity of the gas and decreases with increasing the liquid mass flow rate. All cases have shown that the turbulent viscosity was the largest of its values in the throat.
- ❖ The temperature is not affected much by the gas velocity and the liquid mass flow.
- ❖ The local Nusselt number increases in the convergence until it reaches its maximum value in the throat section and decreases in the diffuser section. This number increases with the increase in the gas velocity and decreases with increases in the Liquid mass flow rate.
- ❖ The water mass fraction is high at the water inlet and concentrates on the wall under the influence of the high velocity of the gas.
- ❖ The gas mass fraction is low at the water inlet and near the wall after the water inlet and concentrates on inside the venturi scrubber.

- ❖ The result of probability density function indicates that the mass transfer in the venturi scrubber is weak and the heat transfer is better with height gas velocity and lowset water mass flow rate..
- ❖ The efficiency of venturi scrubber in cleaning the gas resulting from biomass gasification is up to 98%.
- ❖ The removal efficiency of the venturi scrubber increases with a decrease in the liquid flow rate and an increase in the gas velocity.
- ❖ The temperature does not largely affect the collection efficiency in the venturi scrubber.
- ❖ The REC increases with increasing in the gas velocity and increasing in the liquid mass flow rate.

VI .2 Suggestions

As perspectives, this study can extend to:

- Investigation of the mass transfer through a three-dimensional simulation of cleaning of the gas generated by biomass gasification.
- The study of the performance of venturi scrubber in cleaning the gas generated by biomass gasification experimentally.
- The study of the influence of the venturi scrubber on the cleaning performance of nanofluid.

These suggestions present an interesting study to complete our study.

References

References

- [1] S. B. Kadam and N. P. Gulhane, "Performance Review of Venturi Scrubber," *SSRN Electron. J.*, pp. 1–5, 2019, doi: 10.2139/ssrn.3362216.
- [2] J. Zhou, S. Zhou, and Y. Zhu, "Experiment and Prediction Studies of Marine Exhaust Gas SO₂ and Particle Removal Based on NaOH Solution with a U-Type Scrubber," *Ind. Eng. Chem. Res.*, vol. 56, no. 43, pp. 12376–12384, 2017, doi: 10.1021/acs.iecr.7b02397.
- [3] Q. Xie *et al.*, "Fast microwave-assisted catalytic gasification of biomass for syngas production and tar removal," *Bioresour. Technol.*, vol. 156, pp. 291–296, 2014, doi: 10.1016/j.biortech.2014.01.057.
- [4] R. A. Pulley, "Modelling the performance of venturi scrubbers," *Chem. Eng. J.*, vol. 67, no. 1, pp. 9–18, 1997, doi: 10.1016/S1385-8947(97)00014-4.
- [5] M. Lehner, "Aerosol Separation Efficiency of a Venturi Scrubber Working in Self-Priming Mode," *Aerosol Sci. Technol.*, vol. 28, no. 5, pp. 389–402, 1998, doi: 10.1080/02786829808965533.
- [6] P. Goel, A. Moharana, and A. K. Nayak, "Experimental Investigation of Hydrodynamics Behavior of a Submerged Venturi Scrubber," *Multiph. Sci. Technol.*, vol. 31, no. 1, pp. 45–59, 2019, doi: 10.1615/MultScienTechn.2019029434.
- [7] X. Gamisans, M. Sarrà, F. J. Lafuente, and B. J. Azzopardi, "The hydrodynamics of ejector-Venturi scrubbers and their modelling by an annular flow/boundary layer model," *Chem. Eng. Sci.*, vol. 57, no. 14, pp. 2707–2718, 2002, doi: 10.1016/S0009-2509(02)00171-9.
- [8] X. Gamisans, M. Sarrà, and F. J. Lafuente, "Fluid flow and pumping efficiency in an ejector-venturi scrubber," *Chem. Eng. Process. Process Intensif.*, vol. 43, no. 2, pp. 127–136, 2004, doi: 10.1016/S0255-2701(03)00104-1.
- [9] C. D. Cooper and F. C. Alley, "Air Pollution Control: A Design Approach," Prospect Heights, III, Wavelans Press, Inc, 1994.

- [10] H. P. Robert, W. G. Don, and O. M. James, "Perry's chemical engineers' handbook," Nov. Iorque, 1984.
- [11] T. J. Overcamp and S. R. Bowen, "Effect of Throat Length and Diffuser Angle on Pressure Loss Across a Venturi Scrubber," *J. Air Pollut. Control Assoc.*, vol. 33, no. 6, pp. 600–604, 1983, doi: 10.1080/00022470.1983.10465616.
- [12] S. Viswanathan, "Examination of liquid film characteristics in the prediction of pressure drop in a Venturi scrubber," *Chem. Eng. Sci.*, vol. 53, no. 17, pp. 3161–3175, 1998, doi: 10.1016/S0009-2509(98)00123-7.
- [13] S. Viswanathan, A. W. Gnyp, and C. C. St. Pierre, "Annular flow pressure drop model for pease–anthony-type venturi scrubbers," *AIChE J.*, vol. 31, no. 12, pp. 1947–1958, 1985, doi: 10.1002/aic.690311204.
- [14] S. N. Rudnick, J. L. M. Koehler, K. P. Martin, D. Leith, and D. W. Cooper, "Particle Collection Efficiency in a Venturi Scrubber: Comparison of Experiments with Theory," *Environ. Sci. Technol.*, 1986, doi: 10.1021/es00145a002.
- [15] H. Haller, E. Muschelknautz, and T. Schultz, "Venturi scrubber calculation and optimization," *Chem. Eng. Technol.*, vol. 12, no. 1, pp. 188–195, 1989, doi: 10.1002/ceat.270120125.
- [16] B. J. Azzopardi, "Gas-liquid flows in cylindrical venturi scrubbers: Boundary layer separation in the diffuser section," *Chem. Eng. J.*, vol. 49, no. 1, pp. 55–64, 1992, doi: 10.1016/0300-9467(92)85025-5.
- [17] R. W. K. Allen and A. Van Santen, "Designing for pressure drop in Venturi scrubbers: The importance of dry pressure drop," *Chem. Eng. J. Biochem. Eng. J.*, vol. 61, no. 3, pp. 203–211, 1996, doi: 10.1016/0923-0467(95)03044-1.
- [18] S. Viswanathan, "Examination of liquid film characteristics in the prediction of pressure drop in a Venturi scrubber," *Chem. Eng. Sci.*, 1998, doi: 10.1016/S0009-2509(98)00123-7.
- [19] D. Fernandez Alonso, B. J. Azzopardi, and J. H. Hills, "Gas/liquid flow in laboratory-scale venturis," *Process Saf. Environ. Prot.*, vol. 77, no. 4, pp. 205–211, 1999, doi: 10.1205/095758299530080.

- [20] C.J.Tsai, C.H.Lin, Y-M.Wang, , C.H.Hunag, S.N. Li, , Wu, Z.X. and F-C. Wang, “An efficient venturi scrubber system to remove submicron particles in exhaust gas,” *J. Air Waste Manag. Assoc.*, vol. 55, no. 3, pp. 319–325, 2005, doi: 10.1080/10473289.2005.10464622.
- [21] M. A. Martins Costa, A. P. R. A. Ribeiro, É. R. Tognetti, M. L. Aguiar, J. A. S. Gonçalves, and J. R. Coury, “Performance of a Venturi scrubber in the removal of fine powder from a confined gas stream,” *Mater. Res.*, vol. 8, no. 2, pp. 177–179, 2005, doi: 10.1590/s1516-14392005000200016.
- [22] C. Huang, C. Tsai, and Y. Wang, “Control Efficiency of Submicron Particles by an Efficient Venturi Scrubber System,” *J. Environ. Eng.*, vol. 133, no. 4, pp. 454–461, 2007.
- [23] A. M. Silva, J. C. F. Teixeira, and S. F. C. F. Teixeira, “Experiments in a large-scale venturi scrubber. Part I: Pressure drop,” *Chem. Eng. Process. Process Intensif.*, vol. 48, no. 1, pp. 59–67, 2009, doi: 10.1016/j.cep.2008.02.001.
- [24] I. G. O. S. Wendsida, B. D. Joseph, Z. Belkacem, and C. Xavier, “EXPERIMENTAL STUDY OF GAS CLEANING BY A WET APPROACH VENTURI TYPE,” *Eng. Stud. Res.*, vol. 18, no. 1, pp. 104–110, 2012.
- [25] V. G. Guerra, R. Béttega, J. A. S. Gonçalves, and J. R. Coury, “Pressure drop and liquid distribution in a venturi scrubber: Experimental data and CFD simulation,” *Ind. Eng. Chem. Res.*, vol. 51, no. 23, pp. 8049–8060, 2012, doi: 10.1021/ie202871q.
- [26] A. Majid, Y. Changqi, S. Zhongning, G. Haifeng, and M. Khurram, “Dust particle removal efficiency of a venturi scrubber,” *Ann. Nucl. Energy*, vol. 54, pp. 178–183, 2013.
- [27] R. Desai and O. Sahu, “Study of Venturi Scrubber Efficiency for Pesticide Industry,” *Int. Lett. Nat. Sci.*, vol. 9, pp. 15–26, 2014, doi: 10.18052/www.scipress.com/ilns.9.15.
- [28] Y. Zhou, Z. Sun, H. Gu, and Z. Miao, “Experimental research on aerosols collection performance of self- priming venturi scrubber in FCVS,” *Prog. Nucl. Energy*, vol. 85, pp. 771–777, 2015, doi: 10.1016/j.pnucene.2015.09.009.

- [29] S. Unyaphan, T. Tarnpradab, F. Takahashi, and K. Yoshikawa, "An Investigation of Low Cost and Effective Tar Removal Techniques by Venturi Scrubber Producing Syngas Microbubbles and Absorbent Regeneration for Biomass Gasification," *Energy Procedia*, vol. 105, pp. 406–412, 2017, doi: 10.1016/j.egypro.2017.03.333.
- [30] S. Ali et al., "Experimental investigation of aerosols removal efficiency through self-priming venturi scrubber," *Nucl. Eng. Technol.*, 2020, doi: 10.1016/j.net.2020.03.019.
- [31] S. Calvert, "Venturi and other atomizing scrubbers efficiency and pressure drop," *AIChE J.*, vol. 16, no. 3, pp. 392–396, 1970, doi: 10.1002/aic.690160315.
- [32] R. H. Boll, "Particle Collection and Pressure Drop in Venturi Scrubbers," *Ind. Eng. Chem. Fundam.*, vol. 12, no. 1, pp. 40–50, 1973, doi: 10.1021/i160045a008.
- [33] K. G. T. Hollands and K. C. Goel, "A General Method for Predicting Pressure Loss in Venturi Scrubbers," *Ind. Eng. Chem. Fundam.*, vol. 14, no. 1, pp. 16–22, 1975, doi: 10.1021/i160053a003.
- [34] G. T. Kenneth Hollands and C. Goel Kailash "A General Method for Predicting Particulate Collection Efficiency of Venturi Scrubbers," *Ind. Engng Chem. Fundam*, vol. 2, pp. 186–193, 1977.
- [35] S. C. Yung, S. Calvert, H. F. Barbarlka, and L. E. Sparks, "Venturi Scrubber Performance Model," *Environ. Sci. Technol.*, vol. 12, no. 4, pp. 456–459, 1978, doi: 10.1021/es60140a009.
- [36] T. D. Placek and L. K. Peters, "Analysis of particulate removal in venturi scrubbers—role of heat and mass transfer," *AIChE J*, vol. 28, no. 1, pp. 31–39, 1982, doi: 10.1002/aic.690280106.
- [37] D. W. Cooper and D. Leith, "Venturi scrubber optimization revisited," *Aerosol Sci. Technol.*, vol. 3, no. 1, pp. 63–70, 1984, doi: 10.1080/02786828408958994.
- [38] T. R Azzopardi, B.J., Teixeira, S.F.C.F., Govan, A.H. and Bott, "Improved model for pressure drop in Venturi scrubbers." *Process Saf. Environ. Prot.*, vol. 69, no. 4, pp. 237–245, 1991.

- [39] N. V. Ananthanarayanan and S. Viswanathan, "Estimating Maximum Removal Efficiency in Venturi Scrubbers," *Environ. Energy Eng. Estim.*, no. October 2017, 1998, doi: 10.1002/cjce.5450830206.
- [40] J. A. S. Gonçalves, D. F. Alonso, M. A. M. Costa, B. J. Azzopardi, and J. R. Coury, "Evaluation of the models available for the prediction of pressure drop in venturi scrubbers," *J. Hazard. Mater.*, vol. 81, pp. 123–140, 2001, doi: 10.1016/S0304-3894(00)00336-8.
- [41] H. Sun and B. J. Azzopardi, "Modelling gas-liquid flow in venturi scrubbers at high pressure," *Process Saf. Environ. Prot. Trans. Inst. Chem. Eng. Part B*, vol. 81, no. 4, pp. 250–256, 2003, doi: 10.1205/095758203322299770.
- [42] S. Viswanathan, N. V. Ananthanarayanan, and B. J. Azzopardi, "Venturi Scrubber Modelling and Optimization," *Can. J. Chem. Eng.*, vol. 83, no. 2, pp. 194–203, 2005, doi: 10.1002/cjce.5450830206.
- [43] A. Rahimi, M. Taheri, and J. Fathikakajahi, "Mathematical modelling of non-isothermal venturi scrubbers," *Can. J. Chem. Eng.*, 2005, doi: 10.1002/cjce.5450830302.
- [44] S. Nasseh, A. Mohebbi, Z. Jeirani, and A. Sarrafi, "Predicting pressure drop in venturi scrubbers with artificial neural networks," *Hazard. Mater.* 143, vol. 143, pp. 144–149, 2007, doi: 10.1016/j.jhazmat.2006.09.005.
- [45] A. A. Economopoulou, R. M. Harrison, "Graphical Analysis of the Performance of Venturi Scrubbers for Particle Abatement. Part I: Rapid Collection Efficiency Evaluation," *Aerosol Sci. Technol.*, no. April 2015, pp. 37–41, 2007, doi: 10.1080/02786820601112839.
- [46] M. Taheri and A. Mohebbi, "Design of artificial neural networks using a genetic algorithm to predict collection efficiency in venturi scrubbers," *Hazard. Mater.* 157, vol. 157, pp. 122–129, 2008, doi: 10.1016/j.jhazmat.2007.12.107.
- [47] A. Kumar, P. Kumar, and S. K. Singal, "Performance of A Venturi Scrubbers in Intermediate Drop Reynolds Number Regime for Small Particles at Different Throat Length and Throat Gas Velocity," *Asian J. Water, Environ. Pollut.*, vol. 6, no. 2, pp. 7–13, 2008.

- [48] S. Nasseh, A. Mohebbi, A. Sarrafi, and M. Taheri, "Estimation of pressure drop in venturi scrubbers based on annular two-phase flow model , artificial neural networks and genetic algorithm," *Chem. Eng.*, vol. 150, pp. 131–138, 2009, doi: 10.1016/j.cej.2008.12.011.
- [49] A. Rahimi, A. Niksiar, and M. Mobasheri, "Considering roles of heat and mass transfer for increasing the ability of pressure drop models in venturi scrubbers," *Chem. Eng. Process. Process Intensif.*, vol. 50, no. 1, pp. 104–112, 2011, doi: 10.1016/j.cep.2010.12.003.
- [50] A. A. Shraiber, I. V. Fedinchik, and M. V. Protasov, "On effect of gas flow turbulence on the efficiency of particle collection in a Venturi scrubber," *High Temp.*, vol. 53, no. 1, pp. 80–85, 2015, doi: 10.1134/S0018151X14060145.
- [51] J. Kim, J. W. Park, and S. Korea, "Comparative Study on One-Dimensional Models for Particle Collection Efficiency of a Venturi Scrubber Comparative Study on One-Dimensional Models for Particle Collection Efficiency of a Venturi Scrubber," *Adv. Sci. Technol. Lett. Vol.140*, no. December, 2016, doi: 10.14257/astl.2016.140.47.
- [52] M. Ali, Y. Changqi, S. Zhongning, W. Jianjun, and K. Mehboob, "CFD Simulation of Prediction of Pressure Drop in Venturi Scrubber," *Appl. Mech. Mater.*, vol. 169, pp. 3008–3011, 2012, doi: 10.4028/www.scientific.net/AMM.166-169.3008.
- [53] M. Ali, C. Q. Yan, Z. N. Sun, J. J. Wang, and A. Rasool, "CFD Simulation of throat pressure in venturi scrubber," in *Applied Mechanics and Materials*, 2012, vol. 170, pp. 3630–3634, doi: 10.4028/www.scientific.net/AMM.170-173.3630.
- [54] M. Ali, C. Yan, Z. Sun, J. Wang, and H. Gu, "CFD simulation of dust particle removal efficiency of a venturi scrubber in CFX," *Nucl. Eng. Des.*, vol. 256, pp. 169–177, 2013, doi: 10.1016/j.nucengdes.2012.12.013.
- [55] M. M. Toledo-Melchor et al., "Numerical simulation of flow behavior within a venturi scrubber," *Math. Probl. Eng.*, vol. 2014, 2014, doi: 10.1155/2014/106329.
- [56] S. Kousalya, S .Venkatesh , and Chandrasekaran, "Performance Improvement of Venturi Wet Scrubber," *Mech. Civ. Eng.*, vol. 2, no. April 2015.

- [57] S. A. Qamar, A. Sohail, K. Qureshi, A. Shah, and N. Irfan, "Dust particle collection efficiency of venturi scrubber with varying number of orifices using CFX," ICET 2016 - 2016 Int. Conf. Emerg. Technol., 2017, doi: 10.1109/ICET.2016.7813269.
- [58] Z. Luan, X. Liu, M. Zheng, and L. Zhu, "Numerical Simulation of Square Section Venturi Scrubber with Horizontal Spray," *Procedia Comput. Sci.*, vol. 107, no. Icict, pp. 117–121, 2017, doi: 10.1016/j.procs.2017.03.066.
- [59] M. Bal and B. C. Meikap, "Prediction of Hydrodynamic Characteristics of a Venturi Scrubber by using CFD Simulation," *South African J. Chem. Eng.*, 2017, doi: 10.1016/j.sajce.2017.10.006.
- [60] I. Safdar, A. Khan, M. Ali, and A. Mushtaq, "Numerical Simulation of Particulate Removal Efficiency in Venturi Scrubber," 13th International Conference on Emerging Technologies (ICET) pp. 1–6, 2017, doi:10.1109/ICET.2017.8281727.
- [61] S. Yang, X. Zhao, W. Sun, J. Yuan, and Z. Wang, "Effect of ring baffle configuration in a self-priming venturi scrubber using CFD simulations," *Particuology*, vol. 47, pp. 63–69, 2019, doi: 10.1016/j.partic.2019.02.003.
- [62] A. Ahmed et al., "Investigation of iodine removal efficiency in a venturi scrubber using mass transfer model for CFD," *Prog. Nucl. Energy*, 2020, doi: 10.1016/j.pnucene.2020.103243.
- [63] L. Kumararaja, "Modelling equations for the properties of producer gas generated from biomass gasifiers," *Int. J. Appl. Math. Sci.*, vol. 9, no. 1, pp. 103–112, 2016.
- [64] M. Holz, S. R. Heil, and A. Sacco, "Temperature-dependent self-diffusion coefficients of water and six selected molecular liquids for calibration in accurate ^1H NMR PFG measurements," *Phys. Chem. Chem. Phys.*, vol. 2, no. 20, pp. 4740–4742, 2000, doi: 10.1039/b005319h.
- [65] A. M. Silva, "Numerical and Experimental Study of Venturi Scrubbers" Thesis, p. 138, 2008.